www.reanimatology.com
ISSN 2411-7110 (online)

GENERAL REANIMATOLOGY

SCIENTIFIC-AND-PRACTICAL JOURNAL

ОБЩАЯ РЕАНИМАТОЛОГИЯ

научно-практический журнал

Volume 21 Том 21

№ 3

Директор Федерального научно-клинического центра реаниматологии и реабилитологии (ФНКЦ РР) А. В. Гречко избран Академиком РАН

Директор Федерального научно-клинического центра реаниматологии и реабилитологии (ФНКЦ РР) Министерства науки и высшего образования Российской Федерации, член-корреспондент РАН Андрей Вячеславович Гречко избран Академиком РАН по специальности медико-социальная реабилитация и медико-социальная экспертиза!

Академик РАН — член высшей ступени РАН, ученый, внесший значительный вклад в науку трудами первостепенного научного значения в различных областях знания.

В Академики РАН на выборах 2025 г. было избрано 84 человека, членами-корреспондентами РАН стали 165 ученых. Средний возраст избранных Академиков РАН составил 64,27 лет, членов-корреспондентов РАН — 58,22 лет.

Гречко Андрей Вячеславович — российский ученый, врач высшей категории, доктор медицинских наук, профессор, Академик РАН, специалист в области медико-социальной реабилитации и медико-социальной экспертизы, заведующий кафедрой медико-социальной экспертизы и медико-социальной реабилитации Российского государственного социального университета (РГСУ), член диссертационного совета 24.1246.02 ФНКЦ РР, автор 390 научных работ, из них 18 монографий, суммарное количество цитирований которых в настоящее время превышает 7576 (индекс Хирша РИНЦ — 41, Scopus — 34), имеет 28 патентов, в том числе 5 свидетельств о государственной регистрации программ для ЭВМ и 1 базы данных.

Основные научные результаты А. В. Гречко:

- реализована научно обоснованная разработанная инновационная национальная система этапной нейрореабилитации реанимационных пациентов с тяжелым повреждением головного мозга, нуждающихся в длительном протезировании жизненно-важных функций, позволяющая снизить летальность с доказанной экономической эффективностью;
- сформировано новое научное направление — ранняя медико-социальная реабилитация пациентов с тяжелым повреждением головного мозга, нуждающихся в замещении жизненно важных функций, в том числе ветеранов СВО и лиц, пострадавших на линии боевого соприкосновения;
- разработаны новые методы лечения и реабилитации (новые органопротекторы, технологии фагопрофилактики и фаготерапии, инвазивной нейрореабилитации) на основе изучения общепатологических механизмов развития хронических критических состояний.

Гречко А. В. является экспертом РАН, членом Экспертного совета Министерства Обороны Российской Федерации, Экспертного совета при Комитете Государственной Думы по охране здоровья, Экспертного совета по здравоохранению при Комитете Совета Федерации по социальной политике, Экспертного совета по здравоохранению Совета Федерации Федерального Собрания Российской Федерации, Общественного совета при Росздравнадзоре, Общественного совета при Россотрудничестве МИД России, Общероссийской общественной организации «Федерация анестезиологов и реаниматологов», входит в состав Президиума Союза реабилитологов России, редколлегий 6 научных медицинских журналов.

Гречко А. В. удостоен многих государственных наград и знаков отличия, в числе которых Почетный работник науки и высоких технологий Российской Федерации, лауреат Премии Правительства Российской Федерации, Медаль ордена «За заслуги перед Отечеством» II степени, Орден Мужества, Орден Пирогова.

В 2023 г. совместно с Общероссийским Народным фронтом и Государственным фондом «Защитники отечества» А. В. Гречко создана программа «Возвращение», имеющая целью создание системы эффективной медицинской помощи ветеранам СВО с тяжелыми ранениями головного мозга и максимальную их адаптацию к мирной жизни.

В настоящее время ФНКЦ РР оказывает практическую помощь и поддержку по решению вопросов оказания качественной первичной медико-санитарной и специализированной, в том числе высокотехнологичной, медицинской помощи пострадавшим в ходе проведения СВО. Применение уникальной системы маршрутизации позволяет не только сохранить качество жизни нашим ветеранам, но и обеспечить их эффективную социализацию.

Решение об избрании А. В. Гречко Академиком РАН было поддержано подавляющим большинством на Общем собрании РАН в знак признания его значительного вклада в развитие медицинской науки.

Поздравляем Андрея Вячеславовича с заслуженным высшим научным званием, желаем новых побед и свершений на благо нашей Родины!

С глубоким уважением,
Редакция журнала «Общая реаниматология»

ISSN 1813-9779 (print) ISSN 2411-7110 (online)

GENERAL REANIMATOLOGY

OBSHCHAYA REANIMATOLOGIYA

Scientific-and-Practical Peer-Reviewed Journal
Since 2005

• Covers issues of critical care medicine
• Manuscripts in Russian and English are published free-of-charge
• Included in SCOPUS (since 2015), RINTs, RSCI, DOAJ, and other databases, as well as in the Official list of editions recommended for publication of dissertations (PhD, DSci) by the Russian Higher Attestation Commission

Registration certificate of the Journal «Obshchaya reanimatologiya» (General Reanimatology): ПИ № ФС77-18690, November 2, 2004, Federal Service for Supervision of Compliance with Legislation in the Sphere of Mass Communications and Protection of Cultural Heritage
Publication Frequency: 6 numbers per year.
Founder:

ОБЩАЯ РЕАНИМАТОЛОГИЯ

OBŜAÂ REANIMATOLOGIÂ

научно-практический рецензируемый журнал
Выходит с 2005 г.

• охватывает вопросы медицины критических состояний
• публикует рукописи на русском и английском языках бесплатно
• включен в базы данных SCOPUS (с 2015 г.), РИНЦ, RSCI, DOAJ и др. базы данных; Перечень изданий, рекомендованных ВАК для публикации результатов диссертационных работ

Свидетельство о регистрации: ПИ № ФС77-18690 от 02 ноября 2004 г. Печатное издание журнал «Общая реаниматология» зарегистрирован Федеральной службой по надзору за соблюдением законодательства в сфере массовых коммуникаций и охране культурного наследия.
Периодичность: 6 раз в год
Учредитель: © Фонд «Медицина критических состояний», Москва, Россия

Publisher:
Federal Research and Clinical Center of Intensive Care Medicine and Rehabilitology, Moscow, Russia
Издатель:
Федеральный научно-клинический центр реаниматологии и реабилитологии (ФНКЦ РР), Москва, Россия

Supported by Russian Federation of Anesthesiologists and Reanimatologists
При поддержке Общероссийской общественной организации «Федерация анестезиологов и реаниматологов»

Artwork: Natalia V. Golubeva
Page-proof: Sergey V. Shishkov
Printing House:
Printed at LLC «Advanced Solutions». 19, Leninsky prospekt, build. 1, Moscow, 119071. www.aov.ru
Contacts:
25 Petrovka Str., Bldg. 2, 107031 Moscow, Russia.
Tel. +7-495-694-17-73.
E-mail: **journal_or@mail.ru;**
Web: **www.reanimatology.com**

Subscription:
Index 46338, refer to catalog of «Книга-Сервис»
Signed for printing: 09.09.2025

Оригинал-макет: Н. В. Голубева
Верстка: С. В. Шишков
Типография: отпечатано в ООО «Адвансед солюшнз». 119071, г. Москва, Ленинский пр-т, д. 19, стр. 1. www.aov.ru
Контакты с редакцией:
Россия, 107031, г. Москва, ул. Петровка, д. 25, стр. 2.
Тел.: +7-495-694-17-73.
E-mail: **journal_or@mail.ru;**
сайт: **www.reanimatology.com**

Подписка и распространение: индекс издания по каталогу «Книга-Сервис» — 46338.
Цена свободная
Подписано в печать: 09.09.2025

CONTENTS **СОДЕРЖАНИЕ**

https://doi.org/10.15360/1813-9779-2025-3-2555

The Effect of Fluid Therapy on the Development of Metabolic Disturbances and ICU Length of Stay in Pediatric Patients Undergoing Surgery for Congenital Heart Defects

Nikolay A. Solovyov[1,2]*, Mikhail M. Rybka[1], Denis A. Dibin[1], Gleb E. Gorbunov[1], Sofya M. Tsoi[1], Zera A. Kodzokova[1], Andrey A. Goncharov[1]

[1] A. N. Bakulev National Medical Research Center for Cardiovascular Surgery, Russian Ministry of Health, 135 Rublevskoe shosse, 121552 Moscow, Russia
[2] G. N. Speransky Children's City Clinical Hospital No. 9, Moscow Health Department, 29 Shmitovsky pr., 123317 Moscow, Russia

For citation: *Nikolay A. Solovyov, Mikhail M. Rybka, Denis A. Dibin, Gleb E. Gorbunov, Sofya M. Tsoi, Zera A. Kodzokova, Andrey A. Goncharov.* The Effect of Fluid Therapy on the Development of Metabolic Disturbances and ICU Length of Stay in Pediatric Patients Undergoing Surgery for Congenital Heart Defects. *Obshchaya Reanimatologiya=General Reanimatology.* 2025; 21 (3). https://doi.org/10.15360/1813-9779-2025-3-2555 [In Russ. and Engl.]

***Correspondence to:** Nikolay A. Solovyov, N.A.Solovev@yandex.ru

Summary

Aim: to compare the effects of restrictive versus liberal fluid therapy on the duration of mechanical ventilation (MV), total intensive care unit (ICU) stay, and the need for inotropic and vasopressor support during the post-perfusion period and the first 24 hours after surgery in young children undergoing surgical correction of congenital heart defects (CHD).

Materials and Methods. A prospective, randomized, single-center study included pediatric patients (toddlers) with CHD who were assigned to one of two groups. Group 1 received fluid therapy according to a restrictive protocol (RP group, *N*=65) at 8 mL/kg/h, while group 2 received therapy according to a liberal protocol (LP group, *N*=67) at 16 mL/kg/h. The study evaluated the dynamics of metabolic disturbances, duration of ventilatory support, postoperative weight gain, and total ICU stay.

Results. Mechanical ventilation time and total ICU stay were longer in the RP group compared to the LP group: 14±5 hours vs. 10±3 hours (*P*=0.035) and 27±4 hours vs. 23±2 hours (*P*=0.036), respectively. Mean postoperative weight gain in the LP group was 2.00% vs 0.32% in the RP group (*P*=0.001). No clinically significant metabolic or electrolyte disturbances were observed in either group, except for elevated K^+ ion levels in the LP group.

Conclusion. These findings contradict previously reported data in adult population with CHD. In toddlers, a liberal approach to fluid therapy resulted in shorter duration of ventilation and ICU stay compared to a restrictive approach. Toddlers are more sensitive to fluid volume and their preload requirements are higher than those of adults.

Keywords: fluid therapy; intensive care; pediatric cardiac surgery; cardiopulmonary bypass; congenital heart defects

Funding. This study did not receive any external funding.

Conflict of interest. The authors declare no conflict of interest. Preliminary results were published in the Abstract Book of the XVII International (XXVI All-Russian) Pirogov Scientific Medical Conference for Students and Young Scientists. Moscow: Pirogov Russian National Research Medical University, Ministry of Health of Russia; 2022. p. 22. ISBN: 978-5-88458-591-1.

Information about the authors:
Nikolay A. Solovyov: http://orcid.org/0000-0002-8409-7254
Mikhail M. Rybka: http://orcid.org/0000-0001-8206-8794
Denis A. Dibin: http://orcid.org/0000-0002-4161-7416
Gleb E. Gorbunov: http://orcid.org/0000-0003-3274-4517
Sofya M. Tsoi: http://orcid.org/0000-0002-2733-0355
Zera A. Kodzokova: http://orcid.org/0000-0003-3330-9971
Andrey A. Goncharov: http://orcid.org/0000-0003-2122-7813

Introduction

Recent studies have demonstrated the significant impact of fluid therapy on immediate surgical outcomes and overall clinical outcomes in various surgical disciplines [1–3]. Currently, three main strategies of perioperative fluid management are recognized: restrictive (limiting intravenous fluid volume), liberal (no strict fluid limits), and goal-directed therapy aimed at avoiding both hypovolemia and hypervolemia [4, 5].

Each of these approaches has limitations. The restrictive strategy often requires the use of vasopressors, which, as several studies have shown, may impair peripheral circulation and in some cases lead to anastomotic dysfunction [6, 7]. The liberal strategy does not take into account individual tol-

erance to anemia and increases the risk of iatrogenic edema due to fluid overload [8]. Goal-directed fluid therapy requires the use of invasive monitoring techniques (e. g., PiCCO, Swan–Ganz catheters, or left atrial catheters, CVP monitoring) or specialized noninvasive tools (e. g., USCOM), all of which require a high level of expertise on the part of the anesthesiologist. These considerations remain the subject of ongoing debate and represent an ever persisting challenge in anesthesiology and critical care [9, 10].

International guidelines recommend the use of instrumental methods to assess volume status, primarily based on linear or volumetric flow rate measurements, with the caveat «when technically feasible» [11]. Especially in infants and young children, the applicability of such methods, especially invasive ones, is limited. Studies suggest that there are discrepancies of at least 30% between values obtained by invasive monitoring and echocardiography [12]. At the same time, simpler physical methods, such as serial weighing and careful recording of fluid balance, may offer practical alternatives for assessing volemic status. While a substantial body of research focuses on fluid therapy in neonatology and general pediatrics, early childhood remains relatively understudied. This age group surpasses neonates in metabolic requirements, but is still below the age typically included in pediatric studies.

The aim of the study was to compare the effects of restrictive versus liberal fluid therapy on the duration of mechanical ventilation, total length of stay in the pediatric intensive care unit (PICU), and the need for inotropic and vasopressor support during the postperfusion period and the first 24 hours after surgery in young children undergoing correction of congenital heart defects (CHDs).

Materials and Methods

A single-center, prospective, randomized trial was conducted after approval by the local ethics committee (Protocol No. 001 dated January 30, 2020). The study was not preregistered on ClinicalTrials.gov.

This was a prospective, randomized, observational study that enrolled young children who underwent surgical correction of septal congenital heart defects at the Early Childhood Department of the A. N. Bakulev National Medical Research Center for Cardiovascular Surgery, Ministry of Health of the Russian Federation from February 2020 to February 2022.

The analysis was performed using a per-protocol (PP) approach. All patients had an American Society of Anesthesiologists (ASA) physical status of III–IV, NYHA functional class I–II, Aristotle Basic Complexity score of 1–2 out of 6, and an expected PICU stay of 1–3 days.

Patients enrolled underwent radical correction of CHDs: patch closure or direct suture repair of atrial septal defects (ASD) and/or ventricular septal defects (VSD).

The inclusion criteria were as follows:

- age between 11 and 36 months;
- absence of significant comorbidities;
- written informed consent obtained from the parent or legal guardian;
- congenital heart defect requiring surgical correction under cardiopulmonary bypass (CPB);
- no previous open heart surgery (e. g., no previous pulmonary artery banding [Müller procedure] prior to VSD closure; no history of attempted transcatheter defect closure).

Exclusion criteria were as follows:

- severe genetic syndromes;
- massive intraoperative blood loss;
- emergency surgery;
- severe comorbidities;
- re-sternotomy within the first postoperative day;
- reinitiation of CPB due to low cardiac output in the postperfusion period.

The authors hypothesized that a liberal fluid therapy strategy would be no less effective than a restrictive strategy. Patients were randomized into two groups according to the volume of fluid administered intraoperatively.

Group 1 received restrictive fluid therapy at 8 mL/kg/h (restrictive protocol, RP group, *N*=65), while group 2 received liberal fluid therapy at 16 mL/kg/h (liberal protocol, LP group, *N*=67) (see Fig. 1). Randomization was performed using sealed opaque envelopes one day prior to surgery.

During the study, eight patients were excluded for the following reasons: need for epinephrine infusion (*N*=4), arrhythmia after sternal closure (*N*=2), complete atrioventricular block requiring temporary pacing after CPB (*N*=1), and anaphylactic reaction to protamine (*N*=1).

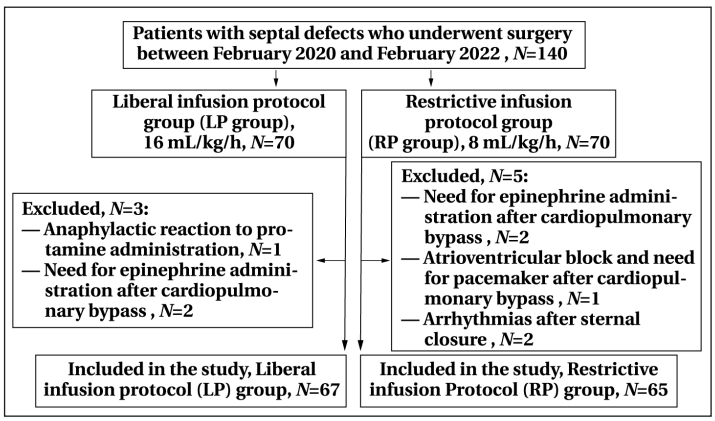

Fig. 1. Study flowchart.

Hemodynamic stabilization after termination of cardiopulmonary bypass (CPB) was achieved by adequate volume loading and titration of inotropic support. Dopamine was administered at doses ranging from 3 to 6 μg/kg/min. In the RP group, all patients required post-CPB norepinephrine infusion at doses ranging from 0.03 to 0.05 μg/kg/min. In 31% of cases, vasopressor support was continued until admission to the ICU.

Anesthesia management was standardized in both groups according to institutional protocol:

- Induction of anesthesia: midazolam 0.2 mg/kg, propofol 2 mg/kg, rocuronium 1 mg/kg, fentanyl 5 μg/kg;
- Maintenance of anesthesia: sevoflurane 1.0–1.2 MAC, fentanyl 5 μg/kg/h, rocuronium 0.5 mg/kg/h;
- Pre-perfusion: All patients received sodium oxybate at a dose of 80–120 mg/kg;
- During CPB: isoflurane was insufflated into the CPB circuit at a concentration of 2 vol%, with continuous fentanyl infusion at 3 μg/kg/h and rocuronium at 0.5 mg/kg/h.

Cardiopulmonary bypass was performed according to institutional protocol. Perfusion was maintained at an index of 2.8–3.2 L/min/m² under normothermic conditions (36°C). Blood cardioplegia was used to induce cardiac arrest and provide myocardial protection.

Arterial blood samples were taken at the following time points: after tracheal intubation, after initiation and termination of extracorporeal circulation, after sternal closure, upon admission to the ICU, and then every 3 hours for the first 12 postoperative hours, at 18 hours, and at the end of the first postoperative day. The following parameters were evaluated: blood glucose, lactate, acid-base balance (pH, base excess, HCO_3^-), electrolytes (Na^+, K^+, Cl^-), and blood gas levels (pO_2, pCO_2, SO_2).

To assess fluid balance, all patients underwent triple body weight measurements. The mean was used for analysis. Weighing was performed in the operating room before skin incision, after tracheal intubation and catheter placement, and again before transfer to the ICU. The first intraoperative weight measurement was compared with the preoperative body weight recorded in the medical record.

Data were analyzed using SPSS software version 11.5 for Windows (SPSS Inc., Chicago, IL) and analysis tools available in Microsoft Excel 2016. No a priori sample size calculation was performed. The Shapiro–Wilk test was used to assess the normality of the data distribution.

Descriptive statistics were presented as means with standard deviations (SD). The independent samples Student's *t*-test was used for comparisons between two independent groups. The paired samples Student's *t*-test was used for related samples, and the one-sample Student's *t*-test was used to compare group values with reference norms. The Mann–Whitney *U* test was used for nonparametric comparisons between two independent groups. Repeated measures were analyzed with the Friedman test. Categorical variables (e. g. sex) were compared using Pearson's chi-squared test.

A $P \leqslant 0.05$ was considered statistically significant. Results were visualized using graphs and charts.

Results

Patients in both groups were comparable with respect to sex, duration of cardiopulmonary bypass, aortic cross-clamp time, surgical complexity, and time to recovery of cardiac function in the postperfusion period (Tables 1 and 2).

Table 1. Comparative characteristics of patients in the two groups by sex.

Sex, *N* (%)	RP (*N*=65)	LP (*N*=67)	*P* (χ^2 test)
Male	32 (49)	33 (49)	0.876
Female	33 (51)	34 (51)	

In the postperfusion and early postoperative periods, acid-base balance (pH<7.36, BE<–2.5 mmol/L, HCO_3^-<22 mmol/L) was assessed. Intergroup comparisons at all time points showed no statistically significant differences in the incidence of metabolic abnormalities (P>0.05). Differences in blood metabolite and electrolyte levels, except for potassium ions (K^+), were also not statistically significant between groups at any time point (P>0.05). However, significant differences in blood K^+ concentrations were observed between the RP and LP groups at baseline (P=0.007) and at ICU admission (P=0.002) (Table 3).

Thus, the use of Sterofundin to maintain the blood electrolyte balance may be sufficient, provided that blood products are used to prime the CPB circuit, as its electrolyte profile is fully balanced. This is supported by previous studies [13–14]. In

Table 2. Comparative characteristics of patients in the two groups.

Parameters	Values in groups		*P* value
	RP (*N*=65)	LP (*N*=67)	
Age, months	19.4±8.6	19.8±8.8	0.920
Height, cm	82.5±7.9	80.5±7.0	0.903
Body weight, kg (according to medical history)	10.17±1.9	10.7±2.1	0.518
Body weight, kg (intraoperatively)	10.1±1.7	9.8±1.7	0.801
Duration of CPB, min	48.12±3.15	43.07±10.2	0.735
Duration of aortic clamping, min	23.6±8.7	20.06±8.1	0.013**
Blood loss, mL	148.1±27.2	150.2±31.2	0.638

Note. ** — Significant differences at $P \leqslant 0.01$ (Mann–Whitney test).

the LP group, a significant dynamic change in the PO_2/FiO_2 ratio was observed (P=0.002): the lowest values were recorded immediately after CPB (3.8), while the highest values were recorded at baseline (4.3) and three hours after admission to the ICU (4.23). In the RP group, changes in the PO_2/FiO_2 ratio were not significant (P=0.289). Comparisons between groups also showed no significant differences (Table 4).

Moderate hypervolemia did not compromise pulmonary oxygenation despite the twofold difference in infusion rates between groups (8 mL/kg/h vs. 16 mL/kg/h). Ventilation modes and parameters were identical in both groups. Duration of mechanical ventilation and total ICU length of stay were significantly longer in the RP group compared to the LP group: 14±5 hours versus 10.3±4 hours (P=0.022) and 27.5±4 hours versus 23±2 hours (P=0.036), respectively (Mann–Whitney test).

Special attention should be paid to accurate weight determination in this patient population (Table 4). Infants and young children should be weighed in the operating room to avoid discrepancies between actual body weight and the weight recorded in the medical chart. Body weight is used to calculate ventilatory volume, doses of inotropes, muscle relaxants, opioid analgesics, antibiotics, and other medications, as well as to determine perfusion and infusion rates, urine output, and blood loss. The mean percentage weight gain was significantly higher in the LP group than in the RP group: 2.00% vs. 0.32% (P=0.001) (Table 5).

Table 3. Analysis of differences and changes in metabolite and electrolyte levels in arterial blood.

Parameter	Group	Values at study stages				**P value
		Baseline	After CPB	In the ICU	After 3 h in the ICU	
pH	RP	7.44±0.05	7.41±0.15	7.44±0.08	7.39±0.09	1.1×10^{-5}**
	LP	7.39±0.06	7.41±0.05	7.45±0.06	7.40±0.05	1.1×10^{-5}**
*P value		0.375*	0.681*	0.458*	0.301*	
HCO_3^-, mmol/L	RP	20.94±2.46	23.49±2.40	23.76±2.96	22.59±2.50	1.3×10^{-12}**
	LP	20.90±2.65	24.56±2.50	24.53±2.59	23.07±2.75	5.6×10^{-13}**
*P value		0.875*	0.116*	0.305*	0.477*	
Osmolality	RP	283.55±35.65	294.28±6.00	296.43±6.60	296.63±6.71	6.4×10^{-13}**
	LP	288.18±4.90	293.07±7.02	295.85±7.13	297.38±15.55	6.8×10^{-10}**
*P value		0.766*	0.436*	0.608*	0.311*	
BE, mmol/L	RP	–3.2±1.8	–0.3±2.1	0.5±2.3	–1.3±0.7	1.2×10^{-15}**
	LP	–3.1±0.17	–0.3±0.19	1.18±0.4	–0.7±0.19	1.2×10^{-11}
*P value		0.982*	0.338*	0.309*	0.104*	
Na^+, mmol/L	RP	135.68±18.32	139.67±3.10	141.31±3.53	140.46±3.70	3.9×10^{-7}**
	LP	135.11±5.19	137.16±2.07	139.13±2.19	138.21±3.16	1.8×10^{-10}**
*P value		0.940*	0.647*	0.809*	0.395*	
K^+, mmol/L	RP	3.82±0.39	4.1±0.31	3.77±0.35	3.78±0.28	3.0×10^{-6}**
	LP	3.65±0.29	4.16±0.29	4.04±0.36	3.51±0.29	9.4×10^{-7}**
*P value		0.007**	0.246*	0.002**	0.568*	
Cl^-, mmol/L	RP	113.23±3.97	111.06±2.68	111.76±3.77	110.19±2.90	3.6×10^{-8}**
	LP	112.35±3.08	110.57±3.47	110.98±3.35	110.33±3.00	7.6×10^{-4}**
*P value		0.395*	0.480*	0.377*	0.579*	
Lactate, mmol/L	RP	1.01±0.30	1.69±0.64	1.49±0.73	1.70±1.02	3.5×10^{-13}**
	LP	0.94±0.30	1.60±0.57	1.32±0.61	1.55±0.89	3.7×10^{-15}**
*P value		0.198*	0.351*	0.238*	0.426*	
Glucose, mmol/L	RP	4.54±0.92	6.72±1.28	6.24±1.57	8.14±2.60	1.2×10^{-22}**
	LP	4.61±0.89	6.72±1.22	6.00±1.31	9.34±3.91	5.2×10^{-18}**
*P value		0.651*	0.936*	0.445*	0.065*	

Note. Differences are statistically significant at $P\leqslant0.05$ (* — Mann–Whitney U test; ** — Friedman test).

Table 4. Changes in PO_2/FiO_2 ratio in arterial blood between groups.

Parameter	Group	Values at study stages				P value
		Baseline	After CPB	In the ICU	After 3 h in the ICU	
PO_2/FiO_2	RP	4.60±0.82	4.05±0.53	4.14±0.4	4.23±0.41	0.289
	LP	4.30±1.10	3.80±0.41	4.10±0.42	4.21±0.45	0.002**
P value		0.174*	0.307*	0.280*	0.151*	

Note. * — Mann–Whitney U test; ** — Friedman test

Table 5. Postoperative weight gain in the two groups.

Parameters	Values in groups		P value
	RP (N=65)	LP (N=67)	
Preoperative weight, kg	11.22±2.80	11.04±2.89	0.396
Postoperative weight, kg	11.26±2.89	11.26±2.92	0.704
P value (Wilcoxon test)	0.332	3.1×10^{-7}**	—
Absolute weight gain, kg	0.05±0.03	0.22±0.03	0.002**
Weight gain, %	0.32±0.29	2.00±0.27	0.001**

Note. $P\leqslant0.01$ indicates statistical significance (Mann–Whitney U test). RP — restrictive protocol; LP — liberal protocol.

Table 6. Association between postoperative weight gain and duration of mechanical ventilation and ICU stay.

Parameter during ICU stay	Statistical test	Weight gain (kg)	Weight gain (%)
Duration of mechanical ventilation, h	Spearman's *R*	–0.160*	–0.119
	P value	0.039	0.128
Total ICU stay, h	Spearman's *R*	0.047	0.041
	P value	0.551	0.603

Note. * — correlation is significant at $P \leqslant 0.05$.

A negative linear correlation was found only between the difference in body weight and the duration of mechanical ventilation in the ICU (R=–0.160; P=0.039): as weight increased, the duration of mechanical ventilation in the ICU decreased (Table 6).

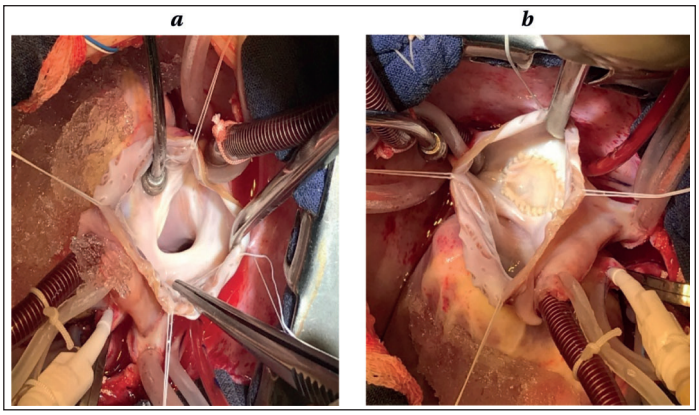

Fig. 2. Atrial septal defect (*a*) before correction and (*b*) after patch closure.

Discussion

Patients with septal defects were selected for this study because these defects are highly prevalent in individuals with congenital heart disease. They are typically associated with hemodynamic stability and can be successfully treated with radical surgical correction in the vast majority of cases (Fig. 2).

Changes in fluid status — particularly hypovolemia — are a major cause of hemodynamic instability in patients undergoing surgery for septal and other congenital heart defects. Because open heart surgery is associated with significant fluctuations in blood volume and vascular tone, optimization of perioperative fluid therapy and accurate assessment of blood loss are critical responsibilities of the anesthesiologist-intensivist. Both fluid overload and hypovolemia increase the risk of postoperative complications. In addition, fluid deficits may occur in the absence of apparent losses due to vasodilation, sweating, and hemodilution.

The study showed that liberal fluid management reduced the length of stay in the pediatric ICU. In this age group, compensatory physiological mechanisms are not fully developed, which may explain the discrepancy with findings from studies of infusion strategies in patients with acquired heart disease (AHD), where more restrictive approaches are often favored due to the severity of the underlying pathology. In one retrospective study [15], patients received restrictive fluid therapy due to the presence of edema and congestive heart failure.

Pulmonary oxygenation function did not differ significantly between the two fluid management strategies, while ventilatory parameters remained consistent in both groups. Based on the present findings, liberal fluid therapy does not compromise pulmonary oxygenation or preclude early mobilization or tracheal extubation in this patient population.

There is ongoing debate regarding the optimal fluid management strategy in young children. In the postoperative period, children with CHD are always at risk for fluid overload, which is known to be associated with adverse outcomes. Several studies have reported that a positive fluid balance greater than 10% of baseline body weight after cardiac surgery is associated with adverse outcomes [16–19]. For example, a single-center study by Hudkins et al. [20] found that early postoperative fluid accumulation in the PICU was associated with increased mortality and prolonged mechanical ventilation. Similarly, a meta-analysis by Bellos [21], which included 12 studies from electronic databases such as Medline, Scopus, CENTRAL, ClinicalTrials.gov, and Google Scholar (a total of 3,111 pediatric patients), yielded comparable results.

In the study by Delpachitra [21], of 1,996 children with a positive fluid balance, 46 (2.3%) died, and of these, 45 (98%) had a fatal outcome associated with prolonged cardiopulmonary bypass time. A 10-minute increase in bypass time was associated with an odds ratio [95% CI] of 1.06 [1.00–1.12]; P=0.03, and with the need for extracorporeal membrane oxygenation in the early postoperative period. Therefore, while early fluid overload was not directly associated with mortality, it was associated with longer duration of mechanical ventilation and prolonged ICU stay.

In a multicenter study involving 2,223 patients [22], the time to first negative 24-hour fluid balance (but not the percentage of fluid overload) was associated with better postoperative outcomes in children after cardiac surgery. Specific management strategies aimed at reducing fluid overload may shorten the duration of postoperative ICU observation in these patients. All authors agree that daily patient weighing is critical for early detection

of fluid overload after cardiac surgery. However, patient weighing practices vary widely among medical centers. Patients with more severe conditions are weighed less frequently [23]. Key recommendations include the use of isotonic balanced solutions and regular monitoring of plasma electrolyte and glucose levels and fluid balance [24].

Conclusion

In patients with congenital heart defects receiving liberal infusion therapy, pulmonary oxygenation function remains unaffected in the postperfusion and early postoperative periods. In addition, there are no significant metabolic or electrolyte disturbances compared to the group receiving restrictive infusion therapy. Weight gain does not prolong the duration of mechanical ventilation or the total ICU stay in patients after radical correction of septal defects.

References

1. *Mathew A., Rai E.* Pediatric perioperative fluid management. *Saudi J Anaesth.* 2021; 15 (4): 435–440. DOI: 10.4103/sja.sja_140_21. PMID: 34658733.
2. *Myles P. S., McIlroy D.R., Bellomo R., Wallace S.* Importance of intraoperative oliguria during major abdominal surgery: findings of the Restrictive versus Liberal Fluid Therapy in Major Abdominal Surgery trial. *Br J Anaesth.* 2019; 122 (6): 726–733. DOI: 10.1016/j.bja.2019.01.010. PMID: 30916001.
3. *Anker A. M., Ruewe M., Prantl L., Baringer M., Pawlik M. T., Zeman F, Goecze I., et al.* Biomarker-guided acute kidney injury risk assessment under liberal versus restrictive fluid therapy — the prospective-randomized MAYDAY-trial. *Sci Rep.* 2024; 14 (1): 17094. DOI: 10.1038/s41598-024-68079-2. PMID: 39048691.
4. *Mathew P. J., Sharma S., Bhardwaj N., Ashok V., Malik M. A.* Goal-directed fluid therapy guided by Plethysmographic Variability Index (PVI) versus conventional liberal fluid administration in children during elective abdominal surgery: a randomized controlled trial. *J Pediatr Surg.* 2023; 58 (4): 735–740. DOI: 10.1016/j.jpedsurg.2022.11.015. PMID: 36631313.
5. *Feng J., Kant S., Sellke F. W.* Microvascular dysfunction following cardioplegic arrest and cardiopulmonary bypass. *Vessel Plus.* 2021; 5: 30. DOI: 10.20517/2574-1209.2021.57.
6. *Guarracino F., Habicher M., Treskatsch S., Sander M., Szekely A., Paternoster G., Salvi L., et al.* Vasopressor therapy in cardiac surgery- an Experts› Consensus Statement. *J Cardiothorac Vasc Anesth.* 2021; 35 (4): 1018–1029. DOI: 10.1053/j.jvca.2020.11.032. PMID: 33334651.
7. *Zieg J., Narla D., Gonsorcikova L., Raina R.* Fluid management in children with volume depletion. *Pediatr Nephrol.* 2024; 39 (2): 423–434. DOI: 10.1007/s00467-023-06080-z. PMID: 37452205.
8. *Старостин Д. О., Кузовлев А. Н.* Роль ультразвука в оценке волемического статуса пациентов в критических состояниях. *Вестник интенсивной терапии имени А.И. Салтанова.* 2018; 4: 42–50. *Starostin D. O., Kuzovlev A. N.* Role of ultrasound in diagnosing volume status in critically ill patients. *Ann Crit Care = Vestnik Intensivnoy Terapii im A. I. Saltanova.* 2018; 4: 42–50. (In Russ.). DOI: 10.21320/1818-474X-2018-4-42-50.
9. *Lobdell K. W., Chatterjee S., Sander M.* Goal-directed therapy for cardiac surgery. *Crit Care Clin.* 2020; 36 (4): 653–662. DOI: 10.1016/j.ccc.2020.06.004. PMID: 32892819.
10. *Habicher M., Perrino A.Jr, Spies C. D., von Heymann C., Wittkowski U., Sander M. J.* Contemporary fluid management in cardiac anesthesia. *J Cardiothorac Vasc Anesth.* 2011; 25 (6): 1141–1153. DOI: 10.1053/j.jvca.2010.07.020. PMID: 20947379.
11. *Кодзокова З. А., Ломакин М. В., Рыбка М. М., Дибин Д. А.* Интраоперационное измерение центральной гемодинамики методом термодилюции с использованием катетера Swan–Ganz у пациента с исправленной транспозицией магистральных артерий. *Клиническая физиология кровообращения.* 2020; 17 (2): 142–147. *Kodzokova Z. A., Lomakin M. V., Rybka M. M., Dibin D. A.* Intraoperative central hemodynamics measurement by thermodilution technique using a Swan–Ganz catheter in a patient with corrected transposition of the great arteries. *Clinical Physiology of Blood Circulation = Klinicheskaya Fiziologiya Krovoobrashcheniya.* 2020; 17 (2). 142–147. (In Russ.). DOI: 10.24022/1814-6910-2020-17-2-142-147.
12. *Langer T., D'Oria V., Spolidoro G. C. I., Chidini G., Catenacci S., Marchesi T., Guerrini M., et al.* Fluid therapy in mechanically ventilated critically ill children: the sodium, chloride and water burden of fluid creep. *BMC Pediatr.* 2020; 20 (1): 424. DOI: 10.1186/s12887-020-02322-3. PMID: 32891127.
13. *Сулайманова Ж. Д., Лазарев В. В.* Кристаллоидные препараты в инфузионной терапии периоперационного периода у детей. *Российский вестник детской хирургии, анестезиологии и реаниматологии.* 2019; 4: 99–107. *Sulaimanova Z. D., Lazarev V. V.* Crystalloid agents used in perioperative infusion therapy in children. *Russian Bulletin of Pediatric Surgery, Anesthesia and Intensive Care = Rossiyskiy Vestnik Detskoy Khirurgii Anesteziologii i Reanimatologii.* 2019; 4: 99–107. (In Russ.). DOI: 10.30946/2219-4061-2019-9-4-99-107.
14. *Ушкалова Е. А., Зырянов С. К., Затолочина К. Э., Бутранова О. И.* Инфузионные растворы: взгляд клинического фармаколога. *Анестезиология и реаниматология.* 2021; (6): 100–106. *Ushkalova E. A., Zyryanov S. K., Zatolochina K. E., Butranova O. I.* Infusion fluids: a clinical pharmacologist's view. *Russian Journal of Anaesthesiology and Reanimatology = Anesteziologiya i Reanimatologiya.* 2021; (6): 100—106. (In Russ.) DOI: 10.17116/anaesthesiology2021061100.
15. *Белоусова Е. И., Матинян Н. В., Мартынов Л. А.* Стратегия инфузионнотрансфузионной терапии при операциях с массивной кровопотерей у детей с опухолями торакоабдоминальной локализации. *Российский вестник детской хирургии, анестезиологии и реаниматологии.* 2018; 8 (2): 56–64. *Belousova E. I., Matinyan N. V., Martynov L. A.* Strategy of infusion-transfusion therapy in operations with massive bloodwork in children with tumor abomalomal localization tumors. *Russian Bulletin of Pediatric Surgery, Anesthesia and Intensive Care = Rossiyskiy Vestnik Detskoy Khirurgii Anesteziologii i Reanimatologii.* 2018; 8 (2): 56–64. (In Russ.). DOI: 10.30946/2219-4061-2018-8-2-56-64.
16. *Хинчагов Д. Я., Рыбка М. М., Мумладзе К. В., Голубев Е. П., Юдин Г. В., Айдашев Ю. Ю., Ворожка И. В.* Выбор стратегии инфузионной терапии при операциях аортокоронарного шунтирования без искусственного кровообращения. *Клиническая физиология кровообращения.* 2022; 19 (4): 338–48. *Khinchagov D. Ya., Rybka M. M., Mumladze K. V., Golubev E. P., Yudin G. V., Aidashev Yu. Y., Vorozhka I. V.* Choosing an infusion therapy strategy for coronary artery bypass surgery without artificial circulation. *Clinical Physiology of Blood Circulation = Klinicheskaya Fiziologiya Krovoobrashcheniya.* 2022; 19 (4): 338–48. (In Russ.). DOI: 10.24022/1814-6910-2022-19-4-338-348.

17. *Sümpelmann R., Zander R., Witt L.* Perioperative Infusionstherapie bei Kindern. *Anasthesiol Intensivmed Notfallmed Schmerzther.* 2020; 55 (5): 324–333. DOI: 10.1055/a-1068-8566. PMID: 32434263.
18. *Brandewie K. L., Selewski D. T., Bailly D. K., Bhat P. N., Diddle J. W., Ghbeis M., Krawczeski C. D., et al; NEPHRON investigators.* Early postoperative weight-based fluid overload is associated with worse outcomes after neonatal cardiac surgery. *Pediatr Nephrol.* 2023; 38 (9): 3129–3137. DOI: 10.1007/s00467-023-05929-7. PMID: 36973562.
19. *Hudkins M. R., Miller-Smith L., Evers P. D., Muralidaran A., Orwoll B. E.* Nonresuscitation fluid accumulation and outcomes after pediatric cardiac surgery: single-center retrospective cohort study. *Pediatr Crit Care Med.* 2023; 24 (12): 1043–1052.
DOI: 10.1097/PCC.0000000000003373. PMID: 37747301.
20. *Bellos I., Iliopoulos D. C., Perrea D. N.* Association of postoperative fluid overload with adverse outcomes after congenital heart surgery: a systematic review and dose-response meta-analysis. *Pediatr Nephrol.* 2020; 35 (6): 1109–1119.
DOI: 10.1007/s00467-020-04489-4. PMID: 32040627.
21. *Delpachitra M. R., Namachivayam S. P., Millar J., Delzoppo C., Butt W. W.* A case-control analysis of postoperative fluid balance and mortality after pediatric cardiac surgery. *Pediatr Crit Care Med.* 2017; 18 (7): 614–622. DOI: 10.1097/PCC.0000000000001170. PMID: 28492405.
22. *Bailly D. K., Alten J. A., Gist K. M., Mah K. E., Kwiatkowski D. M., Valentine K. M., Diddle J. W., et al; NEPHRON Investigators.* Fluid accumulation after neonatal congenital cardiac operation: clinical implications and outcomes. *Ann Thorac Surg.* 2022; 114 (6): 2288–2294.
DOI: 10.1016/j.athoracsur.2021.12.078. PMID: 35245511.
23. *Neumayr T. M., Alten J. A., Bailly D. K., Bhat P. N., Brandewie K. L., Diddle J. W., Ghbeis M., et al; NEPHRON Investigators.* Assessment of fluid balance after neonatal cardiac surgery: a description of intake/output vs. weight-based methods. *Pediatr Nephrol.* 2023; 38 (4): 1355–1364.
DOI: 10.1007/s00467-022-05697-w. PMID: 36066771.
24. *Brossier D. W., Tume L. N., Briant A. R., Chaparro C. J., Moullet C., Rooze S., Verbruggen S. C. A. T., et* al; *Metabolism Endocrinology and Nutrition section of the European Society of Pediatric and Neonatal Intensive Care (ESPNIC).* ESPNIC clinical practice guidelines: intravenous maintenance fluid therapy in acute and critically ill children- a systematic review and meta-analysis. *Intensive Care Med.* 2022; 48 (12): 1691–1708.
DOI: 10.1007/s00134-022-06882-z. PMID: 36289081.

Received 18.12.2024
Accepted 11.04.2025
Online first 19.05.2025

https://doi.org/10.15360/1813-9779-2025-3-2559

Skin Microcirculatory Parameters as Diagnostic Markers of Central and Cerebral Circulatory Disorders in Hemorrhagic Shock (An Experimental Study)

Ivan A. Ryzhkov[1]*, Nadezhda V. Golubova[1,2], Konstantin N. Lapin[1], Sergey N. Kalabushev[1], Viktor V. Dremin[2], Elena V. Potapova[2], Andrey V. Dunaev[2], Vladimir T. Dolgikh[1], Viktor V. Moroz[1]

[1] V. A. Negovsky Research Institute of General Reanimatology, Federal Research and Clinical Center of Intensive Care Medicine and Rehabilitology, 25 Petrovka Str., Bldg. 2, 107031 Moscow, Russia
[2] Orel State University, 95 Komsomolskaya Str., 302026 Orel, Russia

For citation: *Ivan A. Ryzhkov, Nadezhda V. Golubova, Konstantin N. Lapin, Sergey N. Kalabushev, Viktor V. Dremin, Elena V. Potapova, Andrey V. Dunaev, Vladimir T. Dolgikh, Viktor V. Moroz.* Skin Microcirculatory Parameters as Diagnostic Markers of Central and Cerebral Circulatory Disorders in Hemorrhagic Shock (An Experimental Study). *Obshchaya Reanimatologiya=General Reanimatology.* 2025; 21 (3). https://doi.org/10.15360/1813-9779-2025-3-2559 [In Russ. and Engl.]

***Correspondence to:** Ivan A. Ryzhkov, riamed21@gmail.com

Summary

The aim of the study was to evaluate the relationship between skin microcirculatory parameters and central and cerebral hemodynamic parameters during progressive blood loss.

Materials and Methods. A randomized, prospective, controlled in vivo experimental study was performed using male Wistar rats (250–350 g, *N*=23) divided into two groups: «hemorrhagic shock» (HS, *N*=13), with blood loss of 15% and subsequently 35% of estimated circulating blood volume (CBV), and «sham-operated» controls (SO, *N*=10). After combined anesthesia, femoral artery catheterization, and craniotomy, the following were measured at baseline (stage 1): mean arterial pressure (MAP), cortical cerebral perfusion ($LSCI_{brain}$), and skin perfusion in the hindlimb ($LSCI_{skin}$) using laser speckle contrast imaging (LSCI). These measurements were repeated after 15% CBV loss (stage 2) and 35% CBV loss (stage 3). Cerebral (CVC_{brain}=$LSCI_{brain}$/MAP) and cutaneous (CVC_{skin}=$LSCI_{skin}$/MAP) vascular conductance indices were calculated. At stage 3, parameters of post-occlusive reactive hyperemia (PORH) in hindlimb skin were additionally assessed. Statistical analysis was performed using STATISTICA 13.0 with non-parametric methods. Spearman's correlation coefficient (*R*) was used to assess associations between circulatory parameters.

Results. A 15% CBV loss led to a 26% reduction in $LSCI_{skin}$ (*P*=0.003 vs SO), with no significant change in $LSCI_{brain}$. With further blood loss and a 43% reduction in $LSCI_{skin}$ (*P*<0.001 vs SO), $LSCI_{brain}$ decreased by 14% (*P*<0.001 vs SO). These changes were accompanied by a sustained increase in CVC_{brain} (*P*<0.001 vs SO at stage 3), while CVC_{skin} remained unchanged throughout the experiment. In the HS group, blood loss led to a significant decrease in PORH amplitude (*P*=0.003 vs SO), while microvascular flow reserve increased (*P*=0.036 vs SO). Before blood loss, moderate positive correlations were found between $LSCI_{skin}$, CVC_{skin}, and CVC_{brain}. In HS, $LSCI_{brain}$ correlated with the degree of $LSCI_{skin}$ reduction (*R*=0.57, *P*=0.041), and skin microvascular flow reserve showed a strong positive correlation with arterial blood pH and base excess (BE) (*R*=0.84, *P*=0.001). The correlation between $LSCI_{skin}$ and MAP shifted from a moderate negative correlation at stage 1 to a strong positive correlation at stage 3.

Conclusion. Skin microcirculation parameters ($LSCI_{skin}$, CVC_{skin}, and PORH), as assessed by laser speckle contrast imaging, are promising diagnostic markers of central and cerebral hemodynamic impairment during progressive blood loss and warrant further validation.

Keywords: microcirculation; skin; brain; blood loss; laser speckle contrast imaging

Conflict of interest. The authors declare no conflict of interest.

Funding. This study was supported by the Russian Science Foundation (Project No. 24-25-00310).

Information about the authors:
Ivan A. Ryzhkov: AuthorID (RINTs): 781730, http://orcid.org/0000-0002-0631-5666
Nadezhda V. Golubova: AuthorID (RINTs): 1144542, http://orcid.org/0000-0001-5175-1486
Konstantin N. Lapin: AuthorID (RINTs): 1061143, http://orcid.org/0000-0002-7760-3526
Sergey N. Kalabushev: AuthorID (RINTs): 992594, http://orcid.org/0000-0001-7017-7897
Viktor V. Dremin: AuthorID (RINTs): 787806, http://orcid.org/0000-0001-6974-3505
Elena V. Potapova: AuthorID (RINTs): 240669, http://orcid.org/0000-0002-9227-6308
Andrey V. Dunaev: AuthorID (RINTs): 212404, http://orcid.org/0000-0003-4431-6288
Vladimir T. Dolgikh: AuthorID (RINTs): 540900, http://orcid.org/0000-0001-9034-4912
Viktor V. Moroz: AuthorID (RINTs): 168246

Introduction

Hemorrhagic shock (HS) is an acute circulatory failure resulting from significant blood loss. It is characterized by impaired tissue perfusion and oxygen delivery and carries a high risk for the development of multiple organ dysfunction [1]. The primary pathogenic trigger in acute hemorrhage and HS is profound hypovolemia, leading to a reduction in cardiac output, arterial hypotension, and peripheral hypoperfusion [1, 2]. Consequently, the assessment and timely correction of central hemodynamic parameters in the setting of hemorrhage are of critical importance in clinical practice [3].

However, it is the disruption of microcirculatory perfusion and tissue oxygenation that serves as a key mechanism underlying organ dysfunction in hemorrhagic and other forms of shock [4, 5]. Despite certain common features across organs, such as reduced perfused capillary density, heterogeneous microvascular flow, slowed capillary transit, increased blood viscosity, and increased endothelial permeability, microcirculatory disturbances exhibit organ-specific characteristics. These are largely determined by the variable intensity of vascular responses in different tissue beds triggered by hemorrhage and its associated pathophysiological processes [6].

During early blood loss, perfusion of vital organs such as the brain and heart may be temporarily preserved due to effective autoregulation and redistribution of blood flow (circulatory centralization). In contrast, perfusion of non-vital organs, including the skin, skeletal muscles, and abdominal viscera, is markedly reduced [5, 7]. However, as bleeding continues and shock progresses, these compensatory mechanisms are exhausted, leading to circulatory decompensation, global hypoperfusion, and hypoxic injury to even the most critical organs [6, 8, 9]. In cerebral circulatory decompensation during shock, not only the extent and rate of blood loss, but also systemic factors such as the patient's overall physiological condition, intracranial pressure, arterial blood gas composition, and the balance of the autonomic nervous system (between sympathetic and parasympathetic activity) play important pathophysiological roles [10].

Microcirculatory disturbances in internal organs play a central pathophysiological role in determining both the severity and prognosis of hemorrhage. However, most vital organs-such as the heart, brain, and lungs-are not readily accessible for direct visualization, creating methodological challenges in both experimental research and clinical evaluation of organ perfusion in shock and related conditions [4].

Experimental models of hemorrhage and hemorrhagic shock allow direct assessment of perfusion in internal organs through surgical access [11, 12]. On the other hand, superficial tissues such as skin and mucous membranes are readily accessible for non-invasive assessment of microcirculation and are often used as surrogate markers in studies of cardiovascular, endocrine and inflammatory disorders [13, 14].

Despite their relatively high tolerance to hypoxia, these tissues — as well as skeletal muscle and abdominal organs — often exhibit more pronounced microcirculatory impairment during hemorrhage and shock compared to the brain and myocardium [5].

In this context, the investigation of the relationship between cutaneous microcirculation and central and regional hemodynamic parameters is of great scientific and clinical importance. A key point of debate remains whether abnormalities in cutaneous blood flow detected by non-invasive methods accurately reflect disturbances in central or peripheral perfusion of internal organs [15–17]. This question is particularly critical in the context of critical care, where timely identification of circulatory compromise and organ dysfunction directly determines the scope and direction of intensive therapy [3, 18].

Experimental studies using laser Doppler flowmetry (LDF) have shown that the amplitude of microvascular flow oscillations (flowmotion) increases significantly in the early post-hemorrhagic period in both brain and skin, despite differences in the degree of hypoperfusion between these tissues [2]. Notably, even after reperfusion and apparent normalization of central hemodynamic parameters, microcirculatory function and cellular metabolism may remain impaired [19, 20].

In addition, several studies have highlighted the diagnostic and prognostic value of microcirculatory parameters in critical illness. The severity of microcirculatory dysfunction observed in experimental models or in patients with trauma and hemorrhagic shock has been shown to correlate with the extent of organ dysfunction and to be associated with adverse clinical outcomes [19, 21].

A variety of techniques have been developed to directly assess tissue perfusion and visualize the microvascular network. Among these, advanced *in vivo* microscopy, LDF and laser speckle contrast imaging (LSCI) are particularly noteworthy [13, 22]. LSCI is considered one of the most promising non-invasive modalities for clinical perfusion assessment, as it significantly reduces spatial heterogeneity in perfusion measurements. This method is increasingly being used to evaluate the cerebral microcirculation, both in animal models and in neurosurgical practice [23–25].

A critical ongoing challenge is the identification and validation of simple, clinically accessible diagnostic markers of impaired organ perfusion in shock. While LSCI has been used to detect microcirculatory

abnormalities in the skin of patients with cardiovascular, rheumatologic, endocrine, and dermatologic disorders [13], its use in clinical shock research remains limited. Only a handful of studies have used modern microcirculatory assessment techniques to investigate the relationship between cutaneous microcirculation and central hemodynamics or cerebral perfusion in hemorrhagic shock [16, 26], and the results have often been inconsistent.

The aim of the study was to evaluate the relationship between cutaneous microcirculatory parameters and central and cerebral hemodynamic parameters during progressive blood loss.

Material and Methods

This was a randomized, prospective, controlled, experimental study conducted in vivo in laboratory animals. Measures to reduce systematic bias included random assignment of animals to study groups to ensure comparability by body weight, and random sequencing of skin and cerebral blood flow measurements at each time point.

The study was conducted in accordance with national and international bioethical standards, including Directive 2010/63/EU. The experimental protocol was approved by the local ethics committee of the Federal Research and Clinical Center of Intensive Care Medicine and Rehabilitology (Protocol No. 1/24/2, dated April 24, 2024).

The study was conducted on male Wistar rats, aged 3–4 months, weighing 250–350 g. The initial sample size was *N*=30. The animals were randomly assigned to two groups:

- Group 1 (*N*=18): stepwise induction of blood loss leading to the development of hemorrhagic shock (HS group)
- Group 2 (*N*=12): sham-operated control group without blood loss (SO group).

A combined anesthetic protocol was used: tiletamine/zolazepam (Zoletil 100, Virbac, France) at 20 mg/kg and xylazine (Xylanit, NITA-FARM, Russia) at 5 mg/kg, both administered intraperitoneally. If a pain response indicated insufficient depth of anesthesia, an additional dose of Zoletil 100 (10 mg/kg, intraperitoneally) was administered.

For invasive arterial pressure monitoring and arterial blood sampling, the left femoral artery was catheterized with a polyethylene catheter (PE-50, OD 0.95 mm, ID 0.58 mm; SciCat, Russia). For local anesthesia of soft tissues and vessel walls, 1% lidocaine (not more than 0.4 mL per rat) was used. After catheter placement, the surgical wound was closed with temporary sutures. If necessary, the catheter was flushed with unfractionated heparin solution (5 IU/mL) in volumes of 0.1–0.2 mL.

Prior to craniotomy, the anesthetized and catheterized rat was positioned prone in a stereotaxic frame mounted on a temperature-controlled platform. The head was immobilized at three points - via the maxillary incisors and external auditory canals — using a stereotaxic device. Core body temperature was continuously monitored with a rectal probe, with target values maintained between 36.5 and 37.0°C. Animals breathed spontaneously throughout the procedure.

Craniotomy was performed in the left parietal region (corresponding to the vascular territory of the left middle cerebral artery and the sensorimotor cortex of the rat) according to a previously described protocol [27]. The coordinates for the center of the craniotomy were 4 mm caudal to bregma and 2.5 mm lateral to the midline suture. The diameter of the craniotomy was 2.5–3 mm. The dura mater and the inner bone layer (devoid of surface vessels) were left intact to maintain intracranial pressure and avoid injury to the pial vessels. A stabilization period of at least 15 minutes was allowed after craniotomy before measurements were started.

A fixed-volume hemorrhage model was used, with total blood loss set at 35% of the estimated circulating blood volume (CBV), corresponding to a class III hemorrhage (out of four) according to the ATLS classification [28]. The CBV (in mL) was calculated as 6.5% of the animal's body weight. Blood was collected using a sterile syringe in three consecutive draws (15% — 10% — 10% of total CBV), each lasting 2 min, with 8 min intervals between draws. The total bleeding time was 20–22 minutes. Reinfusion of blood was not performed. Animals were monitored for an additional 30 minutes after hemorrhage.

Electrocardiography (ECG) was recorded using needle electrodes integrated into the MouseMonitor S platform (INDUS Instruments, USA). The analog signal was transmitted to a PowerLab 16/35 data acquisition system (ADInstruments, Australia). Digitized ECG signals from three standard leads (I, II, III) were then analyzed using LabChart Pro 8 software (ADInstruments, Australia). Heart rate (HR) was calculated as the average beats per minute over a 5-minute recording period.

Arterial blood pressure (BP) was measured by connecting the femoral artery catheter to a Deltran DPT-100 pressure transducer (Utah Medical Products, USA) via a three-way stopcock and infusion line. The analog pressure signal was transmitted through the BP-100 amplifier (CWE Inc., USA) to the PowerLab 16/35 system. The digitized BP waveform was analyzed using LabChart Pro 8 software to determine mean arterial pressure (MAP) over the 5-minute measurement period.

For assessment of blood gas parameters and acid-base status, arterial blood samples (0.2 mL) were collected through the femoral catheter into 1.0 mL insulin syringes preflushed with a small volume of heparin. Blood gas analysis — including pH, pCO_2, pO_2, base excess (BE), bicarbonate (HCO_3^-),

arterial oxygen saturation (SaO_2), and lactate concentration — was performed using CG4+ reagent cartridges with the i-STAT 1 handheld analyzer (Abbott Point of Care Inc., USA).

Cerebral cortical and limb skin perfusion in rats was assessed using laser speckle contrast imaging (LSCI) with a custom-built setup. The measurement principle and technical specifications of this method have been described previously [27]. Speckle images were acquired from the left parietal region of the skull and the plantar surface of the right hind limb. The acquisition time for each anatomical region was 5 minutes (including a 2.5-minute acquisition between the first and second blood draws).

Monochromatic images were acquired and subsequently processed by pixel-wise calculation of spatiotemporal speckle contrast values over the entire field of view. The images were then color-coded using pseudocolor mapping according to the calculated LSCI perfusion values (defined as $1/K^2$), resulting in laser speckle perfusion maps (see Fig. 1). The derived signal was analyzed to quantify LSCI perfusion in skin ($LSCI_{skin}$) and brain cortex ($LSCI_{brain}$), expressed in arbitrary perfusion units (AU). The anatomical locations used for perfusion measurements are shown in Fig. 1.

Due to the limited field of view of the LSCI setup, sequential imaging of skin and cerebral perfusion was performed at each of the three experimental time points. To minimize systematic measurement bias, the order of imaging (skin followed by brain or vice versa) was randomized for each animal in both groups.

In addition to the mean LSCI perfusion values obtained at each stage of the experiment, cutaneous vascular conductance (CVC_{skin}) was calculated as $LSCI_{skin}$ divided by mean arterial pressure (CVC_{skin} = $LSCI_{skin}$ / MAP, AU/mmHg). This index allows standardization of perfusion relative to systemic blood pressure and serves as an indirect measure of vascular tone [13]. Similarly, cerebral vascular conductance (CVC_{brain} = $LSCI_{brain}$ / MAP) was calculated.

At the end of the experiment, a functional occlusion test was performed on the hind limb of the rat to assess post-occlusive reactive hyperemia (PORH). A pneumatic cuff from the non-invasive blood pressure monitoring system «Systola» (Neurobotics, Russia) was placed around the mid-calf level of the right hind limb and connected to an aneroid manometer. LSCI perfusion was recorded for 30 seconds at baseline (resting state). The cuff was then inflated to 200–220 mmHg and maintained at this pressure for an additional 30 seconds. After rapid cuff deflation, LSCI recording continued for an additional 60 seconds.

PORH parameters were assessed in the same skin area (plantar surface of the limb) used for the previous perfusion measurements. The following PORH variables were calculated:

- LSCI perfusion at rest with cuff in place ($LSCI_{rest}$, AU)

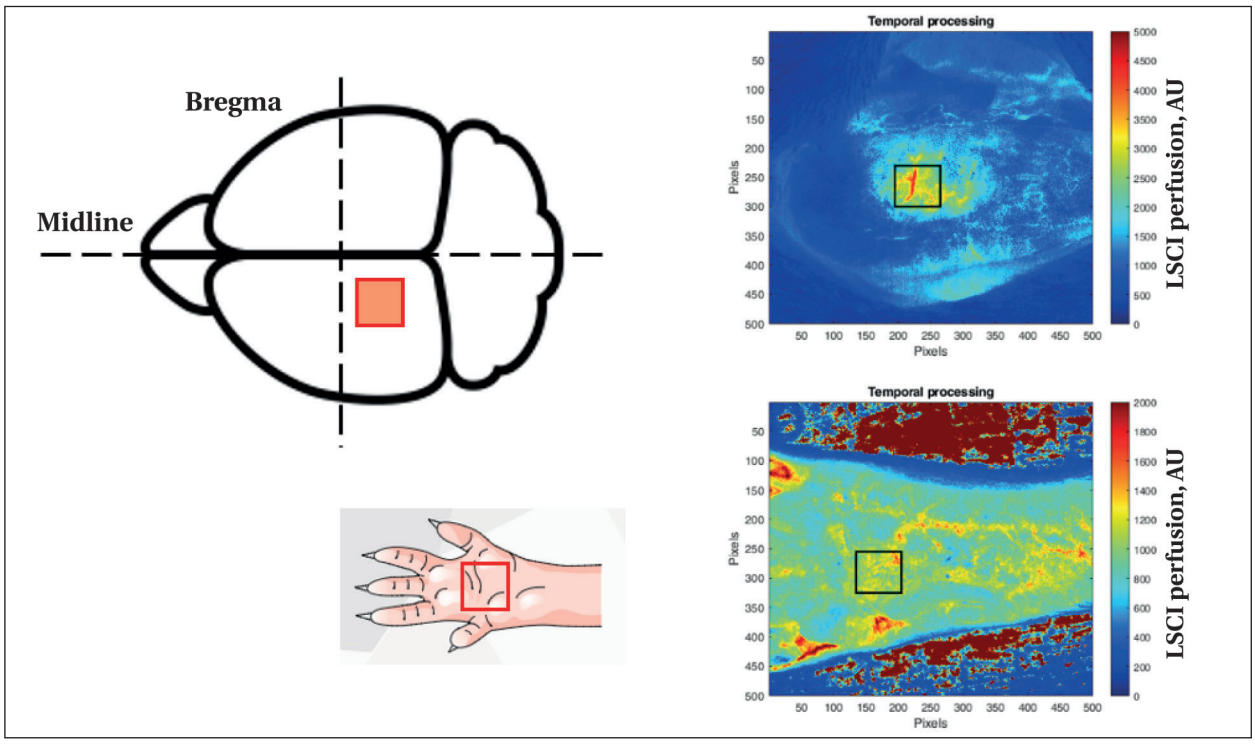

Fig. 1. Anatomical regions of the rat body where microcirculation was assessed using laser speckle contrast imaging (LSCI).
Note: Red squares indicate regions of the organ surface where perfusion was measured. To the right are examples of perfusion mapping in the cerebral cortex and skin of the hind limb.

• minimum LSCI values during occlusion, representing the biological zero ($LSCI_{occl}$, AU)

• peak reactive hyperemia, i.e. the maximum LSCI perfusion after cuff release ($LSCI_{max}$, AU)

• microvascular flow reserve, calculated as $LSCI_{max}$/ $LSCI_{rest}$

• peak cutaneous vascular conductance, calculated as $CVC_{max} = LSCI_{max}/MAP$ (AU/mmHg).

At the end of the procedure, animals were euthanized under general anesthesia (Zoletil 100 + xylazine) by intra-arterial injection of 2.0 mL 2% lidocaine. Death was confirmed by electrocardiographic criteria.

The main time points of the experiment at which physiological and laboratory parameters were recorded included:

1. Baseline — after induction of anesthesia, femoral artery catheterization, craniotomy, and a stabilization period.

2. Blood loss 15% of circulating blood volume (CBV) — measurements of the same physiologic parameters as at baseline (except arterial blood gas and acid-base balance) were performed during the interval between the first and second blood draws.

3. Blood loss 35% of CBV — the same physiological and laboratory parameters as at baseline were recorded 20 to 30 minutes after the end of the bleeding.

Measurements of central, cerebral, and cutaneous hemodynamics — including MAP, HR, and LSCI perfusion of the sensorimotor cortex and hind limb skin — were performed at all time points. Arterial blood gas (ABG) and acid-base balance (ABB) parameters and ECG recordings were obtained only at time points 1 (baseline) and 3 (blood loss 35%) (see Fig. 2).

The occlusion test on the rat hind limb was performed once at the end of the experiment, at the third time point, after LSCI measurements of cerebral and cutaneous perfusion had been completed.

In the sham-operated control group (SO), no blood loss was induced; however, all measurements were performed at the same time intervals as in the bleeding group.

The required sample size was estimated using StatMate 2.0 software (GraphPad Software, USA) based on data from a preliminary series of experiments. The calculation was performed taking into account the variability of the cerebral cortex speckle perfusion index (SD = 287 AU), an expected mortality rate of approximately 30% in the HS group, and a desired statistical power greater than 0.9.

Statistical analysis of the data obtained was performed using Statistica 13.0 software (StatSoft, USA). Because most variables did not follow a normal distribution (as assessed by the Shapiro–Wilk test), intergroup differences were analyzed using the Mann–Whitney *U* test. Within-group changes were assessed using the Friedman test, followed by pairwise comparisons using the Wilcoxon signed-rank test with Bonferroni correction.

Results are expressed as median and interquartile range *Me* ([25%; 75%]). Correlations between parameters were assessed using Spearman's rank

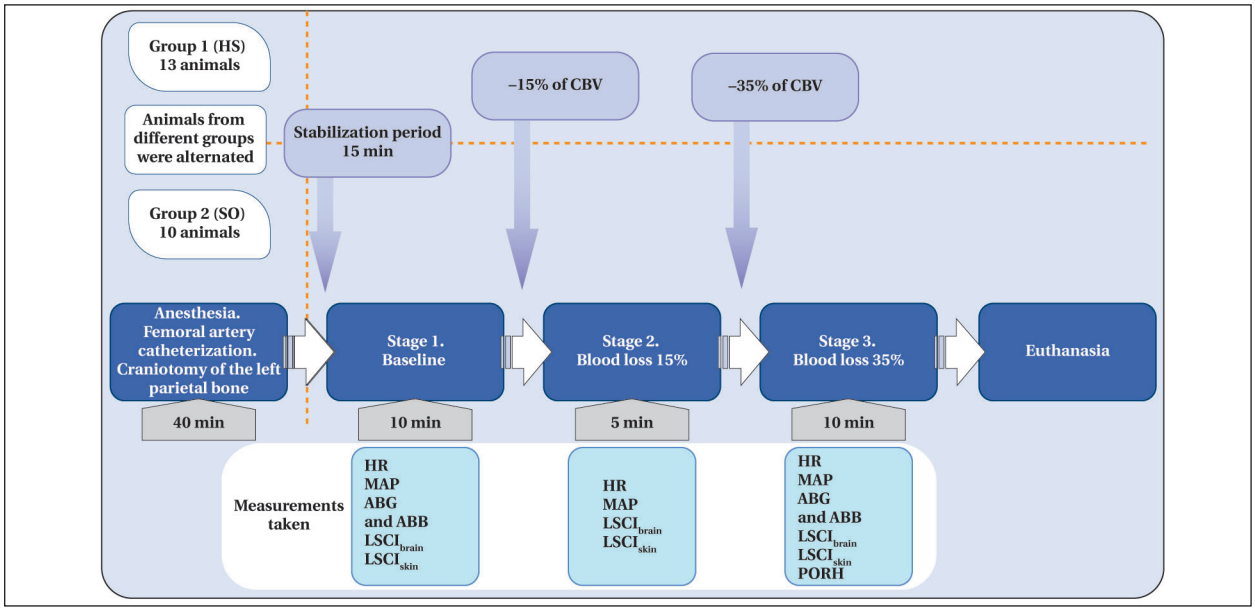

Fig. 2. Schematic representation of the experimental design

Note. During the experiments, 2 animals from the SO group and 5 animals from the HS group were excluded from the study according to predefined exclusion criteria (severe surgical complications, multiple significant protocol deviations). No deaths occurred in either group. Thus, 23 animals were included in the final analysis (SO, *N*=10; HS, *N*=13).

CBV — estimated circulating blood volume; HR — heart rate; MAP — mean arterial pressure; ABG — acid-base status; $LSCI_{brain}$ and $LSCI_{skin}$ — cerebral cortex and skin perfusion, respectively, measured by LSCI; PORH — post-occlusive reactive hyperemia.

correlation coefficient (R). A two-tailed $P<0.05$ was considered statistically significant.

Results

Postmortem examination of the animals' skulls (after euthanasia) revealed that the cranial window area was maximally thinned (⩽0.3 mm) but not perforated. None of the animals included in the analysis showed evidence of intracranial hemorrhage or other evidence of brain injury.

There were no significant differences in central and peripheral hemodynamic parameters between groups at baseline (Stage 1) ($P>0.05$, Mann–Whitney U test, Table 1). However, the total dose of anesthetic tiletamine/zolazepam was lower in the HS group compared to the SO group (40 [30; 40] vs. 53 [50; 55] mg/kg; $P=0.01$), as animals in the HS group required a lower maintenance dose after blood loss to achieve the same depth of anesthesia.

After 15% blood volume loss (stage 2), MAP in the HS group decreased by 26% from baseline and was significantly lower than in the SO group (Fig. 3, *a*). HR decreased by 16% in the HS group compared to baseline, but the difference between the groups for this parameter did not reach statistical significance (HS vs. SO, $P=0.057$) (Fig. 3, *b*).

The $LSCI_{skin}$ index in the HS group decreased by 26% compared to baseline in the same group as well as compared to the SO group (Fig. 4, *a*). $LSCI_{brain}$ in the HS group did not change significantly from stage 1 ($P=0.345$), but was 9% lower than in the SO group, where cerebral perfusion increased slightly (by 7%) relative to baseline in this group ($P=0.017$) (Fig. 4, *b*). In this context, cutaneous vascular conductance (CVC_{skin}) did not differ between the HS and SO groups ($P=0.702$) and remained unchanged from baseline in both groups (Fig. 4, *c*). Meanwhile, cerebral vascular conductance (CVC_{brain}) increased by 43% from baseline in the HS group ($P=0.002$) and was significantly higher than in the SO group (Fig. 4, *d*).

After 35% blood volume loss (stage 3), MAP in the HS group decreased by 32% from baseline and was significantly lower than in the SO group (Fig. 3, *a*). The HR at this stage was not significantly different

Table 1. Central and peripheral hemodynamic parameters in the study groups at Stage 1 (baseline).

Parameter	Values in groups		*P* value
	Group HS	Group SO	
MAP, mmHg	90 [79; 98]	94 [87; 95]	0.651
HR, bpm^{-1}	308 [289; 312]	303 [293; 325]	0.975
$LSCI_{skin}$, AU	1858 [1458; 2419]	1799 [1675; 1953]	0.976
$LSCI_{brain}$, AU	3407 [3066; 3618]	3657 [3291; 3878]	0.166
CVC_{skin}, AU/mmHg	20.3 [14.8; 25.9]	19.6 [18.3; 23.6]	0.917
CVC_{brain}, AU/mmHg	37.0 [29.6; 44.3]	41.3 [36.8; 41.4]	0.508

Note. MAP — mean arterial pressure; HR — heart rate; $LSCI_{skin}$ — laser speckle contrast imaging (LSCI)–derived skin perfusion; $LSCI_{brain}$ — LSCI-derived cerebral perfusion; CVC_{skin} — cutaneous vascular conductance; CVC_{brain} — cerebral vascular conductance. *P-values* represent between-group comparisons (Mann–Whitney U test).

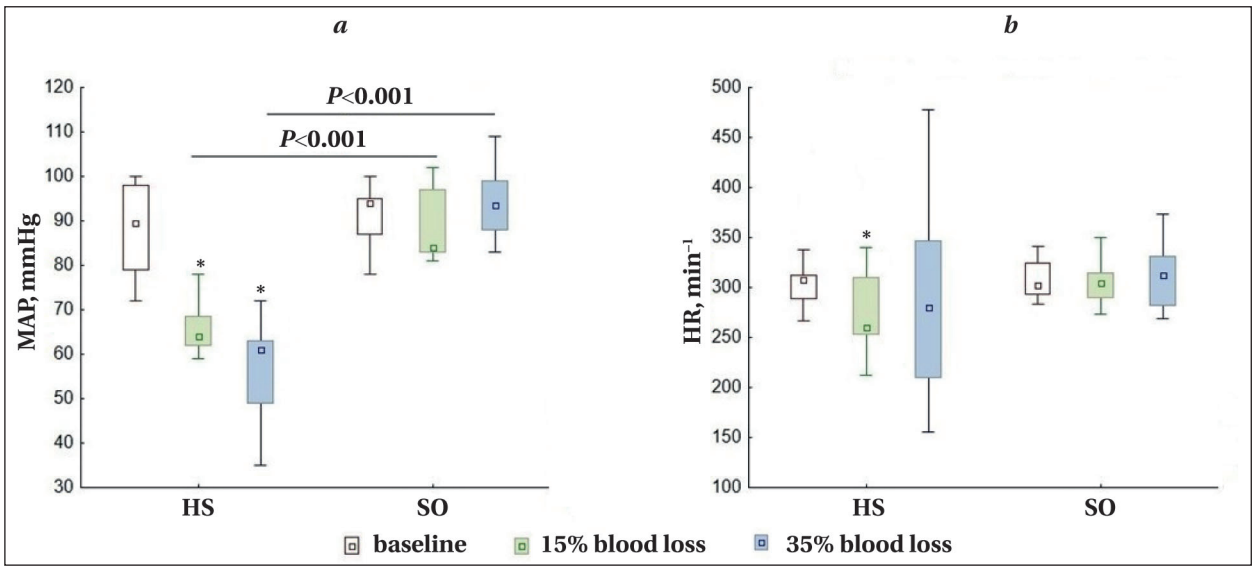

Fig. 3. Key parameters of central hemodynamics in rats at different experimental stages.
Note. *P* values indicate comparisons between groups (HS vs. SO) using the Mann–Whitney U test. * — $P<0.05$ vs. baseline (Wilcoxon test with Bonferroni correction).

from baseline (P=0.046 with Bonferroni correction) or from the SO group (P=0.257), although greater variability in HR values was noted within the HS group (Fig. 3, *b*).

Cutaneous perfusion ($LSCI_{skin}$) in the HS group decreased by 43% compared to both baseline (P=0.001) and SO (Fig. 4, *a*). The reduction in cerebral perfusion ($LSCI_{brain}$) in the HS group compared to stage 1 did not reach the significance level (P=0.116), but was 23% lower than in the SO group (Fig. 4, *b*). CVC_{skin} in the HS group after 35% blood loss did not change significantly from baseline and, as with moderate blood loss, did not differ between the HS and SO groups (P=0.257) (Fig. 4, *c*). In contrast, CVC_{brain} remained elevated by 37% from baseline (P=0.006) and was significantly higher than in the SO group (Fig. 4, *d*).

Characteristic speckle perfusion images of the skin and cerebral cortex obtained during the experiment are shown in Fig. 5.

The results of ABG and ABB measurements in laboratory animals are presented in Table 2.

At baseline, the groups differed only slightly in PaO_2 levels. Thirty minutes after blood loss, animals in the HS group showed changes in arterial blood gas and acid-base status typical of hemorrhagic shock: metabolic lactic acidosis (elevated blood lactate, decreased HCO_3 and BE levels, and decreased blood pH in some animals) with partial respiratory compensation (a trend toward hypocapnia in the

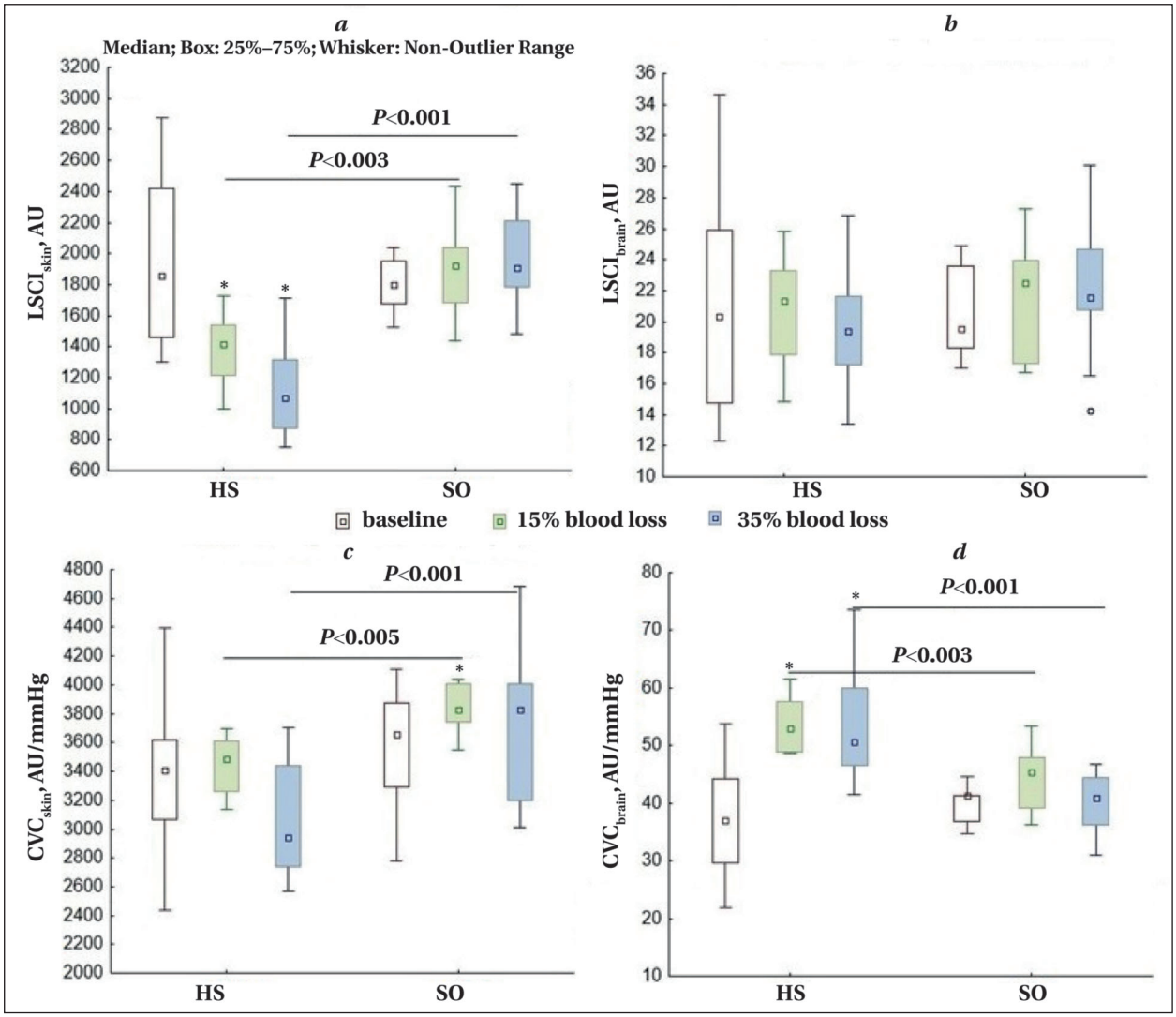

Fig. 4. Key parameters of skin and brain blood flow in rats at different experimental stages.
Note. The figure shows the changes in LSCI-derived skin perfusion (*a*), LSCI-derived brain perfusion (*b*), cutaneous vascular conductance (*c*), and cerebral vascular conductance (*d*) at baseline, after acute blood loss of 15% of the estimated CBV, and 30 min after acute blood loss of 35% CBV. *P* values indicate comparisons between groups (HS vs. SO) using the Mann–Whitney *U* test. * — P<0.05 vs. baseline (Wilcoxon test with Bonferroni correction).

HS group). Arterial blood oxygenation (PaO_2) increased significantly in the HS group at stage 3 compared with stage 1 (P=0.005, Wilcoxon test); however, no between-group differences in PaO_2 or SaO_2 were observed at stage 3 (Table 2).

At the end of stage 3, animals in both groups underwent the PORH test on the hind limb skin after a 30-second occlusion. The results of the occlusion test are shown in Fig. 6.

Correlation analysis was performed to identify biologically significant relationships between skin microcirculation parameters and central and cerebral circulation parameters. Since the groups of animals did not differ in the parameters studied at stage 1 (baseline), the correlation analysis at this stage was performed for the entire sample (N=23). Statistically significant correlations are shown in Fig. 7.

A separate correlation analysis was then performed in the HS group to identify biologically significant associations between skin microcirculation parameters (including PORH parameters) and central and cerebral circulation parameters at stage 3, when the animals developed hemorrhagic shock (Fig. 8).

Discussion

In this study, we investigated the relationship between changes in skin blood flow and cerebral and central circulation during moderate (15% of CBV) and severe (35% of CBV) acute blood loss. As the volume of blood loss increased, animals in the

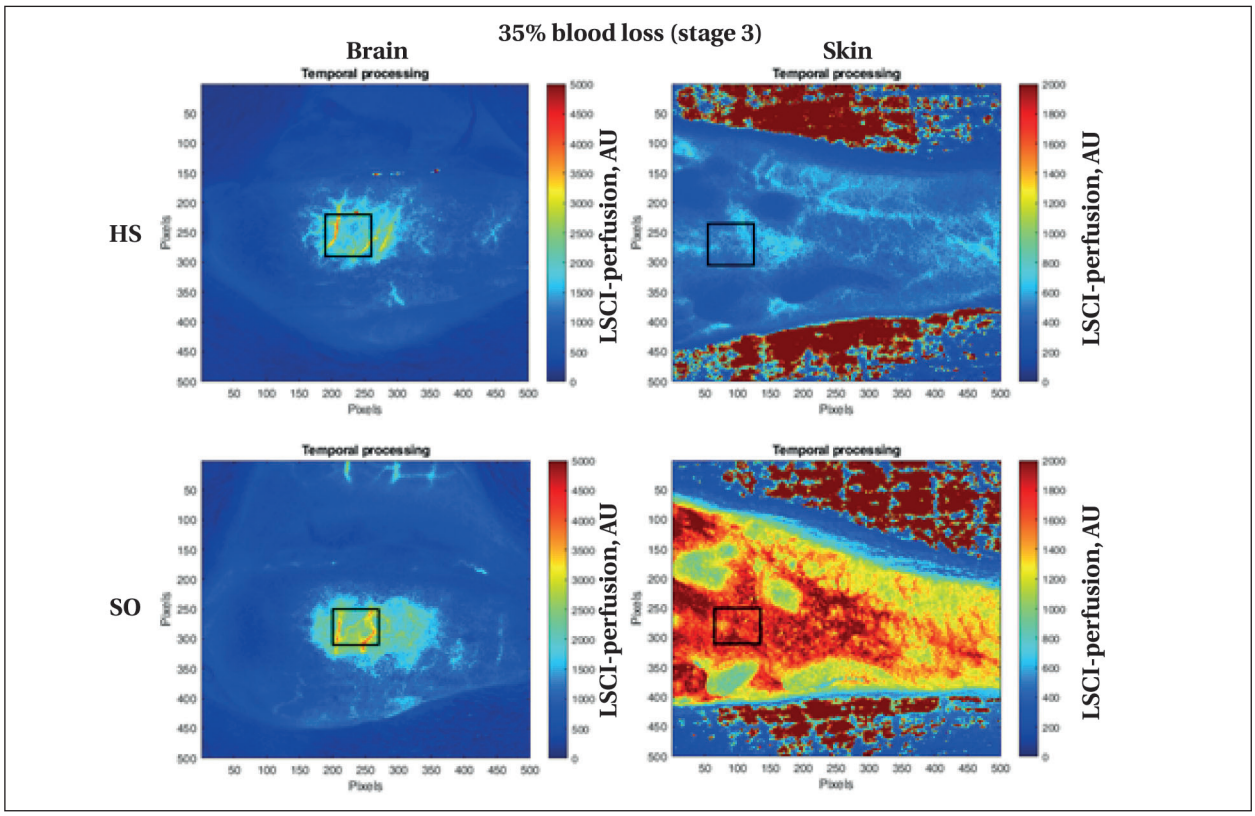

Fig. 5. Examples of speckle perfusion images of the brain and hind limb skin of a rat with 35% blood loss (HS group, top) and a control animal (SO group, bottom) without blood loss.

Table 2. Blood gas composition and acid-base status (ABG) of arterial blood in rats at baseline (Stage 1) and 30 minutes after acute blood loss of 35% blood volume (Stage 3).

Parameter	Values in groups at different stages					
	Stage 1 (baseline)			Stage 3 (blood loss of 35% CBV)		
	HS	SO	*P* value	HS	SO	*P* value
pH	7.40 [7.38; 7.45]	7.41 [7.41; 7.44]	0.257	7.38 [7.33; 7.40]	7.41 [7.39; 7.41]	0.131
$PaCO_2$, mmHg	36.3 [32.2; 38.3]	31.6 [28.6; 36.6]	0.208	27 [23.3; 30.1]	31.95 [29.2; 36.2]	**0.021**
PaO_2, mmHg	75 [70; 80]	83.5 [78; 85]	**0.042**	88 [86; 90]	79 [77; 83]	0.057
BE, mmol/L	–2 [–4; 0]	–2.5 [–4; –1]	0.648	–9 [–11; –6]	–3.5 [–6; –3]	**0.006**
HCO_3^-, mmol/L	21.8 [20.1; 23.0]	20.75 [19.7; 23.0]	0.522	15.1 [12.8; 18.8]	20.4 [18.1; 21.8]	**0.008**
SaO_2, %	95 [93; 96]	96.5 [96; 97]	0.67	97 [96; 97]	96 [95; 96]	0.148
Lactate, mmol/L	1.92 [1.20; 2.25]	1.37 [1.21; 1.73]	0.410	3.18 [2.01; 4.49]	1.76 [1.65; 2.18]	**0.008**

Note. Values with P<0.05 for comparisons between HS and SO groups (Mann–Whitney test) are highlighted in bold.

HS group consistently developed arterial hypotension. At the same time, heart rate variability increased in this group, with a tendency toward moderate bradycardia at stage 2. Tachycardia is known to be a normal compensatory response of the body to hemorrhage [5, 6]. The tendency towards bradycardia observed in this series of experiments can be explained by specific features of the hemorrhagic shock model: the use of combined anesthesia and rapid (within 2–3 minutes) blood removal at each stage of the study, i. e. a high bleeding rate. Both factors lead to a relative predominance of parasympathetic over sympathetic cardiac innervation, which delays the development of tachycardia during bleeding [29].

When measuring LSCI perfusion in the skin of the limb and the sensorimotor cortex of the brain during the post-hemorrhagic period, a consistent pattern was observed: a progressive decrease in skin perfusion with relative preservation of the cerebral microcirculation [7, 12]. To gain additional insight into the mechanisms underlying the reduction (or preservation) of tissue perfusion during blood loss, parameters of cutaneous and cerebral vascular conductance (CVC_{skin} and CVC_{brain}) were calculated. CVC, determined as the ratio of LSCI perfusion to MAP, reflects microvascular tone at the site of measurement and is often used in clinical studies to standardize assessment of skin perfusion under normal and pathological conditions [30]. Analysis of this parameter has shown that maintenance of cerebral microcirculation during blood loss occurs via an increase in cerebral CVC, representing a compensatory response to reduced cerebral perfusion pressure [10]. However, to our knowledge, no studies have used CVC parameters derived specifically from LSCI perfusion values to assess cerebral autoregulation during progressive hemorrhage.

During blood loss, cutaneous vascular conductance did not change significantly despite progressive skin hypoperfusion and other signs of evolving hemorrhagic shock (hypotension, metabolic lactic acidosis). This finding somewhat contradicts the widely accepted concept of «centralization of the circulation» during hypovolemia, which occurs due to activation of the sympathetic nervous system and increased vascular tone in the skin, skeletal muscles, and abdominal organs [3, 6]. However, important factors that also determine the response of the peripheral circulation to blood loss include anesthesia and the core body temperature [4]. The use of combined general anesthesia and maintenance of normal core body temperature during the experiments (to standardize the model) likely explains the absence of a vasoconstrictor response in the skin during bleeding. In addition, as with the observed relative bradycardia, the lack of peripheral vasoconstriction in response to severe blood loss (>30% of estimated blood volume) may be due to phase-dependent inhibition of sympathetic vascular control and impaired baroreflex-mediated blood pressure regulation [31]. This is supported by the shift in

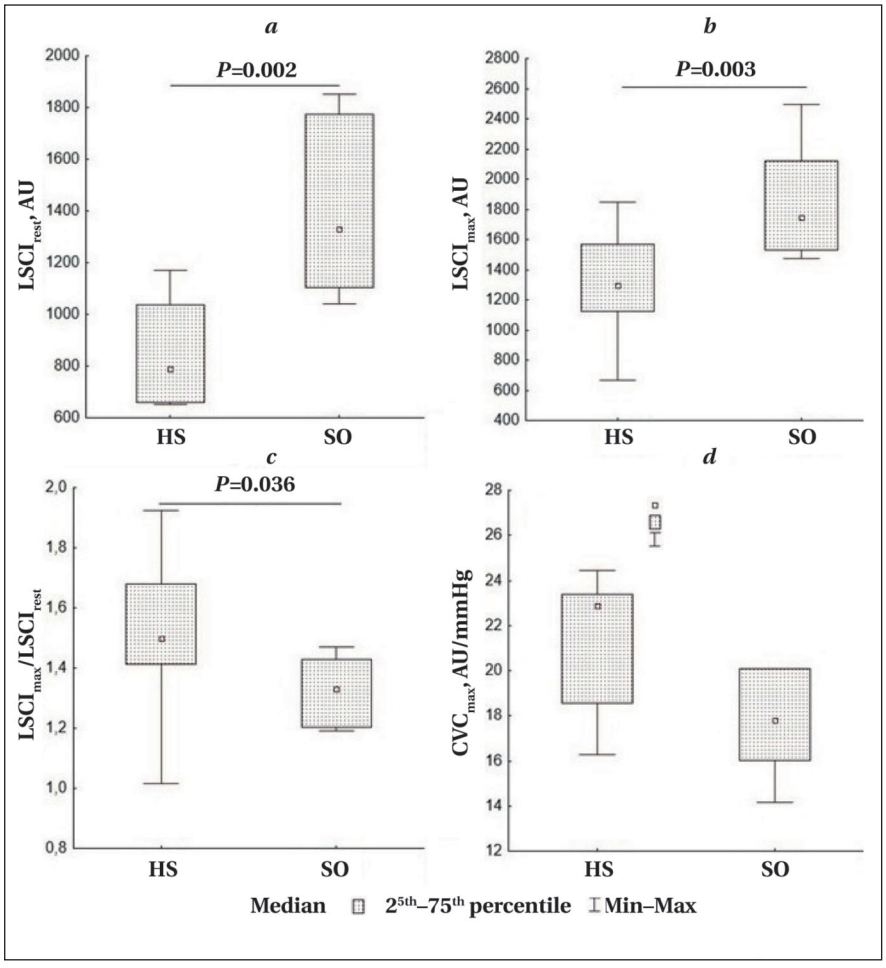

Fig. 6. Parameters of post-occlusive reactive hyperemia (PORH) in the skin of the hind limb of rats after acute blood loss of 35% of the total blood volume (stage 3).
Note. (*a*) Skin perfusion index ($LSCI_{rest}$) of the rat skin at rest with the cuff applied to the limb; (*b*) maximum skin perfusion index after cuff deflation ($LSCI_{max}$); AU — arbitrary units of perfusion; (*c*) skin microvascular blood flow reserve ($LSCI_{max}/LSCI_{rest}$); (*d*) cutaneous vascular conductance for maximum LSCI perfusion values (CVC_{max}).

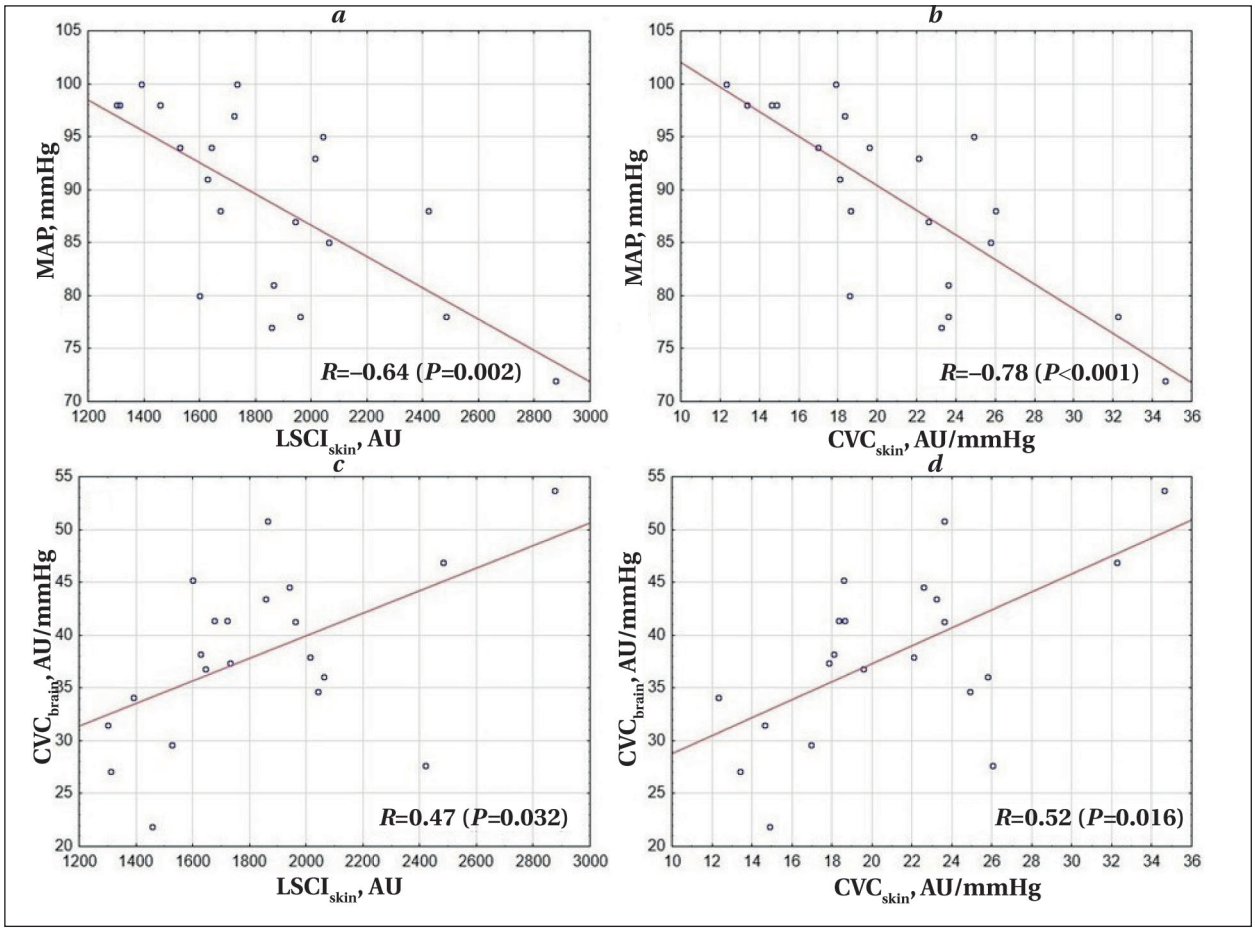

Fig. 7. Scatter plots showing the correlation between cutaneous circulation parameters and central and cerebral circulation parameters in rats (*N*=22) at stage 1 (before blood loss).
Note. MAP — mean arterial pressure, mm Hg; $LSCI_{skin}$ — LSCI perfusion of rat hind limb skin, AU; CVC_{skin} — cutaneous vascular conductance, AU/mm Hg; CVC_{brain} — cerebral vascular conductance, AU/mm Hg. Spearman's rank correlation coefficient (*R*) and corresponding *P* value are shown for each graph. One animal in the SH group was excluded from the analysis due to MAP measurement artifacts.

the correlation between $LSCI_{skin}$ and MAP from a moderately negative value (*R*=–0.64) at stage 1 to a strongly positive value (*R*=0.78) at stage 3. A strong correlation between CVC_{skin} and MAP (*R*=–0.78), present at stage 1, disappeared after the development of hemorrhagic shock.

Correlation analysis also revealed additional biologically and potentially clinically relevant associations between cutaneous and cerebral circulation parameters. At stage 1, a moderate positive correlation (*R*=0.52) was observed between CVC_{skin} and CVC_{brain}. At stage 3, in animals in hemorrhagic shock, cerebral perfusion was partially determined by the extent of skin perfusion reduction (*R*=0.57) — the greater the reduction in skin perfusion, the lower the cerebral blood flow. These findings highlight the potential diagnostic value of skin microcirculation parameters in assessing the severity of conditions such as intraoperative blood loss, particularly when patients are under general anesthesia and spontaneous hypothermia is intentionally prevented.

In this study, an occlusion test followed by analysis of PORH parameters was additionally used to assess skin microcirculation. Under conditions of hemorrhagic shock and pre-existing cutaneous hypoperfusion, a reduction in peak reactive hyperemia and a slight increase in microvascular flow reserve were observed. These findings are consistent with those of a previous experimental study [32] in which PORH was evaluated in rat skin during blood loss using LDF with an occlusion duration of 3 minutes (compared to 30 seconds in our study). They are also consistent with clinical observations showing a marked reduction in PORH in patients with severe blood loss as measured by infrared thermography of the fingers [16].

However, study [32] also reported an increase in peak vascular conductance (CVC_{max}) during the occlusion test in the setting of hemorrhagic shock. In contrast, in our study, the increase in this PORH parameter compared to the control group did not reach statistical significance.

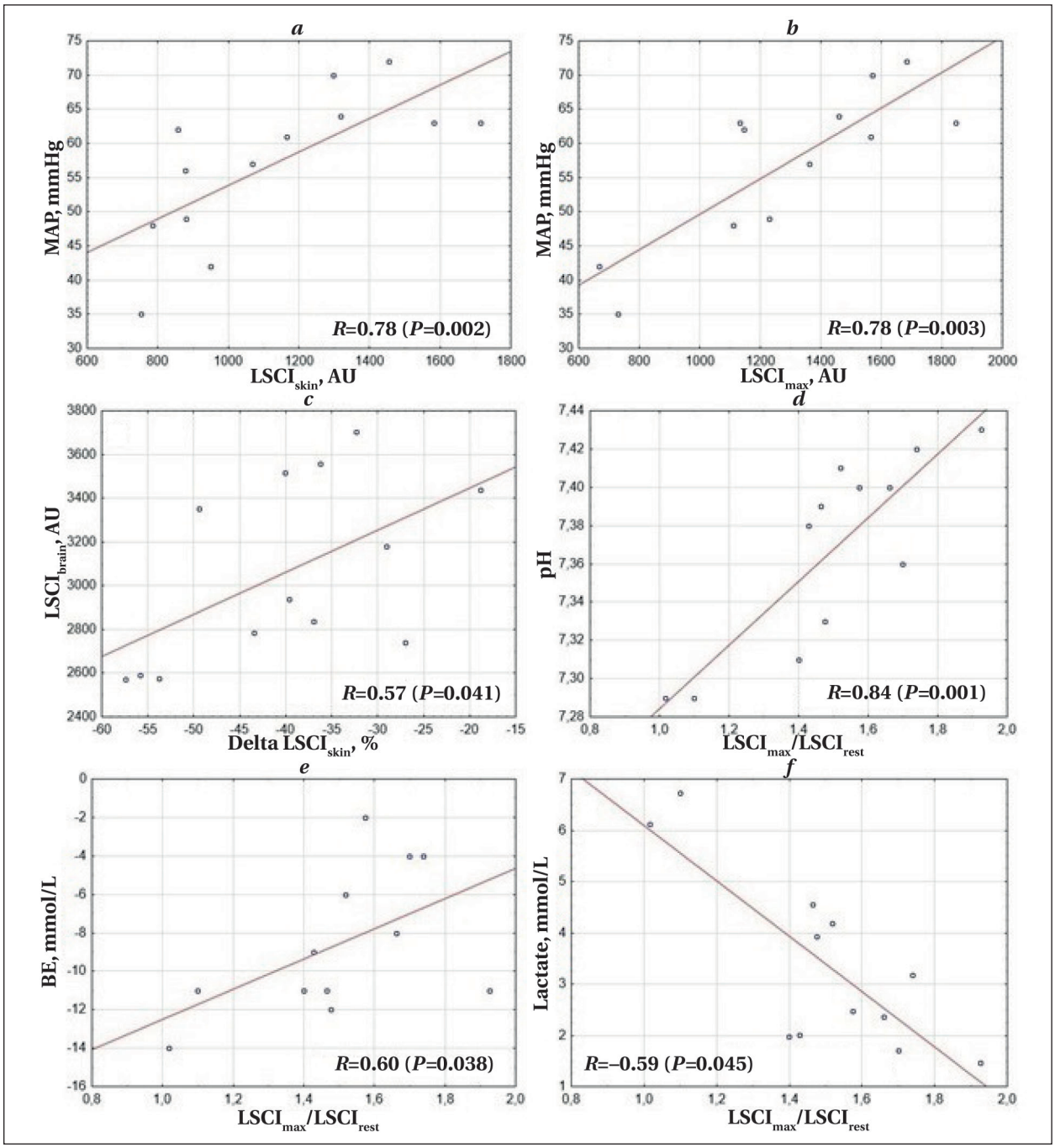

Fig. 8. Scatter plots illustrating the correlation between cutaneous microcirculation parameters and central and cerebral circulation parameters in HS group rats (*N*=12) at stage 3 (after 35% total blood volume loss).
Note. MAP — mean arterial pressure; $LSCI_{skin}$ — LSCI perfusion of rat hind limb skin, AU; $LSCI_{brain}$ — LSCI perfusion of rat cerebral cortex, AU; Delta $LSCI_{skin}$ — relative decrease in LSCI skin perfusion of rat hind limb after 35% blood loss, expressed as a percentage of baseline; $LSCI_{max}$ — maximum LSCI skin perfusion of the rat hind limb after cuff release during the occlusion test, AU; $LSCI_{max}/LSCI_{rest}$ — skin microvascular flow reserve, calculated as the ratio of $LSCI_{max}$ to baseline skin perfusion before vascular occlusion ($LSCI_{rest}$); BE and Lactate — base excess and blood lactate level in arterial blood, mmol/L, respectively. Spearman's rank correlation coefficient (*R*) and corresponding *P* values are shown for each graph. One animal in the HS group was excluded from the analysis due to artifacts in the MAP measurement.

Interestingly, correlation analysis revealed a positive association between cutaneous microvascular flow reserve (expressed as $LSCI_{max}/LSCI_{rest}$ ratio) and both arterial blood pH (*R*=0.84) and base excess (*R*=0.60), and a negative association with blood lactate level (*R*=–0.59). These associations were observed only during the development of hemorrhagic shock. Thus, low values of microvascular

flow reserve during blood loss may indicate the onset of decompensated lactic acidosis, which may have diagnostic value under certain conditions.

This study has several limitations. Cardiac output and total peripheral vascular resistance, important integrative parameters of central hemodynamics, could not be measured during the experiment. Their inclusion would have further improved the understanding of the causal relationships between central and peripheral circulatory changes. In addition, although the LSCI method provides a reliable assessment of perfusion changes over a relatively large area of tissue, it only captures perfusion in superficial layers (up to 0.5–1 mm depth). This limitation precludes the evaluation of microcirculatory changes in deeper tissue regions.

Further validation of skin microcirculatory parameters is warranted to establish their utility not only as diagnostic markers of impaired organ perfusion in hemorrhagic and other forms of shock, but also as prognostic indicators of outcome and therapeutic response in the critical care setting.

Conclusion

Under general anesthesia and normothermia, acute blood loss induces progressive cutaneous hypoperfusion with only minimal impairment of sensorimotor cortical perfusion. These changes are associated with a sustained increase in cerebral vascular conductance, while skin vascular conductance remains unchanged. Hemorrhagic shock is characterized by a reduced amplitude of post-occlusive reactive hyperemia. Before blood loss, moderate positive correlations were observed between cutaneous microcirculatory parameters (LSCI perfusion and cutaneous vascular conductance) and cerebral vascular conductance. In hemorrhagic shock, LSCI cortical perfusion correlates with the severity of skin hypoperfusion (R=0.57; P=0.041), and skin microvascular flow reserve correlates strongly with arterial pH (R=0.84; P=0.001). These findings support the potential of skin microcirculatory metrics as noninvasive indicators of central and cerebral hemodynamic compromise during progressive hemorrhage and hemorrhagic shock. Further studies are needed to validate their diagnostic and prognostic value in the critical care setting.

References

1. *Cannon J. W.* Hemorrhagic shock. *N Engl J Med.* 2018; 378 (19): 1852–1853. DOI: 10.1056/NEJMc1802361. PMID: 29742379
2. *Мороз В. В., Рыжков И. А.* Острая кровопотеря: регионарный кровоток и микроциркуляция (Обзор, Часть II). *Общая реаниматология.* 2016; 12 (5): 65–94. *Moroz V. V., Ryzhkov I. A.* Acute blood loss: regional blood flow and microcirculation (Review, Part II). *General Reanimatology = Obshchaya Reanimatologiya* 2016; 12 (5): 65–94. (in Russ.&Eng.). DOI: 10.15360/1813-9779-2016-5-65-94.
3. *Григорьев Е. В., Лебединский К. М., Щеголев А. В., Бобовник С. В., Буланов А. Ю., Заболотских И. Б., Синьков С. В., с соавт.* Реанимация и интенсивная терапия при острой массивной кровопотере у взрослых пациентов. *Анестезиология и реаниматология.* 2020; (1): 5–24. *Grigoriev E. V., Lebedinsky K. M., Shchegolev A. V., Bobovnik S. V., Bulanov A. Yu., Zabolotskikh I. B., Sinkov S. V., et al.* Resuscitation and intensive care in acute massive blood loss in adults (clinical guidelines). *Russian Journal of Anaesthesiology and Reanimatology = Anesteziologiya i Reanimatologiya.* 2020; (1): 5–24. (in Russ.). DOI: 10.17116/anaesthesiology20200115.
4. *Filho I. T.* Hemorrhagic shock and the microvasculature. *Compr Physiol.* 2017; 8 (1): 61–101. DOI: 10.1002/cphy.c170006. PMID: 29357125.
5. *Harrois A., Tanaka S., Duranteau J.* The microcirculation in hemorrhagic shock. Annual Update in Intensive Care and Emergency Medicine. 2013: 277–289. DOI: 10.1007/978-3-642-35109-9_22.
6. *Мороз В. В., Рыжков И. А.* Острая кровопотеря: регионарный кровоток и микроциркуляция (Обзор, Часть I). *Общая реаниматология.* 2016; 12 (2): 66–89. *Moroz V. V., Ryzhkov I. A.* Acute blood loss: regional blood flow and microcirculation (Review, Part I). *General Reanimatology = Obshchaya Reanimatologiya* 2016; 12 (2): 66–89. (in Russ.&Eng.). DOI: 10.15360/1813-9779-2016-2-66-89.
7. *Wan Z., Sun S., Ristagno G., Weil M. H., Tang W.* The cerebral microcirculation is protected during experimental hemorrhagic shock. *Crit Care Med.* 2010; 38 (3): 928–932. DOI: 10.1097/CCM.0b013e3181cd100c. PMID: 20068466.
8. *Cavus E., Meybohm P., Doerges V., Hugo H. H., Steinfath M., Nordstroem J., Scholz J., et al.* Cerebral effects of three resuscitation protocols in uncontrolled haemorrhagic shock: a randomised controlled experimental study. *Resuscitation.* 2009; 80 (5): 567–572. DOI: 10.1016/j.resuscitation.2009.01.013. PMID: 19217706.
9. *Рева В. А., Самакаева А. Р., Шелухин Д. А., Орлов С. В., Потемкин В. Д., Булгин Д. В., Грачева Г. Ю., с соавт.* Экстренная сверхглубокая гипотермия при остановке сердца, индуцированной кровопотерей (экспериментальное исследование на обезьянах). Общая реаниматология. 2025; 21 (1): 62–74. *Reva V. A., Samakaeva A. R., Shelukhin D. A., Orlov S. V., Potemkin V. D., Bulgin D. V., Gracheva G. Y., et al.* Emergency ultra-deep hypothermia in cardiac arrest induced by blood loss (experimental study on nonhuman primates). *General Reanimatology = Obshchaya Reanimatologiya.* 2025; 21 (1): 62–74. (in Russ.&Eng.). DOI: 10.15360/1813-9779-2025-1-62-74.
10. *Rickards C. A.* Cerebral blood-flow regulation during hemorrhage. *Compr Physiol.* 2015; 5 (4): 1585–1621. DOI: 10.1002/cphy.c140058. PMID: 26426461.
11. *Tonnesen J, Pryds A., Larsen E. H., Paulson O. B., Hauerberg J., Knudsen G. M.* Laser doppler flowmetry is valid for measurement of cerebral blood flow autoregulation lower limit in rats. *Exp Physiol.* 2005; 90 (3): 349–355. DOI: 10.1113/expphysiol.2004.029512. PMID: 15653714.
12. *Рыжков И. А., Заржецкий Ю. В., Новодержкина И. С.* Сравнительные аспекты регуляции кожной и мозговой микроциркуляции при острой кровопотере. *Общая реаниматология.* 2017; 13 (6): 18–27. *Ryzhkov I. A., Zarzhetsky Yu. V., Novoderzhkina I. S.* Comparative aspects of the regulation of cutaneous and cerebral microcirculation during acute blood loss. *General Reanimatology = Obshchaya Reanimatologiya.* 2017; 13 (6): 18–27. (in Russ.&Eng.). DOI: 10.15360/1813-9779-2017-6-18-27.
13. *Cracowski J., Roustit M.* Current methods to assess human cutaneous blood flow: an updated focus on laser-based-techniques. *Microcirculation.* 2016; 23 (5): 337–44. DOI: 10.1111/micc.12257. PMID: 26607042.
14. *Потапова Е. В., Михайлова М. А., Королева А. К., Ставцев Д. Д., Дремин В. В., Дунаев А. В., Якушкина Н. Ю., с соавт.* Мультипараметрический подход к оценке кожной микроциркуляции у пациентов дерматологического профиля (на примере псориаза). Физиол человека. 2021; 47 (6): 33–42. *Potapova E. V., Mikhailova M. A., Koroleva A. K., Stavtsev D. D., Dremin B. B., Dunaev A. V., Yakushkina N. Y., et al.* A multiparametric approach to assessing skin microcirculation in dermatological patients (using psoriasis as an

example). *Human physiology = Physiologiya Cheloveka*. 2021; 47 (6): 33–42. (in Russ.). DOI: 10.31857/S013116462105009X.
15. *Holowatz L. A., Thompson-Torgerson C. S., Kenney W. L.* The human cutaneous circulation as a model of generalized microvascular function. *J Appl Physiol (1985)*. 2008; 105 (1): 370–372. DOI: 10.1152/japplphysiol.00858.2007. PMID: 17932300.
16. *Ураков А. Л., Касаткин А. А., Уракова Н. А., Дементьев В. Б.* Инфракрасная термография пальцев рук человека как метод оценки адаптации регионарного кровообращения к кровопотере. *Регионарное кровообращение и микроциркуляция*. 2016; 15 (3): 24–29. *Urakov A. L., Kasatkin A. A., Urakova N. A., Dement'ev V. B.* Infrared thermography of human fingers as a method for assessing regional circulation adaptation to blood loss. *Regional Blood Circulation and Microcirculation = Regionarnoye Krovoobrashcheniye i Mikrocirkulyatsiya*. 2016; 15 (3): 24–29. (in Russ.). DOI: 10.24884/1682-6655-2016-15-3-24-29.
17. *Танканаг А. В.* Методы вейвлет-анализа в комплексном подходе к исследованию кожной микрогемодинамики как единицы сердечно-сосудистой системы. *Регионарное кровообращение и микроциркуляция*. 2018; 17 (3): 33–41. *Tankanag A. V.* Wavelet analysis methods in the comprehensive study approach of skin microhemodynamics as a cardiovascular unit. *Regional Blood Circulation and Microcirculation = Regionarnoye Krovoobrashcheniye i Mikrocirkulyatsiya*. 2018; 17 (3): 33–41. (in Russ.). DOI: 10.24884/1682-6655-2018-17-3-33-41.
18. *Остапченко Д. А., Гутников А. И., Давыдова Л. А.* Современные подходы к терапии травматического шока (обзор). *Общая реаниматология*. 2021; 17 (4): 65–76. *Ostapchenko D. A., Gutnikov A. I., Davydova L. A.* Current approaches to the treatment of traumatic shock (review). *General Reanimatology = Obshchaya Reanimatologiya*. 2021; 17 (4): 65–76. (in Russ.&Eng.). DOI: 10.15360/1813-9779-2021-4-65-76.
19. *Kerger H., Waschke K. F., Ackern K. V., Tsai A. G., Intaglietta M.* Systemic and microcirculatory effects of autologous whole blood resuscitation in severe hemorrhagic shock. *Am J Physiol*. 1999; 276 (6): H2035–43. DOI: 10.1152/ajpheart.1999.276.6.H2035. PMID: 10362685.
20. *González R., Urbano J., López J., Solana M. J., Botrán M., García A., Fernández S. N., et al.* Microcirculatory alterations during haemorrhagic shock and after resuscitation in a paediatric animal model. *Injury*. 2016; 47 (2): 335–341. DOI: 10.1016/j.injury.2015.10.075. PMID: 26612478.
21. *Tachon G., Harrois A., Tanaka S., Kato H., Huet O., Pottecher J., Vicaut E., et al.* Microcirculatory alterations in traumatic hemorrhagic shock. *Crit Care Med*. 2014; 42 (6): 1433–1441. DOI: 10.1097/CCM.0000000000000223. PMID: 24561562.
22. *Крупаткин А. И., Сидоров В. В.* Функциональная диагностика состояния микроциркуляторно-тканевых систем: Колебания, информация, нелинейность (Руководство для врачей). М: Книжный дом «ЛИБРИКОМ»; 2013: 496. *Krupatkin A. I., Sidorov V. V.* Functional diagnostics of microcirculatory and tissue systems: Fluctuations, information, nonlinearity (A manual for doctors). Moscow: LIBRIKOM Book House; 2013. 496. (in Russ.).
23. *Dunn A. K.* Laser speckle contrast imaging of cerebral blood flow. *Ann Biomed Eng*. 2012; 40 (2): 367–377. DOI: 10.1007/s10439-011-0469-0. PMID: 22109805.
24. *Piavchenko G., Kozlov I., Dremin V., Stavtsev D., Seryogina E., Kandurova K., Shupletsov V., et al.* Impairments of cerebral blood flow microcirculation in rats brought on by cardiac cessation and respiratory arrest. *J Biophotonics*. 2021; 14 (12): e202100216. DOI: 10.1002/jbio.202100216. PMID: 34534405.
25. *Golubova N., Potapova E., Seryogina E., Dremin V.* Time–frequency analysis of laser speckle contrast for transcranial assessment of cerebral blood flow. *Biomedical Signal Processing and Control*. 2023; 85: 104969. DOI: 10.1016/j.bspc.2023.104969.
26. *Ziebart A., Möllmann C., Garcia-Bardon A., Kamuf J., Schäfer M., Thomas R., Hartmann E. K.* Effect of gelatin-polysuccinat on cerebral oxygenation and microcirculation in a porcine haemorrhagic shock model. *Scand J Trauma Resusc Emerg Med*. 2018; 26 (1): 15. DOI: 10.1186/s13049-018-0477-2. PMID: 29426350.
27. *Golubova N., Ryzhkov I., Lapin K., Seryogina E., Dunaev A., Dremin V., Potapova E.* Effect of thinned-skull cranial window on monitoring cerebral blood flow using laser speckle contrast imaging. *IEEE J Select Topics Quantum Electron*. 2025; 31 (4): 1–8. DOI: 10.1109/JSTQE.2025.3533950
28. *Vishwanathan K., Chhajwani S., Gupta A., Vaishya R.* Evaluation and management of haemorrhagic shock in polytrauma: clinical practice guidelines. *J Clin Orthop Trauma*. 2020; 13: 106–15. DOI: 10.1016/j.jcot.2020.12.003. PMID: 33680808.
29. *Secher N. H., Van Lieshout J. J.* Heart rate during haemorrhage: time for reappraisal. *J Physiol*.

2010; 588 (Pt 1): 19.
DOI: 10.1113/jphysiol.2009.184499.
PMID: 20045902.

30. *Tew G. A., Klonizakis M., Crank H., Briers J. D., Hodges G. J.* Comparison of laser speckle contrast imaging with laser Doppler for assessing microvascular function. *Microvasc Res.* 2011; 82 (3): 326–32.
DOI: 10.1016/j.mvr.2011.07.007.
PMID: 21803051.
31. *Schadt J. C., Ludbrook J.* Hemodynamic and neurohumoral responses to acute hypovolemia in conscious mammals. *Am J Physiol.* 1991; 260 (2 Pt 2): H305–18.
DOI: 10.1152/ajpheart.1991.260.2.H305.
PMID: 1671735.
32. *Dubensky A., Ryzhkov I., Tsokolaeva Z;, Lapin K., Kalabushev S., Varnakova L., Dolgikh V.* Post-occlusive reactive hyperemia variables can be used to diagnose vascular dysfunction in hemorrhagic shock. *Microvasc Res.* 2024; 152: 104647.
DOI: 10.1016/j.mvr.2023.104647.
PMID: 38092223.

Received 11.03.2025
Accepted 22.04.2024
Online first 23.04.2025

https://doi.org/10.15360/1813-9779-2025-3-2563

The Effects of Xenon on GSK-3β, NF-κB, and Nrf2 Levels in the Rat Brain: An Experimental Study

Evgeniy E. Beda, Mikhail V. Gabitov*, Ivan V. Redkin, Ivan A. Kryukov, Oleg A. Grebenchikov

V. A. Negovsky Research Institute of General Reanimatology,
Federal Research and Clinical Center of Intensive Care Medicine and Rehabilitology,
25 Petrovka Str., Bldg. 2, 107031 Moscow, Russia

For citation: *Evgeniy E. Beda, Mikhail V. Gabitov, Ivan V. Redkin, Ivan A. Kryukov, Oleg A. Grebenchikov.* The Effects of Xenon on GSK-3β, NF-κB, and Nrf2 Levels in the Rat Brain: An Experimental Study. *Obshchaya Reanimatologiya = General Reanimatology.* 2025; 21 (3). https://doi.org/10.15360/1813-9779-2025-3-2563 [In Russ. and Engl.]

***Correspondence to:** Mikhail V. Gabitov, gabitovmv@gmail.com

Summary

Aim. To evaluate the impact of subanesthetic concentrations of xenon on the brain levels of GSK-3β, NF-κB, and Nrf2 in intact rats.

Materials and Methods. Male laboratory rats were randomly assigned to three groups (*N*=5 per group): the control group received inhalation of a nitrogen-oxygen gas mixture; the Xe-70 group received 70% xenon; and the Xe-35 group received 35% xenon. Following euthanasia, brain tissue samples were analyzed using Western blotting and densitometric quantification to assess levels of phosphorylated GSK-3β, NF-κB, and Nrf2.

Results. Inhalation of xenon-oxygen mixtures led to a statistically significant increase in phosphorylated GSK-3β levels in both the Xe-70 group (95% CI: 593,723–1,018,826; *P*=0.0001; *R*=0.72) and the Xe-35 group (95% CI: 458,413–872,807; *P*=0.0001; *R*=0.80), compared with controls. Xenon exposure also resulted in a significant reduction in NF-κB levels in the Xe-70 (95% CI: 205,138–601,617; *P*=0.0005; *R*=0.95) and Xe-35 (95% CI: 217,700–608,462; *P*=0.0003; *R*=0.95) groups. Furthermore, Nrf2 protein expression was significantly elevated in the Xe-35 group compared to controls (95% CI: 260,926–692,532; *P*=0.0002; *R*=0.91).

Conclusion. Subanesthetic xenon concentrations exert a significant modulatory effect on GSK-3β, NF-κB, and Nrf2 expression in the brain tissue of intact rats.

Keywords: xenon; GSK-3β; NF-κB; Nrf2; brain; rats

Conflict of interest. The authors declare no conflict of interest.

Information about the authors:
Evgeniy E. Beda: https://orcid.org/0009-0008-4637-7598
Mikhail V. Gabitov: https://orcid.org/0009-0005-9615-6118
Ivan V. Redkin: https://orcid.org/0000-0001-7008-2038
Ivan A. Kryukov: https://orcid.org/0000-0003-3121-2981
Oleg A. Grebenchikov: https://orcid.org/0000-0001-9045-6017

Introduction

A complex network of biochemical reactions enables cells to perceive, transmit, and interpret signals, thereby coordinating vital physiological processes such as growth, differentiation, metabolism, and apoptosis. These signaling pathways are usually organized into cascades, in which the number of signaling molecules increases at each successive level as the signal propagates from the initial stimulus. The core components of these cascades include receptors that bind signaling molecules, such as hormones, cytokines, and neurotransmitters, along with intracellular kinases and adaptor proteins that relay the signal and effector molecules that elicit the final cellular response, such as gene activation or metabolic reprogramming. The most extensively studied signaling pathways include PI3K/AKT/mTOR, MAPK/ERK, Wnt, JAK-STAT, Hedgehog, and Fas [1–5].

Glycogen synthase kinase 3 (GSK-3) is a key mediator in several of these signaling cascades. GSK-3 exists in two isoforms, GSK-3α and GSK-3β, which share approximately 85% amino acid sequence homology and display high identity within their kinase domains. Unlike most kinases, GSK-3 is constitutively active and is inactivated by phosphorylation at specific serine residues (Ser21 in GSK-3α and Ser9 in GSK-3β). GSK-3β plays a pivotal role in regulating cellular metabolism, proliferation, apoptosis, and synaptic plasticity [6].

Nuclear factor erythroid 2-related factor 2 (Nrf2) is a transcription factor that serves as a master regulator of the cellular antioxidant response. Consisting of 605 amino acids, Nrf2 includes seven functional domains, designated Neh1–Neh7. Nrf2 governs the expression of genes that encode antioxidant and cytoprotective proteins, such as glutathione S-transferase and heme oxygenase-1, which enable cells to counteract oxidative stress and inflammation [7, 8].

NF-κB (nuclear factor kappa-light-chain-enhancer of activated B cells) is a ubiquitous transcription factor that regulates the cellular inflammatory response. The NF-κB complex comprises several proteins, including NFKB1, NFKB2, REL, RELA, and RELB. This complex controls the expression of proinflammatory cytokines (e. g., TNF-α, IL-6, and IL-1β) and chemokines, playing a central role in orchestrating innate and adaptive immune functions [9].

In recent years, the use of xenon-based general anesthesia in surgical practice has become sporadic. Despite its declining use as an anesthetic, there is growing interest in exploring the therapeutic potential of xenon [10–15]. This trend is driven by the realization that subanesthetic concentrations of xenon–those insufficient to induce anesthesia–can minimize the risk of adverse events such as impaired consciousness or respiratory depression while reducing the consumption of this expensive gas without compromising its pharmacological activity. Notably, the minimum alveolar concentration (MAC) of xenon in humans ranges from 63.1% to 71% [16, 17]. Interestingly, xenon's MAC differs substantially in laboratory animals, reaching 95% in mice and up to 161% in rats [18].

Numerous studies have demonstrated that subanesthetic concentrations of xenon have organ-protecting effects. Several of xenon's molecular targets are of particular pharmacodynamic interest. Xenon inhibits NMDA receptors and activates ATP-sensitive and two-pore domain potassium channels, including TREK-1 and TASK-3. This produces neuroprotective effects. Xenon activates signaling pathways, including MAPK and PI3K/Akt, which contribute to cardioprotection. It also enhances the expression of protein kinase B (Akt) and hypoxia-inducible factor 1-alpha (HIF-1α), underlying its renoprotective action [19–26].

GSK-3β, Nrf2, and NF-κB are key regulators of cellular homeostasis in the central nervous system. They play critical roles in stress resistance, inflammation regulation, and the maintenance of neural integrity. The dynamic interplay and balance among these signaling molecules are essential for normal cerebral function, and their dysregulation has been implicated in the pathogenesis of neurodegenerative and other disorders.

This study aimed to investigate the effect of subanesthetic concentrations of xenon on the levels of GSK-3β, NF-κB, and Nrf2 in intact rat brain tissue.

Materials and Methods

The study was conducted on fifteen male Wistar rats, each weighing between 250 and 350 grams. All experimental procedures were performed in strict compliance with national and international guidelines, including Recommendation No. 33 of the Eurasian Economic Commission, dated November 14, 2023; Directive 2010/63/EU of the European Parliament and Council, regarding the protection of animals used for scientific purposes; national standards for the housing and care of laboratory animals; and facility equipment and procedural regulations (GOST 33215-2014). The animals were housed in ventilated cages under controlled environmental conditions (temperature: 18–22°C; humidity: 30–70%) with a 12-hour light/dark cycle (lights on from 9:00 a.m. to 9:00 p.m.). All rats were provided with standard chow pellets and had ad libitum access to purified drinking water via bottle feeders. On the day before the experiment, food was withheld, but water remained freely available.

The study protocol was approved by the Local Ethics Committee of the Federal Research and Clinical Center of Intensive Care Medicine and Rehabilitology (Approval No. 3/23/2, October 11, 2023).

The animals were randomly assigned to three experimental groups:

- Group 1 (*N*=5): control group that received inhalation of a nitrogen–oxygen gas mixture (70% nitrogen and 30% oxygen) for 60 minutes;
- Group 2 (*N*=5): experimental group that received inhalation of a xenon–oxygen gas mixture (70% xenon and 30% oxygen) for 60 minutes (Xe-70 group);
- Group 3 (*N*=5): experimental group that received inhalation of a xenon–oxygen–nitrogen gas mixture (35% xenon, 30% oxygen, and 35% nitrogen) for 60 minutes (Xe-35 group).

Twenty-four hours after completing the experimental procedures, the animals were euthanized with an overdose of anesthetic. According to the protocol described by Grebenchikov et al. [27], protein concentrations in brain tissue and Western blot analyses were performed. Densitometric quantification was carried out using publicly available ImageJ software (National Institutes of Health, USA). The protein levels of GSK-3β, NF-κB, and Nrf2 were expressed in arbitrary units of chemiluminescence (a.u.c.).

Statistical analyses were conducted using GraphPad Prism (version 10.4.2; GraphPad Software, USA). The Shapiro–Wilk test was used to evaluate the normality of the data distribution. Results are presented as the median [*Q1; Q3*], where *Q1* and *Q3* represent the first and third quartiles, respectively. Nonparametric methods were employed for variables exhibiting non-normal distribution in at least one group. The Mann–Whitney *U* test with Bonferroni correction was used for pairwise comparisons, and the Kruskal–Wallis test was used to assess differences among all three groups. Post hoc pairwise analyses were performed using Dunn's test with Bonferroni adjustment. Effect sizes were estimated as the ratio of medians, and 95% confidence intervals were calculated using a nonparametric bootstrap method.

A two-tailed *P* value of less than 0.05 was considered statistically significant for all analyses.

Results

Inhaling the xenon-oxygen mixture resulted in a statistically significant increase in the phosphorylated form of GSK-3β in the Xe-70 (95% CI: 593,723–1,018,826; *P*=0.0001; *R*=0.72) and Xe-35 (95% CI: 458,413–872,807; *P*=0.0001; *R*=0.80) groups, as compared to the control group (see Table, Fig. *a* and *b*). According to the effect size (r) classification, values between 0.5 and 0.7 indicate a large effect, and values greater than 0.7 indicate a very large effect.

No statistically significant differences were observed between groups receiving xenon-oxygen mixtures at different concentrations (70% and 35% Xe). Although phospho-GSK-3β levels were higher in the Xe-70 group than in the Xe-35 group, the difference was not significant (Xe-70: 1,485,347 [1,283,380–1,711,439] vs. Xe-35: 1,406,472 [1,165,272–1,573,930]; P = 0.075). Similarly, NF-κB levels did not differ significantly between the Xe-70 (731,687 [555,120–912,777]) and Xe-35 (745,535 [531,662–880,721]) groups (*P*=0.069). Analysis of Nrf2 levels across the groups also revealed no statistically significant differences (*P*=0.089).

However, densitometric analysis of the Western blots showed that inhaling the xenon–oxygen mixture led to a significant reduction in NF-κB levels in both the Xe-70 (95% CI: 205,138–601,617; *P*=0.0005; *R*=0.95) and Xe-35 (95% CI: 217,700–608,462; *P*=0.0003; *R*=0.95) groups compared to the control group (see Table, Fig. *c* and *d*).

Inhaling the xenon-oxygen mixture resulted in a non-significant increase in Nrf2 levels in the Xe-70 group, while the Xe-35 group exhibited a significant increase compared to the control group (95% CI: 692,532–260,926; *P*=0.0002; *R*=0.91) (see Table, Fig. *e* and *f*).

Discussion

Determining the modulation of key signaling pathways is a promising strategy for studying agents with potential anti-inflammatory, anti-apoptotic, and cytoprotective properties. It is well-established that the active form of GSK-3β promotes opening of the mitochondrial permeability transition pore (mPTP), which leads to disruption of the membrane potential, activation of caspases, neuronal damage, and apoptosis. Conversely, GSK-3β inactivation via phosphorylation is associated with protective mechanisms, including reduced cell death, enhanced survival, and attenuated inflammation. Various upstream regulators modulate GSK-3β activity in response to signals such as Wnt, phosphoinositide 3-kinase (PI3K)/protein kinase B (AKT), extracellular signal-regulated kinase (ERK), and p38 mitogen-activated protein kinase (MAPK). Therefore, pharmacological inhibition of GSK-3β is a promising therapeutic approach for treating acute brain disorders and chronic neurodegenerative diseases [28].

Using xenon at subanesthetic concentrations (35% and 70%) was associated with a significant increase in the phosphorylated form of GSK-3β in intact rat brains. This indicates xenon's ability to inactivate the enzyme, suggesting potential cytoprotective modulation. Similar findings were reported recently by Ershov et al., who demonstrated that administering a xenon–oxygen mixture at subanesthetic concentrations increased phospho-GSK-3β levels in an ischemia model [29].

Recent studies have shown that GSK-3β phosphorylation enhances Nrf2 expression [30, 31]. In our study, Western blot analysis revealed that inhaling 35% xenon significantly increased Nrf2 levels in laboratory animal brain tissue. These results suggest that subanesthetic concentrations of xenon can modulate the GSK-3β/Nrf2 signaling pathway, promoting cellular protection against oxidative stress.

The NF-κB signaling cascade plays a central role in regulating the expression of pro-inflammatory genes. The canonical NF-κB pathway is activated by IL-1 receptors, TNF receptors, and Toll-like receptors. In contrast, the non-canonical pathway is triggered by specific members of the TNF superfamily, such as CD40 ligand, B-cell activating factor (TNFSF13B), and lymphotoxin. Inhibiting NF-κB activity reduces inflammation and apoptosis, which is particularly relevant in the context of autoimmune diseases [32]. Yang et al. demonstrated that a xenon–

Table. Levels of the investigated markers in rat brain tissue during xenon–oxygen mixture inhalation.

Markers	Values in the groups, a. u. c.		
	Control	Xe-70	Xe-35
Phospho-GSK-3β	739898 [517983–868427]	1485347 [1283380–1711439]	1406472 [1165272–1573930]
P value*		0,0001	0,0001
NF-κB	1157280 [871386–1294758]	731687 [555120–912777]	745535 [531662–880721]
P value*		0,0005	0,0003
Nrf2	1111432 [867718–1241235]	1306910 [220388–1800363]	1550695 [1289715–1785378]
P value*		0,087	0,0002

Note. Data are presented as densitometric analysis results of Western blots; a. u. c. — arbitrary units of chemiluminescence; * — compared to the control group.

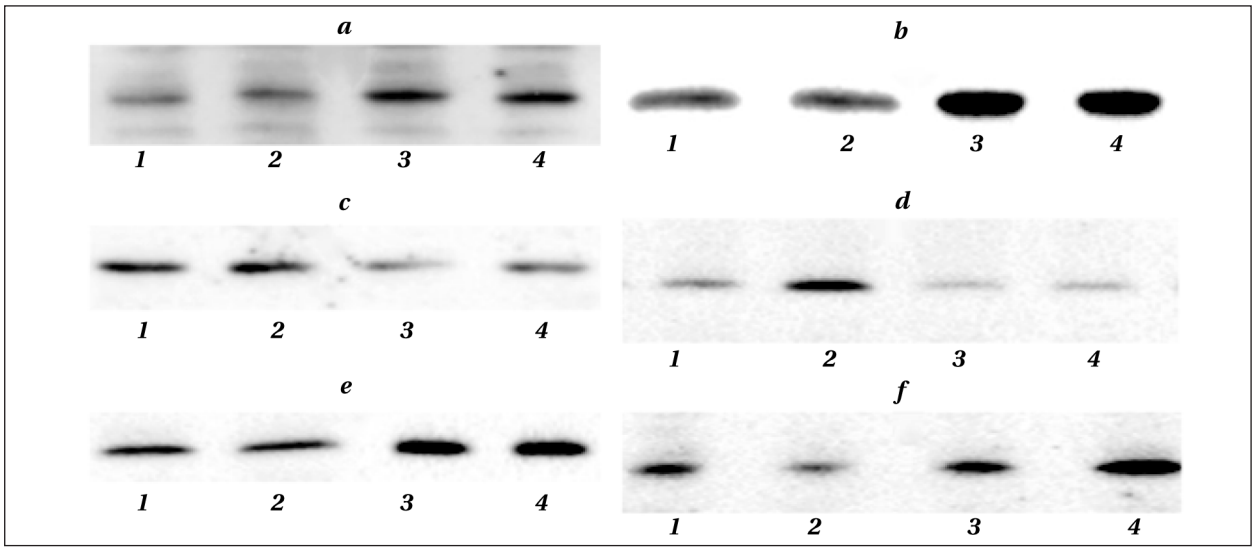

Fig. Western blot analysis of phospho-GSK-3β, NF-κB, and Nrf2 levels in the study groups.
Note. *a, b* — phospho-GSK-3**β**; *c, d* — NF-*κ*B; *e, f* — Nrf2; *1, 2* — control group samples; *3, 4* — experimental group samples

oxygen mixture (70% xenon and 30% oxygen) suppresses NF-*κ*B/NLRP3 inflammasome activation in a murine model of acute lupus nephritis [33].

In vitro studies have demonstrated that xenon modulates the PI3K/AKT/mTOR signaling pathway. This modulation promotes HIF-1*α* activation and suppresses NF-*κ*B-dependent pro-inflammatory and pro-apoptotic signaling. This modulation reduces apoptosis via increased Bcl-2 expression and HMGB-1 inhibition and attenuates inflammation by downregulating NF-*κ*B-mediated pathways [34]. In our study, inhaling xenon–oxygen mixtures at 35% and 70% concentrations significantly reduced NF-*κ*B levels in laboratory animal brain tissue. These results imply that subanesthetic concentrations of xenon have anti-inflammatory and anti-apoptotic effects *in vivo*.

It should be noted, however, that no statistically significant differences were observed between the Xe-35 and Xe-70 groups in terms of GSK-3β, NF-*κ*B, or Nrf2 levels. This may indicate an insufficient sample size or a nonlinear dose-response relationship of the investigated molecular markers within the tested concentration range and exposure time frame.

Conclusion

This study demonstrated that administering xenon at subanesthetic concentrations significantly alters the expression levels of GSK-3β, NF-*κ*B, and Nrf2 in intact rat brain tissue.

Activation of Nrf2 and suppression of the GSK-3β/NF-*κ*B signaling axis under xenon's influence may improve outcomes in cerebral conditions by reducing inflammation and neuronal loss.

These results underscore xenon's cytoprotective potential and highlight the need for further research to elucidate its therapeutic efficacy and underlying mechanisms.

References

1. *Mousavikia S. N., Darvish L., Firouzjaei A. A., Toossi M. T. B., Azimian H. J.* PI3K/AKT/mTOR targeting in colorectal cancer radiotherapy: a systematic review. *Gastrointest Cancer*. 2025; 56 (1): 52. DOI: 10.1007/s12029-024-01160-1. PMID: 39849185.
2. *Park J. I.* MAPK-ERK pathway. *Int J Mol Sci*. 2023; 24 (11): 9666. DOI: 10.3390/ijms24119666. PMID: 37298618.
3. *Iluta S., Nistor M., Buruiana S., Dima D.* Wnt signaling pathway in tumor biology. Genes (Basel). 2024; 15 (12): 1597. DOI: 10.3390/genes15121597. PMID: 39766864.
4. *Hu Q., Bian Q., Rong D., Wang L., Song J., Huang H. S., Zeng J., et al.* JAK/STAT pathway: extracellular signals, diseases, immunity, and therapeutic regimens. *Front Bioeng Biotechnol*. 2023; 11: 1110765. DOI: 10.3389/fbioe.2023.1110765. eCollection 2023. PMID: 36911202.
5. *Острова И. В., Гребенчиков О. А., Голубева Н. В.* Нейропротективное действие хлорида лития на модели остановки сердца у крыс. *Общая реаниматология*. 2019; 15 (3): 73–82. *Ostrova I. V., Grebenchikov O. A., Golubeva N. V.* Neuroprotective effect of lithium chloride in rat model of cardiac arrest. *General Reanimatology= Obshchaya Reanimatologiya*. 2019; 15 (3): 73–82. (in Russ.&Eng.). DOI: 10.15360/1813-9779-2019-3-73-82.
6. *Zhang J., Yang S. G., Zhou F. Q.* Glycogen synthase kinase 3 signaling in neural regeneration *in vivo*. *J Mol Cell Biol*. 2024; 15 (12): mjad075. DOI: 10.1093/jmcb/mjad075. PMID: 38059848.
7. *Saha S., Buttari B., Panieri E., Profumo E., Saso L.* An overview of Nrf2 signaling pathway and its role in inflammation. *Molecules*. 2020; 25 (22): 5474. DOI: 10.3390/molecules25225474. PMID: 33238435.
8. *Шиловский Г. А., Сорокина Е. В., Орловский И. В.* Транскрипционный фактор NRF2 — мишень активирующих антиоксидантную систему клетки препаратов: перспективы применения при возрастных заболеваниях. *Клиническая геронтология*. 2021; 27 (11–12): 57–62. *Shilovsky G. A., Sorokina E. V., Orlovsky I. V.* Transcription factor NRF2 — a target of potential antioxidant drugs: prospects in treatment of age–related diseases. *Clinical Gerontology= Klinicheskaya Gerontologiya*. 2021; 27 (11–12): 57–62. (in Russ.). DOI: 10.26347/1607-2499202111-12057-062.
9. *Barnabei L., Laplantine E., Mbongo W., Rieux-Laucat F., Weil R.* NF-kappaB: at the borders of autoimmunity and inflammation. *Front Immunol*. 2021; 12: 716469. DOI: 10.3389/fimmu.2021.716469. PMID: 34434197
10. *Боева Е. А., Гребенчиков О. А.* Органопротективные свойств аргона (обзор). *Общая реаниматология*. 2022; 18 (5): 44–59. *Boeva E. A., Grebenchikov O. A.* Organoprotective properties of argon (review). *General Reanimatology = Obshchaya Reanimatologiya*. 2022; 18 (5): 44–59. (in Russ.&Eng.). DOI: 10.15360/1813-9779-2022-5-44-59.
11. *Kaufman M. J., Meloni E. G.* Xenon gas as a potential treatment for opioid use disorder, alcohol use disorder, and related disorders. *Med Gas Res*. 2025; 15 (2): 234–253. DOI: 10.4103/mgr.MEDGASRES-D-24-00063. PMID: 39812023.
12. *Antonova V. V., Silachev D. N., Plotnikov E. Y., Pevzner I. B., Yakupova E. I., Pisarev M. V., Boeva E. A., et al.* Neuroprotective effects of krypton inhalation on photothrombotic ischemic stroke. Biomedicines. 2024; 12 (3): 635. DOI: 10.3390/biomedicines12030635. PMID: 38540249.
13. *Гребенчиков О. А., Молчанов И. В., Шпичко А. И., Евсеев А. К., Шабанов А. К., Хусаинов Ш. Ж., Петриков С. С.* Нейропротективные свойства ксенона по данным экспериментальных исследований. *Журнал им. Н. В. Склифосовского Неотложная медицинская помощь*. 2020; 9 (1): 85–95. *Grebenchikov O. A., Molchanov I. V., Shpichko A. I., Evseev A. K., Shabanov A. K., Khusainov S. Z., Petrikov S. S.* Neuroprotective properties of xenon according to experimental studies. *Russian Sklifosovsky Journal «Emergency Medical Care» = Zhurnal im. N. V. Sklifosovskogo «Neotlozhnaya Meditsinskaya Pomoshch»*. 2020; 9 (1): 85–95. (in Russ.). DOI:10.23934/2223-9022-2020-9-l-85-95.
14. *Беда Е. Е., Габитов М. В., Гребенчиков О. А.* Влияние ксенона в различных концентрациях на объем поражения головного мозга и выраженность неврологических нарушений у крыс при моделировании открытой черепно-мозговой травмы. *Патологическая физиология и экспериментальная терапия*. 2024; 68 (1): 26-36. *Beda E. E., Gabitov M. V., Grebenchikov O. A.* The effect of xenon in various concentrations on the volume of brain damage and severity of neurological disorders in rat model of open traumatic brain injury. *Pathological Physiology and Experimental Therapy = Patologicheskaya Fiziologiya i Eksperimentalnaya Terapiya*. 2024; 68 (1): 26-36. (in Russ.). DOI: 10.25557/0031-2991.2024.01.26-36.
15. *Шпичко А. И., Гребенчиков О. А., Молчанов И. В., Шабанов А. К., Шпичко Н. П., Каданцева К. К.* Кардиопротективные свойства ксенона. *Журнал им. Н. В. Склифосовского Неотложная медицинская помощь*. 2020; 9 (2): 266–271. *Shpichko A. I., Grebenchikov O. A., Molchanov I. V., Shabanov A. K., Shpichko N. P., Kadantseva K. K.* Cardioprotective properties of xenon. *Russian Sklifosovsky Journal «Emergency Medical Care» = Zhurnal im. N. V. Sklifosovskogo «Neotlozhnaya Meditsinskaya Pomoshch»*. 2020; 9 (2): 266–271. (in Russ.). DOI: 10.23934/2223-9022-2020-9-2-96-107.
16. *Nakata Y., Goto T., Ishiguro Y., Terui K., Kawakami H., Santo M., Niimi Y., et al.* Minimum alveolar concentration (MAC) of xenon with sevoflurane in humans. *J Am Soc Anesthesiol*. 2001; 94 (4): 611–614. DOI: 10.1097/00000542-200104000-00014. PMID: 11379681.
17. *Cullen S. C., Eger E. D. II, Cullen B. F., Gregory P.* Observations on the anesthetic effect of the combination of xenon and halothane. *Anesthesiology*. 1969; 31: 305-30. DOI: 10.1097/00000542-196910000-00003. PMID: 5811596.
18. *Koblin D. D., Fang Z., Eger E. I., Laster M. J., Gong D., Ionescu P., Halsey M. J., et al.* Minimum alveolar concentrations of noble gases, nitrogen, and sulfur

hexafluoride in rats: helium and neon as nonimmobilizers (nonanesthetics). *Anesth Analg.* 1998; 87 (2): 419–424. DOI: 10.1213/00000539-199808000-00035. PMID: 9706943.

19. *Политов М. Е., Подпругина С. В., Золотова Е. Н., Ногтев П. В., Агакина Ю. С., Жукова С. Г., Яворовский А. Г.* Клиническое применение ксенона в субанестетических концентрациях (обзор). *Общая реаниматология*. 2025; 21 (2): 55–67. *Politov M. E., Podprugina S. V., Zolotova E. N., Nogtev P. V., Agakina Yu. S., Zhukova S. G., Yavorovsky A. G.* Clinical application of xenon in subanesthetic concentrations (review). *General Reanimatology = Obshchaya Reanimatologiya.* 2025; 21 (2): 55–67. (in Russ&Eng.). DOI: 10.15360/1813-9779-2025-2-2554.
20. *Veldeman M., Coburn M., Rossaint R., Clusmann H., Nolte K., Kremer B., Höllig A.* Xenon reduces neuronal hippocampal damage and alters the pattern of microglial activation after experimental subarachnoid hemorrhage: a randomized controlled animal trial. *Front Neurol.* 2017; 8: 511. DOI: 10.3389/fneur.2017.00511. PMID: 29021779.
21. *Amer A. R., Oorschot D. E.* Xenon combined with hypothermia in perinatal hypoxic-ischemic encephalopathy: a noble gas, a noble mission. *Pediatr Neurol.* 2018; 84: 5–10. DOI: 10.1016/j.pediatrneurol.2018.02.009. PMID: 29887039.
22. *Campos-Pires R., Onggradito H., Ujvari E., Karimi S., Valeo F., Aldhoun J., Edge C. J., et al.* Xenon treatment after severe traumatic brain injury improves locomotor outcome, reduces acute neuronal loss and enhances early beneficial neuroinflammation: a randomized, blinded, controlled animal study. *Crit Care.* 2020; 24: 667. DOI: 10.1186/s13054-020-03373-9. PMID: 33246487.
23. *Hollmén C., Parkkola R., Vorobyev V., Saunavaara J., Laitio R., Arola O., Hynninen M., et al.* Neuroprotective effects of inhaled xenon gas on brain structural gray matter changes after out-of-hospital cardiac arrest evaluated by morphometric analysis: a substudy of the randomized xe-hypotheca trial. *Neurocrit Care.* 2025; 42 (1): 131–141. DOI: 10.1007/s12028-024-02053-8. PMID: 38982000.
24. *Brandao W., Jain N., Yin Z., Kleemann K. L., Carpenter M., Bao X., Serrano J. R., et al.* Inhaled xenon modulates microglia and ameliorates disease in mouse models of amyloidosis and tauopathy. *Sci Transl. Med.* 2025; 17 (781): eadk3690. DOI: 10.1126/scitranslmed.adk3690. PMID: 39813317.
25. *Filev A. D., Silachev D. N., Ryzhkov I. A., Lapin K. N., Babkina A. S., Grebenchikov O. A., Pisarev V. M.* Effect of xenon treatment on gene expression in brain tissue after traumatic brain injury in rats. Brain Sci. 2021; 11 (7): 889. DOI: 10.3390/brainsci11070889. PMID: 34356124.
26. *Кабиольский И. А., Симоненко С. Д., Сарычева Н. Ю., Дубынин В. А.* Терапевтические эффекты инертных газов. Российский физиологический журнал им. И. М. Сеченова. 2024; 110 (10): 1582–1601. *Kabiolsky I. A., Simonenko S. D., Sarycheva N.Yu., Dubynin V. A.* Therapeutic effects of inert gases. *I. M. Sechenov Russian Journal of Physiology = Ross. Fiziol. Zh. Im. I. M. Sechenova.* 2024; 110 (10): 1582–1601. (in Russ.). DOI: 10.31857/S0869813924100033.
27. *Гребенчиков О. А., Аврущенко М. Ш., Борисов К. Ю., Ильин Ю. В., Лихванцев В. В.* Нейропротекторные эффекты севофлурана на модели тотальной ишемии-реперфузии. Клиническая патофизиология. 2014; 2: 57–62. *Grebenchikov O. A., Avrushchenko M. Sh., Borisov K.Yu., Ilyin Yu.V., Likhvantsev V. V.* Neuroprotective effects of sevoflurane on a total ischemia-reperfusion model. *Clinical Pathophysiology / Klinicheskaya Patofysiologiya.* (in Russ.). 2014; 2: 57–62.
28. *Ruiz S. A., Rippin I., Eldar-Finkelman H.* Prospects in GSK-3 signaling: from cellular regulation to disease therapy. Cells. 2022; 11 (10): 1618. DOI: 10.3390/cells11101618. PMID: 35626655.
29. *Ершов А. В., Крюков И. А., Антонова В. В., Баева А. А.* Влияние ксенона на активность гликоген-синтазы киназы-3β в перифокальной зоне ишемического инсульта (экспериментальное исследование). Общая реаниматология. 2023; 19 (2): 60–67. *Ershov A. V., Krukov I. A., Antonova V. V., Baeva A. A.* The effect of xenon on the activity of glycogen synthase kinase-3b in the perifocal zone of ischemic cerebral infarction (experimental study). *General Reanimatology = Obshchaya Reanimatologiya.* 2023; 19 (2): 60–67. (in Russ.&Eng.). DOI: 10.15360/1813-9779-2023-2-2274.
30. *Li Y., Chu L, Liu C., Zha Z., Shu Y.* Protective effect of GSK-3β/Nrf2 mediated by dimethyl fumarate in middle cerebral artery embolization reperfusion rat model. *Curr Neurovasc Res.* 2021; 18 (4): 456–464. DOI: 10.2174/1567202618666211109105024. PMID: 34751118.
31. *Niu Q., Sun W., Chen Q., Long Y., Cao W., Wen S., Li A., et al.* Protective effects of ischemic postconditioning on livers in rats with limb ischemia-reperfusion via glycogen synthase kinase 3 beta (GSK-3β)/fyn/nuclear receptor-erythroid-2-related factor (Nrf2) pathway. *Med Sci Monit.* 2020; 26. DOI: 10.12659/MSM.923049. PMID: 32686659.
32. *Yu H., Lin L., Zhang Z., Zhang H., Hu H.* Targeting NF-kappaB pathway for the therapy of diseases: mechanism and clinical study. Signal Transduct Target Ther. 2020; 5 (1): 209. DOI: 10.1038/s41392-020-00312-6. PMID: 32958760.
33. *Yang S. R., Hua K. F., Chu L. J., Hwu Y. K., Yang S. M., Wu C. Y., Lin T. J., et al.* Xenon blunts NF-kappaB/NLRP3 inflammasome activation and improves acute onset of accelerated and severe lupus nephritis in mice. *Kidney Int.* 2020; 98 (2): 378–390. DOI: 10.1016/j.kint.2020.02.033. PMID: 32622527.
34. *Zhao H., Huang H., Ologunde R., Lloyd D. G., Watts H., Vizcaychipi M. P., Lian Q., et al.* Xenon treatment protects against remote lung injury after kidney transplantation in rats. Anesthesiology. 2015; 122: 1312–26. DOI: 10.1097/ALN.0000000000000664. PMID: 25856291.

Received 14.03.2025
Accepted 06.06.2025

https://doi.org/10.15360/1813-9779-2025-3-2540

The Impact of Interleukin-6 and Hypoxia on the Expression of Brain Injury Marker Proteins in a Cellular Model of the Neurovascular Unit

Artem A. Ivkin[1]*, Evgeniy V. Grigoriev[1], Elena D. Khilazheva[2]

[1] Research Institute of Complex Problems of Cardiovascular Disease, Ministry of Education and Science of the Russian Federation, 6 Academician L. S. Barbarash Boulevard, 650002 Kemerovo, Russia

[2] Research Institute of Molecular Medicine and Pathobiochemistry, Prof. V.F. Voino-Yasenetsky Krasnoyarsk State Medical University, Ministry of Health of Russia,
1 Partizana Zheleznyaka Str., 660022 Krasnoyarsk, Krasnoyarsk area, Russia

For citation: *Artem A. Ivkin, Evgeniy V. Grigoriev, Elena D. Khilazheva.* The Impact of Interleukin-6 and Hypoxia on the Expression of Brain Injury Marker Proteins in a Cellular Model of the Neurovascular Unit. *Obshchaya Reanimatologiya = General Reanimatology.* 2025; 21 (3). https://doi.org/10.15360/1813-9779-2025-3-2540 [In Russ. and Engl.]

***Correspondence to:** Artem A. Ivkin, ivkiaa@kemcardio.ru

Summary

The high incidence of postoperative cognitive dysfunction in children undergoing cardiac surgery underscores the urgent need for effective neuroprotective strategies.

Aim. To examine the effects of hypoxia and interleukin-6 (IL-6) on the expression of claudin-5, occludin-1, and interleukin-1 (IL-1) and IL-6 receptors in neurovascular unit (NVU) cells.

Materials and methods. An *in vitro* NVU model comprising neurons, astrocytes, and endothelial cells was established. The cells were cultured under normoxic and hypoxic conditions with oxygen concentrations of 15%, 10%, 7%, and 5%. The cultures were also treated with patient-derived sera containing high or low levels of IL-6. All incubations were conducted under normothermic conditions for 30 minutes. Injury marker expression was then assessed using fluorescence analysis.

Results. Significant reductions in claudin-5 fluorescence intensity were observed at oxygen levels of 10% and below (15.2 vs. 34.3 in controls, P=0.0105). Hypoxia did not affect occludin-1 expression. IL-1 receptor fluorescence intensity increased under 7% and 5% oxygen conditions (12.2 and 12.9 versus 9.9 in the control group, P=0.0105), while IL-6 receptor expression remained unchanged. In both normoxic and hypoxic conditions, adding patient sera significantly altered marker expression; hypoxia enhanced these effects. Sera with the highest IL-6 levels induced the most pronounced reduction in injury marker fluorescence.

Conclusion. IL-6 had a more significant impact on injury marker expression in NVU cells than hypoxia did. Hypoxic conditions with oxygen concentrations down to 10% did not affect marker expression.

Keywords: neurovascular unit, neurons, astrocytes, endothelial cells, hypoxia, interleukin-6, IL-1 receptor, claudin-5, occludin-1

Conflict of interest. The authors declare no conflict of interest.

Funding. This study was supported by the Russian Science Foundation (grant No. 22-15-00258). https://rscf.ru/project/22-15-00258.

Information about the authors:

Artem A. Ivkin: http://orcid.org/0000-0002-3899-1642.

Evgeniy V. Grigoriev: http://orcid.org/0000-0001-8370-3083.

Elena D. Khilazheva: http://orcid.org/0000-0002-9718-1260

Introduction

Contemporary advances in cardiac surgery and anesthesiology have advanced to the point that surgical interventions must not only preserve vital functions, but also maintain patients' quality of life. Cognitive function is a critical component of quality of life and should be preserved at or near preoperative levels whenever possible. However, numerous studies have demonstrated that pediatric cardiac surgery is often associated with a high risk of postoperative cognitive dysfunction (POCD). Postoperative delirium (POD) occurs in 40–65% of cases. POD significantly prolongs the duration of stay in intensive care units due to increased requirements for mechanical ventilation, sedative administration, and other supportive measures. Consequently, hospital length of stay and overall mortality increase as well [6].

Moreover, the adverse impact of POD extends beyond its immediate effects. It has been shown to have long-term consequences that reduce cognitive performance in children for months following surgery. These long-term outcomes may result from POD itself or from cerebral injury sustained during the surgical procedure [7, 8]. Studies indicate that children experiencing POD are more likely to exhibit negative behavioral changes, such as difficulties with attention, emotional instability, and impaired social interactions. These disturbances can persist, adversely affecting the child's psychosocial well-being and overall quality of life [9]. These issues can lead to challenges in applying previously acquired

skills and difficulties in learning new information, which is particularly critical for preschool-aged children [10, 11]. Delirium in pediatric patients also leads to increased medical and financial burdens [12]. Given the high incidence of cognitive impairment following surgical correction of congenital heart defects in children, it is important to recognize that cardiac surgery involves numerous pathophysiological factors that can adversely affect the brain and contribute to cerebral injury.

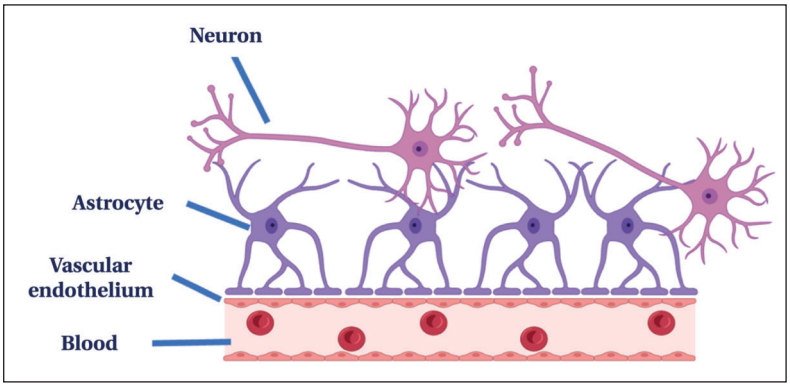

Fig. 1. Schematic representation of the neurovascular unit (illustration by the authors).

Contributing factors include the effects of anesthetic agents, which have been shown to induce neuronal apoptosis and disrupt synaptic plasticity — mechanisms that may ultimately lead to cognitive impairment. Additionally, episodes of hypoxia and hemodynamic instability, use of sympathomimetic drugs, and overall surgery duration must be considered — factors that are common, though not unique, to this type of intervention [13–15]. However, a distinctive feature of cardiac surgery is the frequent use of cardiopulmonary bypass (CPB). CPB-related phenomena that increase the risk of cerebral injury include microembolism, non-pulsatile blood flow, and periods of circulatory arrest. Hypothermia, which is routinely used in pediatric cardiac surgery for various reasons, may have both beneficial and harmful effects. The latter include altered blood rheology, microcirculatory disturbances, and the initiation of neuroinflammatory processes via the activation of cold-inducible RNA-binding protein (CIRBP) [16–18]. These factors require close monitoring and strict control to minimize the risk of brain injury.

The function of brain cells relies on the coordinated interaction of components within a structural complex that comprises blood vessels and astrocytes, forming the blood-brain barrier (BBB), as well as neurons (Fig. 1). This integrated system is referred to as the neurovascular unit (NVU). When exposed to direct damaging factors or systemic inflammation, the BBB's integrity is compromised, enabling systemic cytokines to enter the NVU. These cytokines exacerbate neuroinflammation and disrupt NVU function through multiple mechanisms. Notably, interleukin-1β (IL-1β) has been shown to impair glymphatic system function by interacting with astrocytes. This hinders the clearance of neurotoxic substances and amplifies the cycle of neuroinflammation [19–23].

Thus, interleukin-1β can serve as a marker of neuroinflammation. Two additional potential markers are claudin-5 and occludin-1, which are tight junction proteins of the blood–brain barrier. Their expression reflects the structural integrity of this interface. Numerous studies have demonstrated correlations between circulating levels of these proteins and clinical manifestations of brain injury. Furthermore, evidence suggests that claudin-5 and occludin-1 are directly involved in the neuroinflammatory process. This supports their potential utility in assessing the functional state of the NVU [24–26].

Based on the above, it can be concluded that brain injury results from a combination of direct damaging factors and indirect mechanisms mediated by systemic inflammation, which ultimately leads to the destruction of the NVU (see Fig. 2). In this context, strategies aimed at attenuating the systemic inflammatory response (SIR) in children undergoing surgical correction of congenital heart defects (CHDs) are of particular interest. One approach is to minimize the use of donor blood components during the intraoperative and postoperative periods. This concept is especially critical in pediatric cardiac surgery, where transfusions are often given ahead of time to prevent excessive hemodilution. This is due to the difference between the child's circulating blood volume and the volume needed to prime the cardiopulmonary bypass circuit [21].

However, studies have shown that donor blood components themselves may cause SIR [27, 28]. Despite this complexity, the use of donor blood products during CPB is not governed by standardized protocols, but rather depends on the anesthesiologist's or perfusionist's discretion.

Currently, a restrictive transfusion strategy is favored in pediatric practice due to the multitude of associated risks. These risks include infection, acute hemolytic reactions, metabolic complications such as hyperkalemia or hypocalcemia, allergic reactions, transfusion-associated circulatory overload (TACO), and transfusion-related acute lung injury (TRALI). Nevertheless, transfusions remain widely used in cardiac surgery due to concerns about complications from hemodilution during extracorporeal circulation [29–31].

This raises a critical, unresolved question: which has a more damaging effect on the NVU — hypoxia resulting from hemodilution or systemic inflammation triggered by exposure to donor blood components?

This experimental study aimed to determine the effects of hypoxia and interleukin-6 (IL-6) on the expression of claudin-5, occludin-1, and IL-1 and IL-6 receptors in neurovascular unit cells.

Materials and Methods

At Krasnoyarsk State Medical University (KrasSMU), a brain injury model associated with cardiac surgery was developed using an NVU cellular model cultured under intraoperative conditions. The experimental study was conducted at KrasSMU in the following steps:

1. Retrieval of primary brain cell cultures *in vitro*.

The procedure for obtaining primary brain cell cultures and forming experimental groups has been described in detail in a previously published study [32]. The concentration of interleukin-6 (IL-6) in patient serum was used as an indicator of systemic inflammation intensity.

2. Experimental Design and Group Allocation.

To evaluate the impact of IL-6 on the NVU cellular model *in vitro*, serum samples containing either minimal or maximal IL-6 concentrations were added to the culture medium. This approach allowed for the simulation of systemic inflammation of varying severity.

The experimental groups were classified based on IL-6 concentration as follows:

1. Control group: intact NVU model without serum exposure.
2. The minimum IL-6 group consisted of cultures treated with serum containing the lowest IL-6 levels.
3. The maximum IL-6 group consisted of cultures treated with serum containing the highest IL-6 levels.

Additional groups were formed according to hypoxic incubation conditions:

1. Control: standard culture conditions: N_2 75%, O_2 20%, CO_2 5%.
2. Hypoxia 1: N_2 80%, O_2 15%, CO_2 5%.
3. Hypoxia 2: N_2 85%, O_2 10%, CO_2 5%.
4. Hypoxia 3: N_2 88%, O_2 7%, CO_2 5%.
5. Hypoxia 4: N_2 90%, O_2 5%, CO_2 5%.

Incubation was performed at 37°C for 30 minutes.

Each experimental condition was replicated five times.

At this stage of the study, we evaluated the effects of sera with high and low IL-6 concentrations, as well as varying oxygen conditions, on the following parameters:

- expression of tight junction proteins (claudin-5 and ZO-1);
- expression of interleukin 1 and 6 receptors;
- cytokine levels (IL-1 and IL-6) in the culture medium.

3. Immunocytochemical Analysis.

A double indirect immunocytochemical staining method was employed to detect target molecular markers, following the manufacturer's protocol for each antibody. The following primary antibodies were used: Claudin-5 (AF0130, Affinity Biosciences); Occludin-1 (ZO1) (AF5145, Affinity Biosciences); Interleukin-1 Receptor Type I (PAA066Ra01, Cloud-Clone Corp.); and Interleukin-6 Receptor (DF2530, Affinity Biosciences). The detailed staining procedure has been previously described in an earlier study of ours [32].

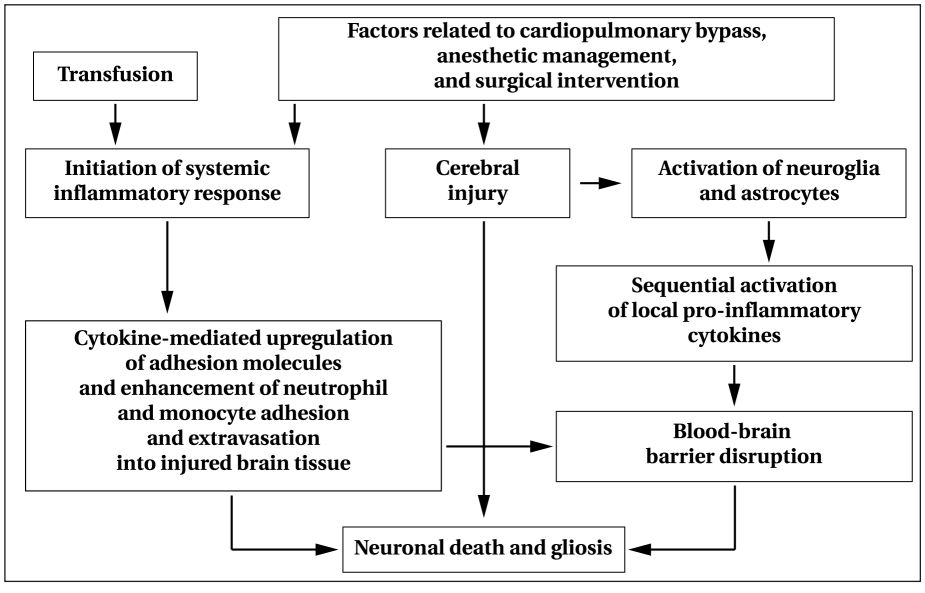

Fig. 2. Schematic representation of the effects of pathological factors on the neurovascular unit during cardiac surgery (illustration by the authors).

Statistical Analysis

Data were statistically analyzed using BioStat Pro 5.9.8. Since most variables did not follow a normal distribution (as determined by the Shapiro–Wilk test, $P<0.05$), the results are presented as medians *(Me)* with lower *(Q1)* and upper *(Q3)* quartiles. Quantitative variables were compared using the one-tailed Mann–Whitney *U* test. Differences were considered statistically significant at $P<0.05$.

To compare multiple independent groups, the

Kruskal–Wallis test was used. For pairwise group comparisons, the Mann–Whitney *U* test was used with Bonferroni correction. When evaluating the effects of hypoxia on the NVU, four experimental groups were compared to one control group. This resulted in a Bonferroni-adjusted significance threshold of $P<0.0125$. When assessing the effects of IL-6, comparisons were made between the maximum and minimum IL-6 groups with a Bonferroni-adjusted significance level of $P<0.017$.

Results and Discussion

Exposure to hypoxic conditions decreased claudin-5 fluorescence intensity from 34.3 arbitrary units (a. u.) to 27.0 a. u. This reduction was statistically significant in the 10%, 7%, and 5% oxygen groups (Table 1).

Exposure to hypoxia at an oxygen concentration of 15% did not result in a statistically significant reduction in claudin-5 expression. However, the combined effect of hypoxia and IL-6 decreased fluorescence intensity in the subgroup exposed to serum with minimal IL-6 level (P=0.0043). Pairwise comparisons showed that claudin-5 fluorescence intensity was significantly lower in the Hypoxia 2, Hypoxia 3, and Hypoxia 4 groups compared to the normoxic control group (P=0.0105 for each comparison).

The most pronounced decrease in claudin-5 expression was notably observed in the Maximum IL-6 group, even under normoxic conditions (P=0.0105). Further reductions of fluorescence intensity under hypoxic conditions were not observed in this group (P=0.0734). In contrast, under minimal IL-6 exposure, a progressive decrease in fluorescence intensity was noted with increasing hypoxia severity (P=0.043).

An important comparison is the difference in claudin-5 fluorescence intensity between groups exposed to minimal or maximal IL-6 concentrations and a group exposed to 5% oxygen. Statistical analysis revealed no significant difference between the minimal IL-6 group and the 5% hypoxia group (13.0 [11.5–13.6] a. u. vs. 13.5 [11.2–15.8] a. u., P=0.5637). However, the high IL-6 group had significantly lower fluorescence intensity than the hypoxia group (3.6 [3.3–3.8] a. u. vs. 13.0 [11.5–13.6] a. u., P=0.0105).

These findings suggest that severe hypoxia (5% O_2) has a similar effect on claudin-5 expression as minimal systemic inflammation (low IL-6). However, elevated IL-6 levels—and, consequently, a heightened systemic inflammatory response—had a more profound impact on the NVU than hypoxia alone.

Thus, IL-6 had a greater effect on claudin-5 expression than hypoxia. Higher IL-6 concentrations led to maximal suppression of claudin-5 expression, as assessed by fluorescence intensity. Furthermore, hypoxia appeared to potentiate the effects of IL-6, even at low cytokine levels.

Table 1. Claudin-5 fluorescence intensity.

Group	Values in different O_2 levels					*P* value				
	Normoxia (20% O_2)	15% O_2	10% O_2	7% O_2	5% O_2	15% vs 10% vs 7% vs 5%	Control vs 15%	Control vs 10%	Control vs 7%	Control vs 5%
Control	34.3 [30.9–36.9]	27.0 [25.1–28.7]	15.2 [13.5–16.9]	10.6 [8.5–12.5]	13.0 [11.5–13.6]	0.0029	0.0416	0.0105	0.0105	0.0105
Minimum IL-6	13.5 [11.2–15.8]	10.7 [10.0–11.6]	8.6 [8.0–9.0]	7.4 [6.4–8.3]	6.9 [6.4–7.4]	0.0043	0.0956	0.0105	0.0105	0.0105
Maximum IL-6	3.6 [3.3–3.8]	4.7 [3.9–4.9]	2.5 [2.1–2.8]	3.8 [3.7–4.2]	3.6 [3.2–3.7]	0.0734	—	—	—	—
Control vs Minimum vs Maximum, *P*	0.0073	0.0073	0.0073	0.0125	0.0073					
Control vs Minimum, *P*	0.0105	0.0105	0.0105	0.0105	0.0105					
Control vs Maximum, *P*	0.0105	0.0105	0.0105	0.0105	0.0105					
Minimum vs Maximum, *P*	0.0105	0.0105	0.0105	0.0105	0.0105					

Note. Here and in tables 2–4: All values are expressed in arbitrary fluorescence units (a. u.).

Table 2. Occludin-1 fluorescence intensit.

Group	Values in different O_2 levels					*P* value			
	Normoxia (20% O_2)	15% O_2	10% O_2	7% O_2	5% O_2	15% vs 10% vs 7% vs 5%	Control vs 15%	Control vs 10%	Control vs 7%	Control vs 5%
Control	53.8 [51.6–56.9]	58.7 [56.4–60.4]	54.7 [53.2–58.2]	60.6 [58.8–62.0]	62.2 [61.0–64.0]	0.2092	—	—	—	—
Minimum IL-6	26.3 [25.0–28.1]	26.2 [24.9–26.8]	22.1 [21.6–23.4]	19.8 [18.9–20.4]	20.4 [19.4–21.2]	0.0106	0.3864	0.0416	0.0105	0.0105
Maximum IL-6	8.2 [7.8–8.6]	9.1 [8.3–9.3]	8.0 [7.7–8.5]	11.0 [10.3–11.6]	12.3 [11.3–12.9]	0.0065	0.1932	0.4423	0.0105	0.0105
Control vs Minimum vs Maximum, *P*	0.0073	0.0073	0.0073	0.0073	0.0073					
Control vs Minimum, *P*	0.0105	0.0105	0.0105	0.0105	0.0105					
Control vs Maximum, *P*	0.0105	0.0105	0.0105	0.0072	0.0105					
Minimum vs Maximum, *P*	0.0105	0.0105	0.0105	0.0105	0.0105					

The second protein involved in maintaining the functional activity of the blood-brain barrier is the tight junction protein occludin-1.

Hypoxic exposure did not cause a statistically significant change in the fluorescence intensity of occludin-1, which ranged from 58.7 to 62.2 arbitrary units (*P*=0.2092). Only a slight trend toward increased fluorescence intensity was observed (Table 2).

The presence of patient serum in the culture medium led to a significant decrease in occludin-1 fluorescence intensity in both the low IL-6 (*P*=0.0151) and high IL-6 (*P*=0.0105) groups.

Under hypoxic conditions, a further reduction in fluorescence intensity was observed in only two groups: the Hypoxia 3 group (*P*=0.0105) and the Hypoxia 4 group, which contained serum with both low and high IL-6 levels (*P*=0.0105).

These findings suggest that IL-6 significantly affects occludin-1 at all tested concentrations. Furthermore, the effect of IL-6 was concentration-dependent; higher IL-6 levels were associated with lower occludin-1 fluorescence intensity.

In contrast, hypoxia alone did not have a statistically significant effect on occludin-1 expression.

The next set of experiments focused on assessing the expression of the interleukin-1 receptor (IL-1R).

Under hypoxic conditions and in the absence of IL-6 in the culture medium, changes in IL-1 receptor (IL-1R) fluorescence intensity were observed in the Hypoxia 3 and Hypoxia 4 groups (oxygen concentrations of 7 and 5%, respectively). Increases were 23% (*P*=0.0105) and 30% (*P*=0.0105), respectively (Table 3).

Under normoxic conditions, low IL-6 concentrations led to a more than twofold increase in IL-1R fluorescence intensity (from 9.9 to 22.7 a. u.; *P*=0.0105), whereas high IL-6 concentrations caused a 2.8-fold increase, up to 27.6 a. u. compared to 9.9 a. u. in the control group (*P*=0.0105).

As hypoxia deepened, IL-1R fluorescence intensity increased progressively. The most pronounced changes were observed in the Maximum IL-6 subgroup under severe hypoxia (Hypoxia 4), with a fourfold increase compared to intact cells cultured in normoxia (*P*=0.0105). In the Minimum subgroup, a threefold increase in IL-1R fluorescence intensity was observed (*P*=0.0105).

In the group with minimal IL-6, hypoxia at 15% oxygen did not yet have a statistically significant effect on IL-1R fluorescence. Significant differences only emerged in groups with oxygen concentrations of 10% or lower.

Thus, it was found that hypoxia only modestly affected IL-1R fluorescence intensity, with changes remaining within a 20% range. In contrast, the presence of IL-6 in the culture medium resulted in more significant alterations than hypoxic exposure

Table 3. Expression levels of interleukin-1 receptors (IL-1R).

Group	Values in different O_2 levels					*P* value			
	Normoxia (20% O_2)	15% O_2	10% O_2	7% O_2	5% O_2	15% vs 10% vs 7% vs 5%	Control vs 15%	Control vs 10%	Control vs 7%	Control vs 5%
Control	9,9 [9,8–10,1]	10,1 [9,8–10,4]	10,6 [10,3–10,9]	12,2 [11,7–12,7]	12,9 [12,1–13,3]	0,0117	0,2819	0,0956	0,0105	0,0217
Minimum IL-6	22,7 [21,7–23,7]	22,0 [21,3–22,4]	28,8 [27,7–29,7]	32,6 [31,3–34,1]	33,1 [32,3–33,8]	0,0027	0,2339	0,0105	0,0105	0,0105
Maximum IL-6	27,6 [26,6–29,0]	32,2 [31,0–34,4]	36,0 [33,6–37,8]	38,3 [34,9–41,0]	39,8 [38,5–40,7]	0,0218	0,0416	0,0217	0,0217	0,0105
Control vs Minimum vs Maximum, *P*	0,0097	0,0073	0,0073	0,0073	0,0073					
Control vs Minimum, *P*	0,0105	0,0105	0,0105	0,0105	0,0105					
Control vs Maximum, *P*	0,0105	0,0105	0,0105	0,0105	0,0105					
Minimum vs Maximum, *P*	0,0217	0,0105	0,0105	0,0745	0,0105					

Table 4. Expression levels of interleukin-6 receptors (IL-6R).

Group	Values in different O_2 levels					*P* value			
	Normoxia (20% O_2)	15% O_2	10% O_2	7% O_2	5% O_2	15% vs 10% vs 7% vs 5%	Control vs 15%	Control vs 10%	Control vs 7%	Control vs 5%
Control	8.6 [7.9–9.0]	8.0 [7.5–8.5]	8.5 [8.3–8.6]	8.6 [8.4–8.8]	8.9 [8.6–9.2]	0.0552	—	—	—	—
Minimum IL-6	8.8 [8.2–9.4]	10.9 [10.3–12.3]	16.0 [14.1–17.8]	21.1 [17.7–24.1]	20.7 [19.7–22.2]	0.0034	0.0217	0.0105	0.0105	0.0105
Maximum IL-6	8.9 [8.3–10.1]	16.2 [15.0–17.0]	19.4 [17.1–22.3]	33.6 [30.6–36.0]	41.3 [39.2–44.4]	0.0014	0.0105	0.0105	0.0105	0.0105
Control vs Minimum vs Maximum, *P*	0.6678	0.0097	0.0169	0.0073	0.0073					
Control vs Minimum, *P*	—	0.0105	0.0105	0.0105	0.0105					
Control vs Maximum, *P*	—	0.0105	0.0105	0.0105	0.0105					
Minimum vs Maximum, *P*	—	0.0217	0.0956	0.0105	0.0105					

alone. At the same time, the study observed a potentiating effect of hypoxia on IL-6-mediated IL-1R responses.

Under hypoxic conditions without IL-6 in the culture medium, no statistically significant changes in IL-6 receptor (IL-6R) fluorescence intensity were detected (*P*=0.5152) (Table 4).

Even under intensified hypoxic conditions, with an ambient oxygen concentration as low as 5%, no statistically significant changes in fluorescence intensity were observed compared to normoxic conditions.

When patient-derived serum containing IL-6 was added to the culture under normoxia, no statistically significant changes in fluorescence intensity were observed, either in the group with minimal IL-6 (*P*=0.2819) or in the group with maximal IL-6 levels (*P*=0.1933).

In the group with minimal IL-6, exposure to increasing hypoxia led to significant elevations in IL-6R fluorescence intensity at 10% (*P*=0.0105), 7% (*P*=0.0105), and 5% (*P*=0.0105) oxygen, relative to normoxic conditions.

In groups with high IL-6 levels, a progressive increase in IL-6R fluorescence intensity was also observed with greater degrees of hypoxia. This effect became statistically significant at 15% oxygen (*P*=0.0105) and continued to increase proportionally as oxygen levels decreased.

Similar to the IL-1R response, the highest fluorescence values were detected in the group with maximal IL-6 under 5% oxygen, where IL-6R expression was 4.8 times higher than in the control group (*P*=0.0105).

These findings demonstrate that the presence of IL-6 in the culture medium promotes increased IL-6R expression as measured by fluorescence intensity and that the effects of IL-6 are amplified under hypoxic conditions. The observed changes closely mirrored the combined effects of hypoxia and IL-6 on IL-6R.

All experiments demonstrated that the cellular NVU model was less impacted by hypoxia than by IL-6. However, increasing degrees of hypoxia progressively decreased fluorescence intensity across all investigated markers.

These results imply that strategies to avoid the use of donor blood components during pediatric cardiac surgery could be effective. Although restrictive transfusion strategy carries the risk of hemic hypoxia,

transfusion itself significantly enhances the SIRS and subsequent neuroinflammation, as previously described by our group [27, 28].

These results are consistent with those of other studies examining the impact of transfusion on the NVU in children. These studies have shown an association between transfusion and an increased risk of postoperative delirium and cognitive dysfunction [33, 34].

Furthermore, a previous clinical study demonstrated that surgical repair of septal CHD using cardiopulmonary bypass can be safely performed without transfusion in children weighing over 8 kg without preoperative anemia [35]. The study also found that children who did not receive donor blood components had lower levels of SIRS and cerebral injury.

Several limitations of the present study must be acknowledged.

First, the evaluation of only a limited number of experimental groups with varying oxygen concentrations may have reduced the statistical power to detect the robust effects of hypoxia on the NVU model.

Second, the study used an imperfect in vitro model. Several types of NVU models are currently available. The simplest consists of a monoculture of endothelial cells [36]. A more advanced approach is the Transwell model, which uses a semipermeable membrane insert to simulate the vascular lumen. This enables the study of BBB permeability and modeling of brain diseases [37]. This model is currently the most widely used and was applied in our study.

More complex systems include three-dimensional (3D) matrix-based BBB models, which incorporate extracellular matrix scaffolds [38]. These models represent an early step toward spatially accurate models that better simulate cellular interactions. However, these models face challenges, including limited nutrient delivery to the matrix, the absence of blood flow, and the poor reproducibility of matrix composition. These issues restrict their widespread use.

A more recent innovation involves spheroid-based models [39]. These models are formed via co-culture of endothelial cells, astrocytes, and pericytes. This results in self-organizing spheroids in which endothelial cells form the outer layer, astrocytes form the core, and pericytes reside in the intermediate zone. Spheroid models exhibit higher expression of tight and adherens junction proteins (ZO-1, occludin, and claudin-5). They also offer ease of handling, reproducibility, and long viability — up to 21 days. Their limitations include an insufficient nutrient supply to the core of the spheroid and an inability to measure transendothelial electrical resistance (TEER).

The most advanced and promising approach is the use of microfluidic models [40]. These models have a 3D architecture and a defining feature: continuous laminar flow through microchannels. This allows for automated nutrient delivery, reduces the risk of contamination, and induces shear stress that promotes cell morphology resembling in vivo conditions. However, these systems have limitations, such as the difficulty of measuring TEER and the need for expensive, specialized equipment.

Using spheroid or microfluidic models may have provided more detailed insights into the effects of hypoxia and systemic inflammation on the NVU. However, the current lack of materials and technical infrastructure prevents their wide implementation.

Conclusion

Using an in vitro NVU model, this study demonstrated that hypoxia had a smaller impact on the expression of cerebral injury markers than IL-6 concentration.

Claudin-5 expression increased significantly only under hypoxic conditions with 10% oxygen or less. Occludin-1 expression did not respond to changes in oxygen levels, similar to IL-1 receptor expression. In contrast, IL-6 receptor expression significantly changed under more severe hypoxia, specifically at 7% and 5% oxygen.

Adding patient serum to the NVU culture induced greater changes in fluorescence intensity than hypoxia alone and potentiated its effects. Notably, the negative impact increased proportionally with higher IL-6 concentrations in the added serum.

References

1. *Staveski S. L., Pickler, R.H., Khoury P. R., Ollberding N. J., Donnellan A. L.D., Mauney J. A., Lincoln, P.A., et al.* Prevalence of ICU delirium in postoperative pediatric cardiac surgery patients. *Pediatr Crit Care Med*. 2021; 22 (1): 68–78. DOI: 10.1097/PCC.0000000000002591. PMID: 33065733.
2. *Patel A. K., Biagas K. V., Clarke E. C., Gerber L. M., Mauer E., Silver G., Chai P., et al.* Delirium in children after cardiac bypass surgery. *Pediatr Crit Care Med*. 2017; 18 (2): 165–171. DOI: 10.1097/PCC.0000000000001032. PMID: 27977539.
3. *Alvarez R. V., Palmer C., Czaja A. S., Peyton C., Silver, G. Traube C., Mourani P. M., et al.* Delirium is a common and early finding in patients in the pediatric cardiac intensive care unit. *J Pediatr*. 2018; 195: 206–212. DOI: 10.1016/j.jpeds.2017.11.064.
4. *Köditz H., Drouche A., Dennhardt N., Schmidt M., Schultz M., Schultz B.* Depth of anesthesia, temperature, and postoperative delirium in children and adolescents undergoing cardiac surgery. *BMC Anesthesiol*. 2023; 23 (1): 148. DOI: 10.1186/s12871-023-02102-3. PMID: 37131120.
5. *Chomat M. R., Said A. S. Mann J. L., Wallendorf M., Bickhaus A., Figueroa M.* Changes in sedation practices in association with delirium screening in infants after cardiopulmonary bypass. *Pediatr Cardiol*. 2021; 42 (6): 1334–1340. DOI: 10.1007/s00246-021-02616-y. PMID: 33891134.
6. *Dechnik A., Traube C.* Delirium in hospitalised children. *Lancet Child Adolesc Health* 2020; 4 (4): 312–321. DOI: 10.1016/s2352-4642 (19)30377-3. PMID: 32087768.
7. *Goldberg T. E., Chen C., Wang Y., Jung E., Swanson A., Ing C., Garcia P. S., et al.* Association of delirium with long-term cognitive decline. *JAMA Neurol*. 2020; 77 (11): 1373–1381. DOI: 10.1001/jamaneurol.2020.2273. PMID: 32658246.
8. *Gunn J. K., Beca J., Hunt R. W., Goldsworthy M., Brizard C. P., Finucane K., Donath S., et al.* Perioperative risk factors for impaired neurodevelopment after cardiac surgery in early infancy. *Arch Dis Child*. 2016; 101 (11): 1010–1016. DOI: 10.1136/archdischild-2015-309449. PMID: 27272973.
9. *Houben A., Ghamari S., Fischer A., Neumann C., Baehner T., Ellerkmann R. K.* Pediatric emergence delirium is linked to in-creased early postoperative negative behavior within two weeks after adenoidectomy: an observational study. *Braz J Anesthesiol*. 2024; 74 (5): 744114. DOI: 10.1016/j.bjane.2021.03.008. PMID: 33887334.
10. *Koch S., Stegherr A.-M., Rupp L., Kruppa J., Prager C., Kramer S., Fahlenkamp A., et al.* Emergence delirium in children is not related to intraoperative burst suppression — prospective, observational electrography study. *BMC Anesthesiol*. 2019; 19 (1): 146. DOI: 10.1186/s12871-019-0819-2. PMID: 31395011.
11. *Hansen T. G.* Anesthesia-related neurotoxicity and the developing animal brain is not a significant problem in children. *Paediatr Anaesth*. 2015; 25 (1): 65–72. DOI: 10.1111/pan.12548. PMID: 25266176.
12. *Jevtovic-Todorovic V.* General anesthetics and neurotoxicity: how much do we know? *Anesthesiol Clin*. 2016; 34 (3): 439–451. DOI: 10.1016/j.anclin.2016.0 4.001. PMID: 27521190.
13. *Dahmani S., Stany I., Brasher C., Lejeune C., Bruneau B., Wood C., Nivoche Y., et al.* Pharmacological prevention of sevoflurane- and desflurane-related emergence agitation in children: a meta-analysis of published studies. *Br J Anaesth*. 2010; 104 (2): 216–223. DOI: 10.1093/bja/aep376. PMID: 20047899.
14. *Hogue C. W. Jr., Palin C. A., Arrowsmith J. E.* Cardiopulmonary bypass management and neurologic outcomes: an evidence- based appraisal of current practices. *Anesth Analg*. 2006; 103 (1): 21–37. DOI: 10.1213/01.ane.0000220035.82989.79. PMID: 16790619.
15. *Hori D., Brown C., Ono M., Rappold T., Sieber F., Gottschalk A., Neufeld K. J., et al.* Arterial pressure above the upper cerebral autoregulation limit during cardiopulmonary bypass is associated with postoperative delirium. *Br J Anaesth*. 2014; 113 (6): 1009–1017. DOI: 10.1093/bja/aeu319. PMID: 25256545ю
16. *Hirata Y.* Cardiopulmonary bypass for pediatric cardiac surgery. *Gen Thorac Cardiovasc Surg*. 2018; 66 (2): 65–70. DOI: 10.1007/s11748-017-0870-1. PMID: 29185163.
17. *Toomasian C. J., Aiello S. R., Drumright B. L., Major T. C., Bartlett R. H., Toomasian J. M.* The effect of air exposure on leucocyte and cytokine activation in an *in-vitro* model of cardiotomy suction. *Perfusion*. 2018; 33 (7): 538–545. DOI: 10.1177/0267659118766157. PMID: 29638199.
18. *Liu M., Li Y., Gao S., Yan S., Zhang Q., Liu G., Ji B.* A novel target to reduce microglial inflammation and neuronal damage after deep hypothermic circulatory arrest. *J Thorac Cardiovasc Surg*. 2020; 159 (6): 2431–2444.e7. DOI: 10.1016/j.jtcvs.2019.06.115. PMID: 31564537.
19. *Pozhilenkova E. A., Lopatina O. L., Komleva Y. K., Salmin V. V., Salmina A. B.* Blood-brain barrier-supported neurogenesis in healthy and diseased brain. *Nat Rev Neurosci*. 2017; 28 (4): 397–415. DOI: 10.1515/revneuro-2016-0071. PMID: 28195555.
20. *Cerejeira J., Firmino H., Vaz-Serra A., Mukaetova-Ladinska E. B.* The neuroinflammatory hypothesis of delirium. *Acta Neuropathol*. 2010; 119 (6): 737–754. DOI: 10.1007/s00 401-010-0 674-1. PMID: 20309566.
21. *Sun Y., Koyama Y., Shimada S.* Inflammation from peripheral organs to the brain: how does systemic inflammation cause neuroinflammation? *Front Aging Neurosci*. 2022; 14: 903455. DOI: 10.3389/fnagi.2022.903455. PMID: 35783147.
22. *Linnerbauer M., Wheeler M. A., Quintana F. J.* Astrocyte crosstalk in CNS inflammation. *Neuron*. 2020; 108 (4): 608–622. DOI: 10.1016/j.neuron.2020.08.012. PMID: 32898475.
23. *Kress B. T., Iliff J. J., Xia M., Wang M., Wei H. S., Zeppenfeld D., Xie L., et al.* Impairment of para-vascular clearance pathways in the aging brain. *Ann Neurol*. 2014; 76 (6): 845–861. DOI: 10.1002/ana.24271. PMID: 25204284.
24. *Kuo W. T., Odenwald M. A., Turner J. R., Zuo L.* Tight junction proteins occludin and ZO-1 as regulators of epithelial proliferation and survival. *Ann N Y Acad Sci*. 2022; 1514 (1): 21–33. DOI: 10.1111/nyas.14798. PMID: 35580994.
25. *Li Y., Liu B., Zhao T., Quan X., Han Y., Cheng Y., Chen Y., et al.* Comparative study of extracellular vesicles derived from mesenchymal stem cells and brain endothelial cells attenuating blood-brain barrier permeability via regulating Caveolin-1-dependent ZO-1 and Claudin-5 endocytosis in acute ischemic stroke. *J Nanobiotechnology*. 2023; 21 (1): 70. DOI: 10.1186/s12951-023-01828-z. PMID: 36855156.
26. *Yang Z., Lin P., Chen B., Zhang X., Xiao W., Wu S., Huang C., et al.* Autophagy alleviates hypoxia-induced blood-brain barrier injury via regulation of CLDN5 (claudin 5). *Autophagy*. 2021; 17 (10): 3048–3067. DOI: 10.1080/15548627.2020.1851897. PMID: 33280500.
27. *Baker R. A., Nikolic A., Onorati F., Alston R. P.* 2019 EACTS/EACTA/ EBCP guidelines on cardiopulmonary bypass in in adult cardiac surgery: a tool to better clinical practice. *Eur J Cardio-Thorac Surg*. 2020; 57 (2): 207–209. DOI: 10.1093/ejcts/ezz358. PMID: 31942985.
28. *Ivkin A., Grigoriev E., Mikhailova A.* Impact of intraoperative blood transfusion on cerebral injury in pediatric patients undergoing congenital septal heart defect surgery. *J Clin Med*. 2024; 13 (20): 6050. DOI: 10.3390/jcm13206050. PMID: 39458000.
29. *Wittenmeier E., Piekarski F., Steinbicker A. U.* Blood product transfusions for children in the perioperative period and for critically ill children. *Dtsch Arztebl Int*. 2024; 121 (2): 58–65. DOI: 10.3238/arztebl.m2023.0243. PMID: 38051160.
30. *Ивкин А. А., Григорьев Е. В., Балахнин Д. Г., Чермных И. И.* Интраоперационная трансфузия как фактор риска церебрального повреждения после кардиохирургических

вмешательств у детей: проспективное наблюдательное исследование. *Вестник интенсивной терапии имени А. И. Салтанова*. 2023; (1): 101–114. *Ivkin A. A., Grigoryev E. V., Balakhnin D. G., Chermnykh I. I.* Intraoperative transfusion is a risk factor for cerebral injury after cardiac surgery in children: a prospective observational study. *Ann Crit Care = Vestnik Intensivnoy Terapii im AI Saltanova*. 2023; 1: 101–114. (in Russ.). DOI: 10.21320/1818-474X-2023-1-101-114.

31. *Malati Z. A., Pourfathollah A. A., Dabbaghi R., Balagholi S., Javan M. R.* Evaluation of a new method of leukocyte extractions from the leukoreduction filter. *Indian J Hematol Blood Transfus*. 2023; 39 (3): 478–486. DOI: 10.1007/s12288-022-01618-x. PMID: 37304478.
32. *Ивкин А. А., Григорьев Е. В., Хилажева Е. Д., Моргун А. В.* Влияние трансфузии и гипоксии на клетки модели нейроваскулярной единицы *in vitro*. *Общая реаниматология*. 2024; 20 (1): 37–42. *Ivkin A. A., Grigoriev E. V., Khilazheva E. D., Morgun A. V.* The effect of transfusion and hypoxia on cells in an *in vitro* model of the neurovascular unit. *General Reanimatology = Obshchaya Reanimatologiya*. 2024; 20 (1): 37–42. (in Russ/&Eng.). DOI: 10.15360/1813-9779-2024-1-2350.
33. *Ивкин А. А., Григорьев Е. В., Цепокина А. В., Шукевич Д. Л.* Послеоперационный делирий у детей при коррекции врожденных септальных пороков сердца. *Вестник анестезиологии и реаниматологии*. 2021; 18 (2): 62–68. *Ivkin A. A., Grigoriev E. V., Tsepokina A. V., Shukevich D. L.* Postoperative delirium in children in undergoing treatment of congenital septal heart defects. *Messenger of Anesthesiology and Resuscitation = Vestnik Anesteziologii i Reanimatologii*, 2021; 18 (2): 62–68. (In Russ.). DOI: 10.21292/2078-5658-2021-18-2-62-68.
34. *Naguib A. N., Winch P. D., Tobias J. D., Simic J., Hersey D., Nicol K., Preston T., et al. A* single-center strategy to minimize blood transfusion in neonates and children undergoing cardiac surgery. *Paediatr Anaesth*. 2015; 25 (5): 477–486. DOI: 10.1111/pan.12604. PMID: 25581204.
35. *Борисенко Д. В., Ивкин А. А., Шукевич Д. Л., Корнелюк Р. А.* Значение эритроцитсодержащих компонентов донорской крови в объеме первичного заполнения контура искусственного кровообращения в развитии системного воспаления при коррекции врожденных пороков сердца у детей. *Общая реаниматология*. 2022; 18 (3): 30–37. *Borisenko D., Ivkin A. A., Shukevich D. L., Kornelyuk R. A.* The effect of erythrocyte containing donor blood components in the priming of the cardiopulmonary bypass circuit on the development of systemic inflammation during correction of congenital heart defects in children. *General Reanimatology = Obshchaya Reanimatologiya*. 2022; 18 (3): 30–37. (in Russ.&Eng.). DOI: 10.15360/1813-9779-2022-3-30-37.
36. *Siddharthan V., Kim Y. V., Liu S., Kim K. S.* Human astrocytes/astrocyte-conditioned medium and shear stress enhance the barrier properties of human brain microvascular endothelial cells. *Brain Res*. 2007; 1147: 39–50. DOI: 10.1016/j. brainres.2007.02.029. PMID: 17368578.
37. *Cenini G., Hebisch M., Iefremova V., Flitsch L. J., Breitkreuz Y., Tanzi R. E., Kim D. Y., et al.* Dissecting Alzheimer's disease pathogenesis in human 2D and 3D models. *Mol Cell Neurosci*. 2021; 110: 103568. DOI: 10.1016/j.mcn.2020.103568. PMID: 33068718.
38. *Wang H., Yang H., Shi Y., Xiao Y., Yin Y., Jiang B., Ren H., et al.* Reconstituting neurovascular unit with primary neural stem cells and brain microvascular endothelial cells in three-dimensional matrix. *Brain Pathol*. 2021; 31 (5): e12940. DOI: 10.1111/bpa.12940. PMID: 33576166.
39. *Sokolova V., Nzou G., Van Der Meer S. B., Ruks T., Heggen M., Loza K., Hagemann N., et al.* Ultrasmall gold nanoparticles (2 nm) can penetrate and enter cell nuclei in an *in vitro* 3D brain spheroid model. *Acta Biomater*. 2020; 111: 349–362. DOI: 10.1016/j.actbio.2020.04.023. PMID: 32413579.
40. *Teixeira M. I., Amaral M. H., Costa P. C., Lopes C. M., Lamprou D. A.* Recent developments in microfluidic technologies for central nervous system targeted studies. *Pharmaceutics*. 2020; 12 (6): 542. DOI: 10.3390/pharmaceutics12060542. PMID: 32545276.

Received 05.12.2024
Accepted 09.06.2025

https://doi.org/10.15360/1813-9779-2025-3-2568

Assessment of Structural Changes in Neutrophil Membranes Induced by Plasma from Newborns with Infection

Vladimir A. Inozemtsev[1], Igor V. Obraztsov[2], Ekaterina A. Sherstyukova[1]*, Snezhanna S. Kandrashina[1], Mikhail A. Shvedov[1], Maxim E. Dokukin[1], Viktoria A. Sergunova[1]

[1] V. A. Negovsky Research Institute of General Reanimatology, Federal Research and Clinical Center of Intensive Care Medicine and Rehabilitology, 25 Petrovka Str., Bldg. 2, 107031 Moscow, Russia
[2] G.N. Speransky Children's City Clinical Hospital No. 9, Moscow Health Department, 29 Shmitovsky pr., 123317 Moscow, Russia

For citation: *Vladimir A. Inozemtsev, Igor V. Obraztsov, Ekaterina A. Sherstyukova, Snezhanna S. Kandrashina, Mikhail A. Shvedov, Maxim E. Dokukin, Viktoria A. Sergunova.* Assessment of Structural Changes in Neutrophil Membranes Induced by Plasma from Newborns with Infection. *Obshchaya Reanimatologiya = General Reanimatology.* 2025; 21 (3). https://doi.org/10.15360/1813-9779-2025-3-2568 [In Russ. and Engl.]

***Correspondence to:** Ekaterina A. Sherstyukova, kmanchenko@yandex.ru

Summary

This study aimed to identify neutrophil membrane characteristics that could serve as clinical biomarkers for the development of infectious complications in newborns.

Materials and Methods. Neutrophils isolated from healthy donors were used as a model system. The cells were incubated with plasma samples (S) isolated from blood of newborns categorized into three groups: apparently healthy (normal) (NS) (N=6), with localized infection (LIS) (N=7), and with generalized infection (GIS) (N=8). We assessed cellular morphology and membrane roughness before and after stimulation with phorbol 12-myristate 13-acetate (PMA) using fluorescence and atomic force microscopy. We quantified nuclear and membrane surface areas, the intensity of neutrophil extracellular trap (NET) formation, and membrane arithmetic average roughness (R_a).

Results. A standardized protocol for neutrophil preparation and evaluation was developed. Optimal incubation conditions were established; 1% bovine serum albumin (BSA) yielded minimal background activation. Dose-dependent activation of neutrophils by PMA was observed in the presence of 1% plasma. PMA stimulation significantly increased nuclear area (P<0.001), membrane area (P<0.001), and R_a (P<0.001), regardless of plasma sample group. The most significant changes occurred in neutrophils incubated with plasma from the GIS group. Generalized infection was associated with enhanced NET activation, which may contribute to the pathogenesis of thrombotic complications in neonatal sepsis.

Conclusion. Microscopy-based neutrophil characteristics are promising biomarkers for evaluating infection including sepsis in newborns.

Keywords: neutrophil membranes; newborns; infectious and septic complications; sepsis; neutrophil extracellular traps; membrane roughness; atomic force microscopy; fluorescence microscopy

Conflict of interest. The authors declare no conflict of interest.

Information about the authors:
Vladimir A. Inozemtsev: http://orcid.org/0000-0002-4693-5624
Igor V. Obraztsov: http://orcid.org/0000-0002-6649-853X
Ekaterina A. Sherstyukova: http://orcid.org/0000-0002-9962-6315
Snezhanna S. Kandrashina: http://orcid.org/0000-0002-2185-3817
Mikhail A. Shvedov: http://orcid.org/0009-0004-4288-2758
Maxim E. Dokukin: http://orcid.org/0000-0001-6856-1953
Viktoria A. Sergunova: http://orcid.org/0000-0002-8425-0845

Introduction

Inflammation is a universal pathological process triggered by infectious agents, mechanical or thermal injury, or major surgical interventions [1,2]. According to the epidemiological data from 2019–2020, the incidence of sepsis in the European region is approximately 750 cases per 100,000 people in developed countries [3].

Neonatal sepsis remains a major medical concern due to its high mortality rate and poor response to treatment. This is largely attributed to the immaturity of the innate immune system, which includes impaired functional activity of neutrophils and monocytes [4–6].

Studies have shown that, in cases of neonatal sepsis and multi-organ failure of mixed etiology, there is increased expression of CD64 and decreased expression of CD16 on neutrophils, which is an important diagnostic biomarker [7].

Stimulating neutrophils with physiological and pharmacological agents, such as hydrogen peroxide, lipopolysaccharides (LPS), phorbol 12-myristate 13-acetate (PMA), and calcium ionophore A23187, enhances their effector functions and induces sig-

nificant morphological changes, including transitioning from spherical to flattened shapes. This transformation is a critical component of the cell's adaptation to its protective role [8–13].

Recent studies have demonstrated that septic serum profoundly impacts neutrophils by inducing their activation and apoptosis and altering their functional properties [14, 15].

These findings underscore the importance of investigating modulatory factors that could mitigate the harmful effects of septic serum on neutrophils, with the ultimate goal of developing novel therapeutic approaches to sepsis [16].

In the present study, we performed a thorough analysis of neutrophil alterations using advanced microscopy techniques.

Despite the considerable existing research, many structural and functional aspects of neutrophils remain poorly understood. Modern optical methods are limited in their ability to elucidate neutrophil function and investigate intracellular processes [14].

In recent years, atomic force microscopy (AFM) has become increasingly utilized for investigating biological samples [17, 18], particularly cells [19–22]. AFM provides a distinct advantage by enabling the acquisition of topographic images alongside high-resolution maps of the physical properties of the cell surface [23, 24], making it a powerful tool for identifying biophysical markers.

This study aimed to identify neutrophil membrane characteristics that could serve as clinical biomarkers for the development of infectious and septic complications in neonates.

Materials and Methods

Neutrophils were isolated from the peripheral blood of a healthy adult donor. All experimental procedures, including the collection and analysis of biological samples, were conducted in strict accordance with international ethical standards, including the 2000 Declaration of Helsinki on principles of medical research and the 1999 Council of Europe Convention on Human Rights and Biomedicine. This study was conducted in accordance with the regulatory framework and protocols of the Federal Research and Clinical Center of Intensive Care Medicine and Rehabilitology (protocol no. 427, dated October 17, 2023) and was approved by the Speransky Children's City Clinical Hospital No. 9's local ethics committee (protocol no. 45, dated May 31, 2022).

For neutrophil isolation, freshly collected donor blood was layered onto a two-step Ficoll gradient (Paneco, Russia) with densities of 1.119 g/cm³ and 1.077 g/cm³. Centrifugation was performed at 400×g for 40 minutes at room temperature. The resulting fraction containing neutrophils and residual erythrocytes was collected. The erythrocytes were lysed in ice-cold water for 30 seconds and then double-strength phosphate-buffered saline (PBS) was added to restore osmotic balance [25, 26]. The isolated neutrophils were resuspended in PBS for counting. Light microscopy confirmed that the neutrophil purity exceeded 98%, and cell viability, as assessed by trypan blue exclusion, was greater than 96%.

Experiments were conducted in 24-well plates with sterile, round coverslips in each well. To promote cell adhesion, 2×10^5 neutrophils were resuspended in RPMI 1640 medium (Paneco, Russia), supplemented with 10 mM HEPES (Paneco, Russia). The cells were then allowed to adhere to the coverslips for 30 minutes at 37°C in a 5% CO_2 atmosphere.

In all experiments, plasma samples were obtained from three groups of neonatal patients:

- NS (normal sample): apparently healthy neonates without confirmed infectious or inflammatory complications (*N*=6);
- LIS (localized infection sample): neonates with laboratory- and imaging-confirmed localized infection and no signs of organ dysfunction (*N*=7);
- GIS (generalized infection sample): neonates with a confirmed infection focus and organ dysfunction (pSOFA score>8) (*N*=8).

A total of 21 plasma samples were analyzed.

A preliminary experiment was performed to optimize the culture medium. The basal medium (RPMI 1640 + 10 mM HEPES) was compared to the same medium supplemented with 1% fetal bovine serum (FBS), 1% heat-inactivated FBS (hiFBS), or 1% bovine serum albumin (BSA) (all from Paneco, Russia). The incubation time was three hours. Based on the results, the basal medium was selected as RPMI 1640 supplemented with 10 mM HEPES and 1% BSA for subsequent experiments.

To determine the optimal plasma concentration, the basal medium was supplemented with 1%, 10%, or 50% plasma from apparently healthy neonates. The cells were then activated with 25nM PMA for three hours.

To optimize the activator concentration, 1%, 10%, or 50% normal or septic plasma was added to the basal medium. Then, the cells were activated with PMA at concentrations of 5, 10, or 25 nM for three hours.

In the main experiment, neutrophils were incubated in the basal medium supplemented with 1% plasma from each patient group. To assess activation, the cells were stimulated with 25nM PMA. The incubation period was three hours.

After the incubation period, the cells were fixed with 4% paraformaldehyde at 37°C for 30 minutes, followed by three washes with 1× PBS.

Neutrophil morphology and surface roughness were assessed using atomic force microscopy (AFM). Prior to scanning, the samples were washed three times with distilled water for 30 seconds each to remove residual salts and then dried in a Jeio Tech

VDC-11U vacuum desiccator at a pressure of 1×10^{-3} MPa for one hour.

To acquire 2D and 3D images, we performed AFM scanning in semicontact mode using NTEGRA Prima and NTEGRA BIO microscopes (NT-MDT SI, Russia). NSG01 cantilevers (NT-MDT SI, Russia) with a spring constant of 5 N/m and a tip radius of 10 nm were used. Scanning was conducted at various settings: scan areas of 100×100 μm² and 2×2 μm², with 512 data points, and a scanning frequency ranging from 0.3 to 0.7 Hz.

Image analysis was performed using Gwyddion 2.65 and Image Analysis software (NT-MDT SI, Russia). The surface roughness (R_a) of the cells was quantified using a cutoff value of 0.440 μm to ensure maximum sensitivity and consistent analysis of all images obtained.

Widefield fluorescence microscopy was employed to evaluate neutrophil activation and measure the area of the cell membrane and nucleus. Imaging was performed using a Leica Microsystems (Germany) Thunder microscope equipped with an LED excitation source and a ×63 oil-immersion objective.

Image processing was performed using LAS X software (Leica Microsystems, Germany) and ImageJ [29]. ImageJ was used specifically for quantitative analysis of cell activation and measurement of cellular structure areas.

For widefield fluorescence microscopy, the cells were fixed and permeabilized in a solution of 0.05% Triton X-100 (Sigma, USA) in PBS for five minutes at 4°C. The cells were then washed with PBS and incubated with 3% BSA to block nonspecific binding.

DNA was stained with 1:1000 diluted Hoechst 33342 (Sigma, USA) in PBS and incubated for 30 minutes. Neutrophil membranes were visualized using a 1:500 dilution of Alexa Fluor 594-conjugated wheat germ agglutinin (WGA; Thermo Fisher Scientific, USA), and F-actin was stained with a 1:1000 dilution of Alexa Fluor 488-conjugated phalloidin (Thermo Fisher Scientific, USA). All staining steps were performed in the dark. After staining, the coverslips were washed three times with PBS, mounted onto microscope slides, and fixed using ibidi mounting medium (ibidi, Germany).

Statistical analysis was conducted using OriginPro 2019 (OriginLab Corporation, USA). Quantitative data were expressed as the median (*Me*) and interquartile range (*Q1; Q3*). The Shapiro–Wilk test was used to assess the distribution of variables. Since most parameters did not follow a normal distribution, nonparametric methods were employed. The Mann–Whitney *U* test was used to compare two independent groups and the Wilcoxon signed-rank test was used for paired data. The

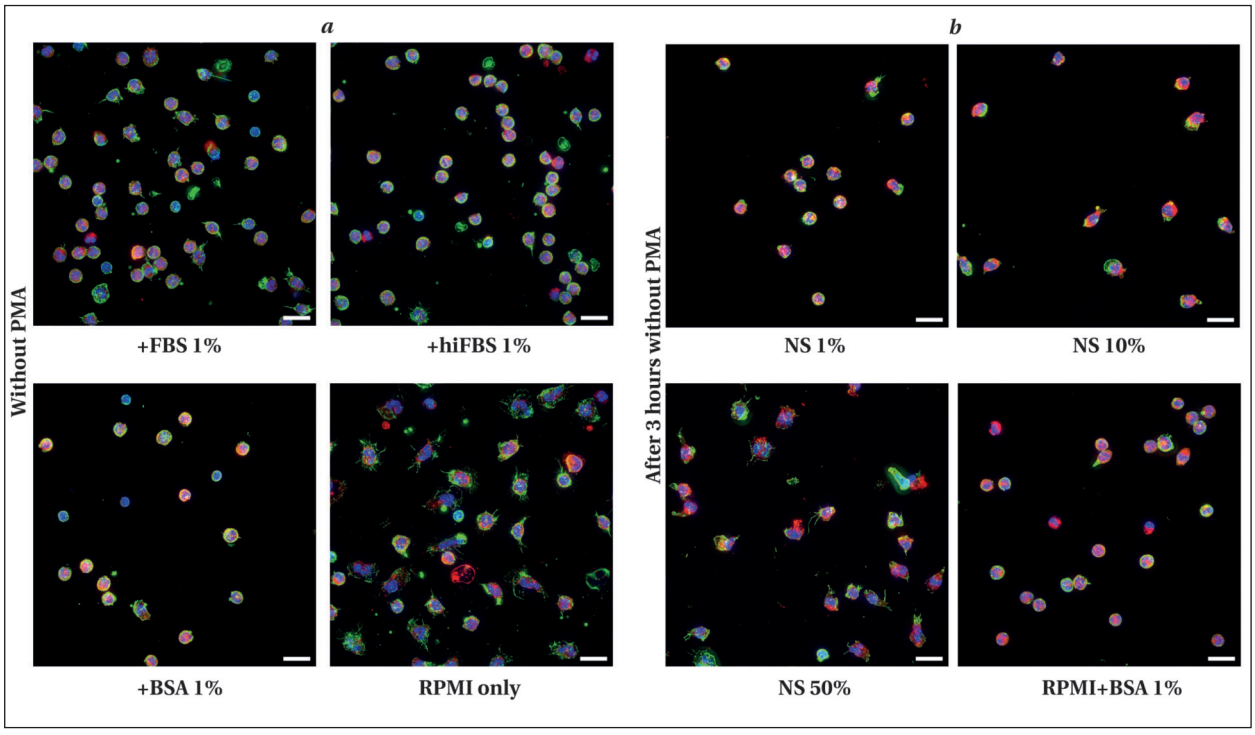

Fig. 1. Fluorescence images of neutrophils under different incubation conditions: effect of medium components (*a*) and plasma concentration (*b*).

Note. Blue indicates the nucleus, green indicates F-actin, and red indicates the membrane. Scale bar: 20 μm. FBS — fetal bovine serum; hiFBS — heat-inactivated fetal bovine serum; BSA — bovine serum albumin; NS — serum from apparently healthy (normal) newborns.

Kruskal–Wallis test was used to compare three independent groups, followed by a Dunn's multiple comparison test for post hoc analysis. Differences were considered statistically significant at $P<0.05$ (two-tailed).

Results and Discussion

The initial phase of the study focused on optimizing the experimental conditions for the main investigation. The basal medium was RPMI supplemented with HEPES. The goal was to determine the appropriate additional components of the medium and the optimal concentrations of neonatal plasma and PMA.

As part of the preliminary experiments, we compared the effects of 1% fetal bovine serum (FBS), 1% heat-inactivated FBS (hiFBS), 1% bovine serum albumin (BSA), and the basal medium alone on neutrophil status. Neutrophil morphology was assessed under each condition. Incubation of neutrophils in the basal medium alone resulted in widespread adhesion to the glass surface, indicating premature cell activation. Adding 1% FBS, hiFBS, or BSA equally suppressed this premature activation (Fig. 1, *a*).

BSA at 1% produced the most suitable reduction in neutrophil adhesion under our experimental conditions.

To determine the optimal dose of neonatal plasma, we assessed the effect of varying plasma concentrations on neutrophils (Fig. 1, *b*). Specifically, we compared the effects of 1%, 10%, and 50% plasma supplementation versus the basal medium. Representative images of neutrophils are shown in Fig. 1, *b*.

Adding 1% plasma to the working medium best preserved neutrophils in their intact state, while 10% and 50% plasma concentrations promoted adhesion to the surface.

Neutrophils were activated using PMA. In studies on NETs, PMA is commonly applied at concentrations ranging from 1 to 100 nM. For this experiment, the optimal PMA concentration was defined as the minimal dose that induces neutrophil activation in the presence of plasma.

Representative images of control and PMA-activated neutrophils are presented in Fig. 2.

Fluorescence microscopy data were used to quantify the number of activated neutrophils that

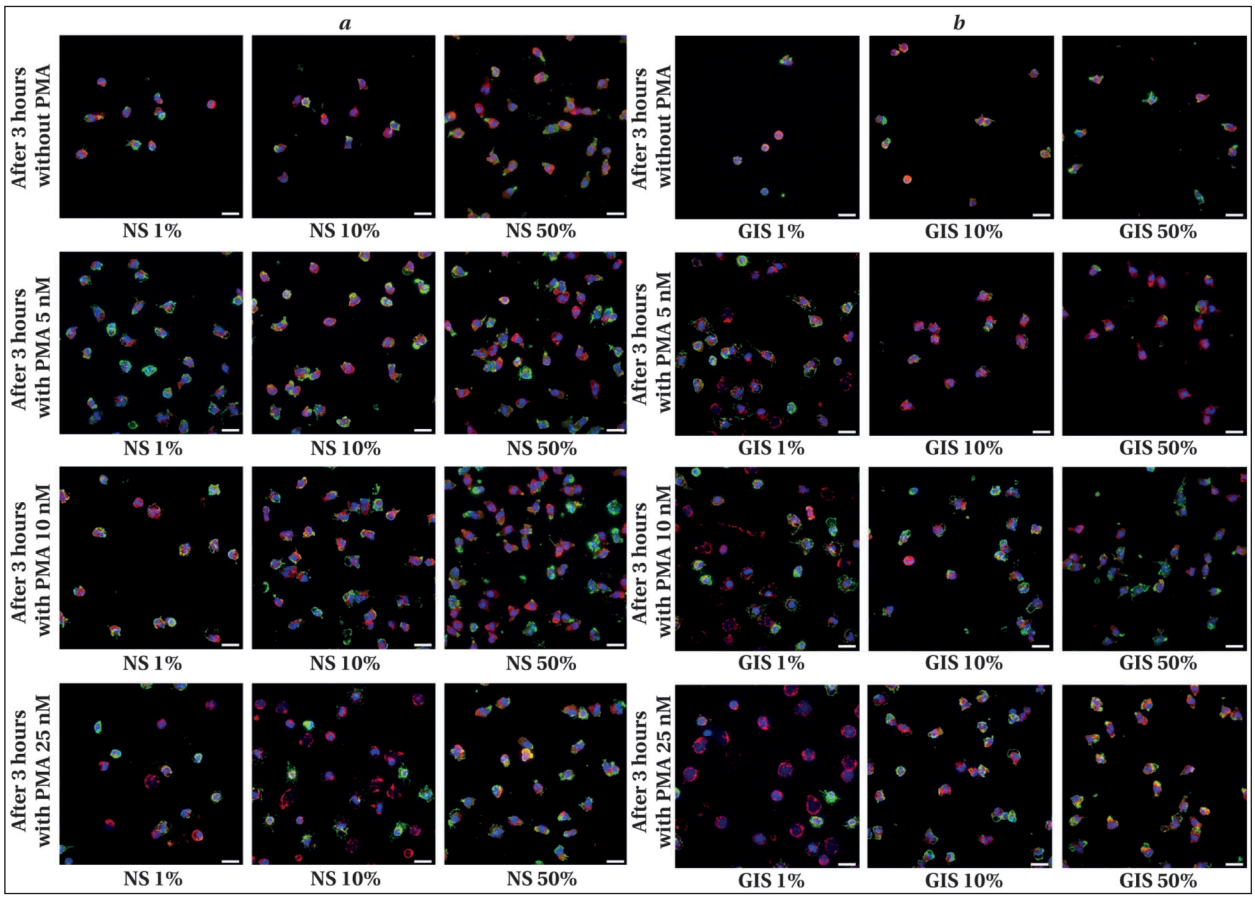

Fig. 2. Fluorescence images of neutrophils in working medium with added plasma from an apparently healthy newborn, at varying PMA concentrations.
Note. *a* — control neutrophils; *b* — neutrophils after activation. Blue indicates the nucleus, green indicates F-actin, and red indicates the membrane. Scale bar: 20 μm. NS — plasma samples from apparently healthy (normal) newborns; GIS — plasma samples from generalized infection group.

released NETs in each group. The analysis revealed that higher plasma concentrations, regardless of type, inhibited NET formation by neutrophils. The most effective condition for NET induction was observed with 1% plasma supplementation.

The number of NET-activated cells was calculated based on morphology and nuclear status. Representative fluorescence images used for quantification are shown in Fig. 3, *a* and 3, *b*.

Cells were considered NET-activated if they exhibited the following features: (1) disrupted segmented nuclear morphology, where the nucleus appeared as either a large «cloud» lacking structural organization or an elongated «arrow»-like shape; (2) absence of the actin cytoskeleton, where the presence of cortical actin is an indirect marker of functional integrity; and (3) the membrane no longer maintained a continuous structure. All other cells were classified as non-activated and intact. These included round or oval neutrophils with a diameter of 6–9 μm that exhibited segmented nuclei and cortical actin, as well as adherent cells with segmented nuclei that were spread across the glass surface and displayed prominent filopodia.

We analyzed morphological changes in neutrophils following incubation with various types of

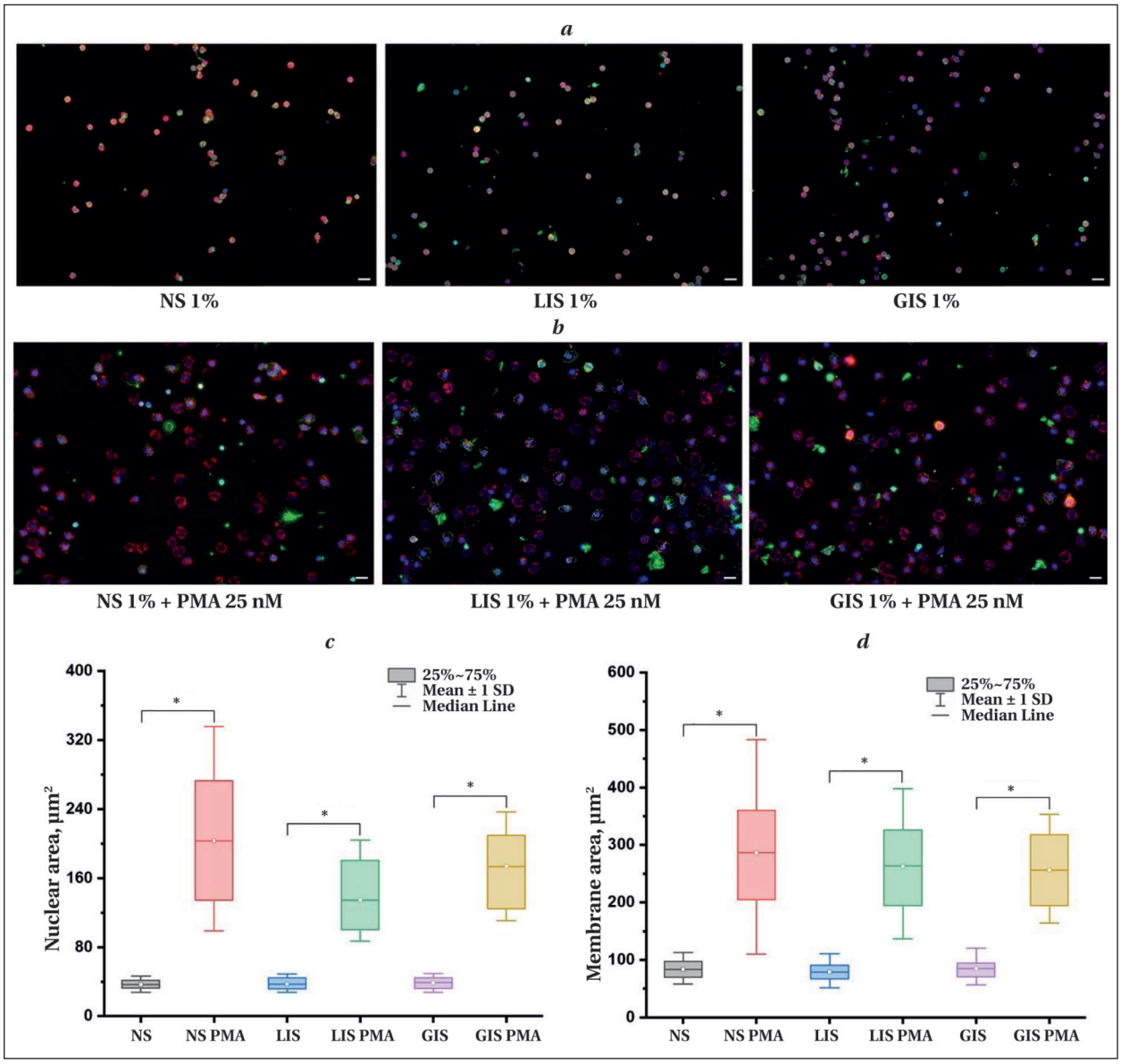

Fig. 3. Effect of different plasma types on neutrophil morphological changes following PMA stimulation.
Note: *a*, *b* — fluorescence images of neutrophils incubated with 1% plasma of various types, without stimulation (*a*) and after addition of PMA (*b*). Blue indicates the nucleus, green indicates F-actin, and red indicates the membrane. Scale bar: 20 μm. *c*, *d* — quantitative analysis of nuclear and membrane areas of neutrophils under different conditions. NS — serum from apparently healthy (normal) newborns; LIS — serum from newborns with localized infection; GIS — serum from newborns with generalized infection. Statistically significant differences within groups are indicated ($P<0.001$).

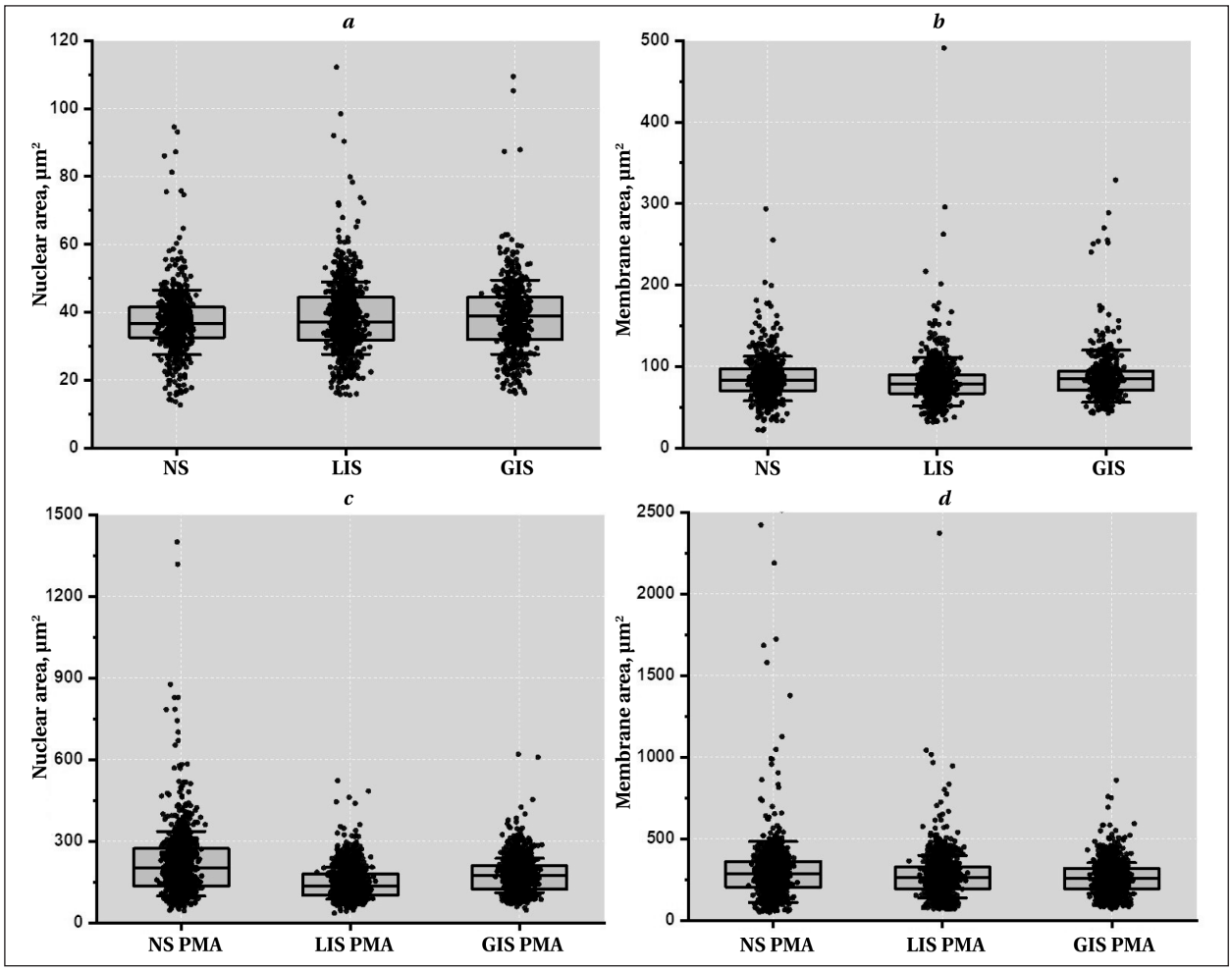

Fig. 4. Graphs showing changes in neutrophil nuclear and membrane areas.
Note. *a, b* — values prior to PMA stimulation; *c, d* — values after addition of PMA.

plasma and subsequent PMA stimulation. To this end, we examined the obtained fluorescent images and measured the areas of neutrophil nuclei and cytoplasmic membranes. It is well established that NET activation is accompanied by nuclear swelling and an increase in overall cell size [26] (Fig. 3, *c*, *d*). Following PMA stimulation, we observed a significant increase in nuclear area: in the NS group, from 37 μm² (33–42 μm²) to 203 μm² (135–273 μm²) (P<0.001); in the LIS group, from 37 μm² (32–44 μm²) to 134 μm² (101–180 μm²) (P<0.001); and in the GIS group, from 39 μm² (32–44 μm²) to 173 μm² (124–210 μm²) (P<0.001). Similar trends were observed for membrane area: NS, from 83 (70; 97) to 286 (205; 361) μm² (P<0.001); LIS, from 79 (67; 90) to 263 (194; 326) μm² (P<0.001); and GIS, from 85 (70; 95) to 256 (195; 318) μm² (P<0.001).

Analysis of the graphs revealed that non-activated neutrophils retained their segmented nuclear morphology and spherical shape. Following PMA stimulation, neutrophils exhibited a significant increase in nuclear and membrane area. At the same time, there was considerable variation in morphological parameters within the same plasma group, indicating heterogeneity in the effect of plasma on cells. Despite this variability, the general trend of morphological changes associated with NET activation was observed across all examined samples.

Figure 4 presents distribution plots of all measured nuclear and membrane areas of neutrophils before and after PMA stimulation, stratified by plasma type. Neutrophils incubated with plasma from neonates with generalized infection exhibited a significantly larger nuclear area prior to PMA stimulation compared to those treated with control plasma (χ^2=9.366; P=0.009).

After PMA activation, the distribution pattern of nuclear area values changed. The largest nuclear area was recorded in neutrophils incubated with plasma from apparently healthy neonates. Next were those exposed to plasma from the GIS group, followed by those treated with plasma from patients with localized infection (χ^2=339.295; P<0.001).

A similar trend was observed for the membrane area. Before PMA activation, the smallest membrane areas were found in neutrophils incubated with plasma from the LIS group (χ^2 = 26.396; P<0.001). However, after PMA stimulation, the largest mem-

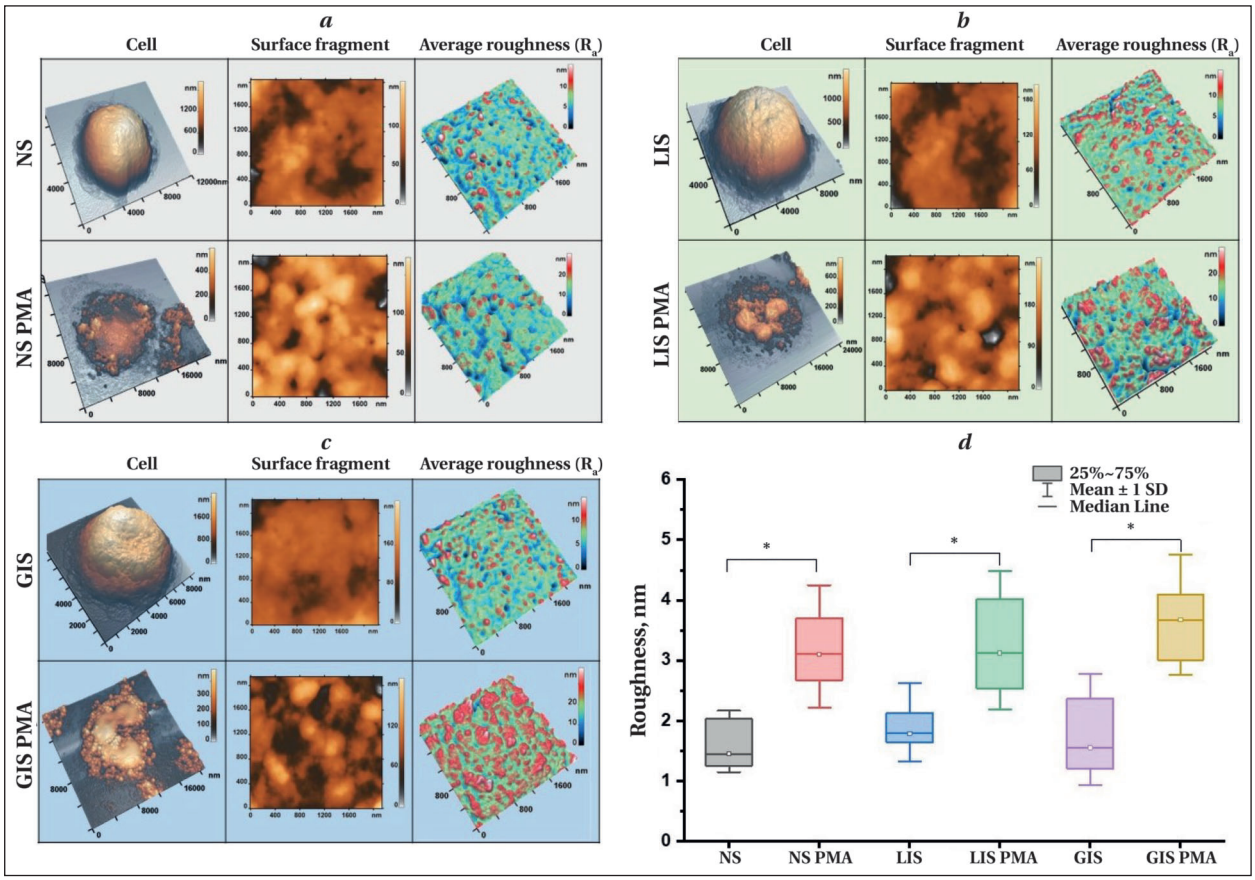

Fig. 5. AFM images of neutrophils and analysis of membrane roughness after exposure to plasma from different groups.
Note. *a–c* — 3D images of neutrophils (first column), membrane surface fragments (second column), and corresponding R_a maps (third column), obtained by atomic force microscopy (AFM) after incubation with plasma from the control group (NS) and from patients with localized (LIS) or generalized (GIS) infection, before and after PMA stimulation. *d* — graph showing changes in average membrane surface roughness across all experimental groups. Statistically significant within-group differences are indicated ($P<0.001$).

brane areas were found in neutrophils treated with control plasma ($\chi^2=37.663$; $P<0.001$).

Fig. 5 shows the mean membrane roughness values of neutrophils measured by AFM. Comparing non-activated groups, neutrophils incubated with plasma from apparently healthy donors, as well as those from LIS and GIS patients, demonstrated comparable roughness values. R_a values were 1.4 (1.2; 2.0) nm for NS, 1.8 (1.6; 2.1) nm for LIS, and 1.5 (1.2; 2.4) nm for GIS. Differences between groups were not statistically significant ($\chi^2=4.001$; $P=0.135$).

Detailed topographic images of neutrophil surfaces obtained by AFM were used for further analysis of cell surface features (Fig. 5, *a–c*).

After PMA activation, the membrane's shape changed significantly. All the studied groups had significantly higher R_a values than their non-activated controls. Neutrophils exposed to plasma from the NS group in the presence of PMA increased in R_a to 3.1 (2.7; 3.7) nm. The R_a values were 3.1 (2.5; 4.0) and 3.7 (3.0; 4.0) nm in the LIS and GIS PMA groups, respectively. While there was a general trend towards higher roughness, an intergroup comparison revealed a *P*-value of 0.072 ($\chi^2=5.255$), indicating no significant differences across groups. However, pairwise comparisons of PMA-activated and non-activated groups showed significant differences ($P<0.001$), indicating that activation affects membrane roughness characteristics.

The increase in R_a reflects the increased heterogeneity of the neutrophil surface after activation. Furthermore, PMA stimulation caused significant lateral expansion of the cells, consistent with recognized morphological characteristics of NET activation.

Fluorescence microscopy results showed that none of the plasma samples examined, regardless of patient group, had a deleterious effect on neutrophil morphology. The vast majority of cells in the control group, which did not receive PMA stimulation, maintained their morphology.

Neutrophils incubated with plasma from patients with localized infections exhibited the weakest response to stimulation, as indicated by nuclear area measurements. In contrast, neutrophils exposed to plasma from patients with generalized infections demonstrated comparable levels of NET activation to those in the control group. These results imply that the soluble factor profile in plasma from

localized infections stabilizes neutrophils within the circulation. Conversely, neutrophils appear more susceptible to chromatin network formation in the context of systemic infection, which may increase the risk of thrombosis and disseminated intravascular coagulation (DIC) in septic patients [30].

The results of the AFM analysis confirmed that, regardless of its origin, plasma did not have a significant damaging effect on neutrophils. In the absence of stimulation, neutrophils incubated with different plasma types maintained comparable membrane roughness values, indicating no substantial structural alterations. Upon PMA stimulation, all groups exhibited a similar increase in Ra values, reflecting a consistent rise in membrane surface heterogeneity. These observations suggest that NET-associated morphological changes to the cell surface occur to a similar extent, regardless of plasma origin.

Limitations. This study is limited by its relatively small sample size and the absence of neutrophil phenotypic characterization following incubation with plasma from neonates with varying degrees of infectious and septic complications.

Conclusion

Our findings shed light on the mechanisms underlying neutrophil alterations in neonates during infectious and septic conditions. These findings may also aid in developing new diagnostic and therapeutic approaches. We showed that plasma has different effects on neutrophil NET activation depending on the severity of the infectious and septic condition.

Based on these findings, future research could employ advanced biochemical and biophysical assays, along with flow cytometry, to examine the molecular composition of plasma and its influence on neutrophil responses. These approaches could help us better understand the signaling pathways and effector mechanisms that control neutrophil activation.

The methodology used here and its refinement pave the way for more in-depth investigations into the pathophysiology of neonatal sepsis. Changes in neutrophil membrane properties induced by plasma may be useful biomarkers for determining the severity of infectious and septic conditions in newborns.

Acknowledgments. The authors gratefully acknowledge the staff of the Core Facility Center at the N. K. Koltsov Institute of Developmental Biology of the Russian Academy of Sciences. Special thanks are extended to Dr. Elena E. Voronezhskaya, Head of the Center, for her invaluable support with fluorescence microscopy.

References

1. *Liu D., Huang S. Y., Sun J. H., Zhang H. C., Cai Q. L., Gao C., Li L., et al.* Sepsis-induced immunosuppression: mechanisms, diagnosis and current treatment options. *Mil Med Res.* 2022; 9 (1): 56. DOI: 10.1186/s40779-022-00422-y. PMID: 36209190.
2. *Понасенко А. В., Синицкий М. Ю., Хуторная М. В., Барбараш О. Л.* Генетические макеры системной воспалительной реакции в кардиохирургии (обзор). *Общая реаниматология.* 2017; 13 (6): 48–59. *Ponasenko A. V., Sinitsky M. Y., Khutornaya M. V., Barabash O. L.* Genetic markers of systemic inflammatory response in cardiac surgery (Review). *Gen Reanimatol = Obshchaya Reanimatologiya.* 2017; 13 (6): 48–59. (in Russ.&Eng.). DOI: 10.15360/1813-9779-2017-6-48-59.
3. *Mellhammar L., Wollter E., Dahlberg J., Donovan B., Olséen C.-J., Wiking P. O., Rose N., et al.* Estimating sepsis incidence using administrative data and clinical medical record review. *JAMA Netw Open.* 2023; 6 (8): e2331168. DOI: 10.1001/jamanetworkopen.2023.31168. PMID: 37642964.
4. *Образцов И. В., Рябов А. Ю., Цуранова Н. С., Балыкова Е. В., Парамонов А. И.* Функциональная активность нейтрофилов у пациентов с послеоперационными инфекционно-септическими осложнениями. *Российский иммунологический журнал.* 2019; 22 (4): 1393–401. *Obraztsov I. V., Ryabov A.Yu., Tsuranova N. S., Balykova E. V., Paramonov A. I.* Neutrophil function in patients with postsugery infectious septic complications. *Russian Journal of Immunology = Ross Immunol Zhurnal.* 2019; 22 (4): 1393–1401. (in Russ.). DOI: 10.31857/S102872210007042-1.
5. *Celik I. H., Hanna M., Canpolat F. E., Mohan Pammi.* Diagnosis of neonatal sepsis: the past, present and future. *Pediatr Res.* 2022; 91 (2): 337–350. DOI: 10.1038/s41390-021-01696-z. PMID: 34728808.
6. *Glaser M. A., Hughes L. M., Jnah A., Newberry D.* Neonatal sepsis: a review of pathophysiology and current management strategies. *Adv Neonatal Care.* 2021; 21 (1): 49–60. DOI: 10.1097/ANC.0000000000000769. PMID: 32956076.
7. *Образцов И. В., Жиркова Ю. В., Черникова Е. В., Крапивкин А. И., Брунова О. Ю., Абдраисова А. Т., Давыдова Н. В.* Значение функционального анализа фагоцитов для диагностики неонатального сепсиса. *Российский вестник перинатологии и педиатрии.* 2023; 68 (1): 24–29. *Obraztsov I. V., Zhirkova Y. V., Chernikova E. V., Krapivkin A. I., Brunova O. Y., Abdraisova A. T., Davydova N. V.* Feasibility of phagocytes functional testing in neonatal sepsis diagnostics. *Russian Bulletin of Perinatology and Pediatrics = Rossiyskiy Vestnik Perinatologii i Pediatrii.* 2023; 68 (1): 24–29. (in Russ.). DOI: 10.21508/1027-4065-2023-68-1-24-29.
8. *Ohbuchi A., Kono M., Kitagawa K., Takenokuchi M., Imoto S., Saigo K.* Quantitative analysis of hemin-induced neutrophil extracellular trap formation and effects of hydrogen peroxide on this phenomenon. *Biochem Biophys Reports.* 2017; 11: 147–153. DOI: 10.1016/j.bbrep.2017.07.009. PMID: 28955779.
9. *Parker H., Winterbourn C. C.* Reactive oxidants and myeloperoxidase and their involvement in neutrophil extracellular traps. *Front Immunol.* 2012; 3: 424. DOI: 10.3389/fimmu.2012.00424. PMID: 23346086.
10. *Zhang J., Shao Y., Wu J., Zhang J., Xiong X., Mao J.,Wei Y., et al.* Dysregulation of neutrophil in sepsis: recent insights and advances. *Cell Commun Signal.* 2025; 23 (1): 87. DOI: 10.1186/s12964-025-02098-y. PMID: 39953528.
11. *Sergunova V., Inozemtsev V., Vorobjeva N., Kozlova E., Sherstyukova E., Lyapunova S., Chernysh A.* Morphology of neutrophils during their activation and NETosis: atomic force microscopy study. *Cells.* 2023; 12 (17): 2199. DOI: 10.3390/cells12172199. PMID: 37681931.
12. *Dewitt S., Hallett M.* Leukocyte membrane «expansion»: a central mechanism for leukocyte extravasation. *J Leukoc Biol.* 2007; 81 (5): 1160–4. DOI: 10.1189/jlb.1106710. PMID: 17360954.
13. *Hallett M. B., Dewitt S.* Ironing out the wrinkles of neutrophil phagocytosis. *Trends Cell Biol.* 2007; 17 (5): 209–14. DOI: 10.1016/j.tcb.2007.03.002. PMID: 17350842.
14. *Гребенчиков О. А., Касаткина И. С., Каданцева К. К., Мешков М.А., Баева А. А.* Влияние лития хлорида на активацию нейтрофилов под действием сыворотки пациентов с септическим шоком. *Общая реаниматология.* 2020; 16 (5): 45–55. *Grebenchikov O. A., Kasatkina I. S., Kadantseva K. K., Meshkov M. A., Bayeva A. A.* The effect of lithium chloride on neutrophil activation on exposure to serum of patients with septic shock. *Gen Reanimatol = Obshchaya Reanimatologiya.* 2020; 16 (5): 45–55. (in Russ.&Eng.). DOI: 10.15360/1813-9779-2020-5-45-55.
15. *Образцов И. В., Годков М. А., Кулабухов В. В., Владимирова Г. А., Измайлов Д. Ю., Проскурнина Е. В.* Функциональная активность нейтрофилов при ожоговом сепсисе. *Общая реаниматология.* 2017; 13 (2): 40–51. *Obraztsov I. V., Godkov M. A., Kulabukhov V. V., Vladimirova G. A., Izmailov D. Y., Proskurnina E. V.* Functional activity of neutrophils in burn sepsis. *Gen Reanimatol = Obshchaya Reanimatologiya.* 2017; 13 (2): 40–51. (in Russ.&Eng.). DOI: 10.15360/1813-9779-2017-2-40-51.
16. *Starostin D. O., Kuzovlev A. N., Dolgikh V. T., Grebenchikov O. A., Polyakov P. A., Grechko A. V.* Influence of sevoflurane on neutrophils in patients with sepsis. *Russ J Anesthesiol Reanimatol.* (in Russ.&Eng.). 2024; (5): 50. DOI: 10.17116/anaesthesiology202405150.
17. *Liu S., Han Y., Kong L., Wang G., Ye Z.* Atomic force microscopy in disease-related studies: exploring tissue and cell mechanics. *Microsc Res Tech.* 2024; 87 (4): 660–684. DOI: 10.1002/jemt.24471. PMID: 38063315.
18. *Dumitru A. C., Koehler M.* Recent advances in the application of atomic force microscopy to structural biology. *J Struct Biol.* 2023; 215 (2): 107963. DOI: 10.1016/j.jsb.2023.107963. PMID: 37044358.
19. *Kerdegari S., Canepa P., Odino D., Oropesa-Nuñez R., Relini A., Cavalleri O., Canale C.* Insights in cell biomechanics through atomic force microscopy. *Mate-*

rials (Basel). 2023; 16 (8): 2980.
DOI: 10.3390/ma16082980. PMID: 37109816.
20. *Sokolov I., Iyer S., Woodworth C. D.* Recovery of elasticity of aged human epithelial cells *in vitro*. *Nanomedicine*. 2006; 2 (1): 31–36.
DOI: 10.1016/j.nano.2005.12.002. PMID: 17292113.
21. *Pérez-Domínguez S., Kulkarni S. G., Rianna C., Radmacher M.* Atomic force microscopy for cell mechanics and diseases. *Neuroforum*. 2020; 26 (2): 101–109. DOI: 10.1515/nf-2020-0001.
22. *Makarova N., Kalaparthi V., Seluanov A., Gorbunova V., Dokukin M. E., Sokolov I.* Correlation of cell mechanics with the resistance to malignant transformation in naked mole rat fibroblasts. *Nanoscale*. 2022; 14 (39): 14594–14602.
DOI: 10.1039/D2NR01633h. PMID: 36155714.
23. *Burn G. L., Foti A., Marsman G., Patel D. F., Zychlinsky A.* The Neutrophil. *Immunity*. 2021; 54 (7): 1377–1391.
DOI: 10.1016/j.immuni.2021.06.006. PMID: 34260886.
24. *Tilley D. O., Abuabed U., Arndt U. Z., Schmid M., Florian S., Jungblut P. R., Brinkmann V., et al.* Histone H3 clipping is a novel signature of human neutrophil extracellular traps. *Elife*. 2022; 11: e68283.
DOI: 10.7554/eLife.68283. PMID: 36282064.
25. *Thiam H. R., Wong S. L., Qiu R., Kittisopikul M., Vahabikashi A., Goldman A. E., Goldman R. D., et al.* NETosis proceeds by cytoskeleton and endomembrane disassembly and PAD4-mediated chromatin decondensation and nuclear envelope rupture. *Proc Natl Acad Sci*. 2020; 117 (13): 7326–7337.
DOI: 10.1073/pnas.1909546117. PMID: 32170015.
26. *Inozemtsev V., Sergunova V., Vorobjeva N., Kozlova E., Sherstyukova E., Lyapunova S., Chernysh A.* Stages of NETosis Development upon Stimulation of Neutrophils with Activators of Different Types. *Int J Mol Sci*. 2023; 24 (15): 12355.
DOI: 10.3390/ijms241512355. PMID: 37569729.
27. *Wei M., Zhang Y., Wang Y., Liu X., Li X., Zheng X.* Employing atomic force nicroscopy (AFM) for microscale investigation of interfaces and interactions in membrane fouling processes: new perspectives and prospects. *Membranes (Basel)*. 2024; 14 (2): 35.
DOI: 10.3390/membranes14020035. PMID: 38392662.
28. *Миронов В. Л.* Основы сканирующей зондовой микроскопии. Нижний Новгород: Российская академия наук, Институт физики микроструктур; 2004: 110. *Mironov V. L.* Fundamentals of scanning probe microscopy. Nizhny Novgorod: Russian Academy of Sciences, Institute of Physics of Microstructures; 2004: 110. (in Russ.).
29. *Schneider C. A., Rasband W. S., Eliceiri K. W.* NIH Image to imageJ: 25 years of image analysis. *Nat Methods*. 2012; 9 (7): 671–675.
DOI: 10.1038/nmeth.2089. PMID: 22930834.
30. *Zhou Y., Xu Z., Liu Z.* Impact of neutrophil extracellular traps on thrombosis formation: new findings and future perspective. *Front Cell Infect Microbiol*. 2022; 12: 910908.
DOI: 10.3389/fcimb.2022.910908. PMID: 35711663.

Received 01.04.2025
Accepted 27.05.2025
Online first 09.06.2026

https://doi.org/10.15360/1813-9779-2025-3-2566

Sepsis: A Brief Overview of the Key Concepts

Pavel G. Malkov[1]*, Georgy A. Frank[2]

[1] M. V. Lomonosov Moscow State University,
1 Leninskiye gory Str., 119991 Moscow, Russia
[2] Russian Medical Academy of Continuous Professional Education, Ministry of Health of Russia,
2/1 Barrikadnaya Str., Bldg. 1, 125993 Moscow, Russia

For citation: *Pavel G. Malkov, Georgy A. Frank.* Sepsis: A Brief Overview of the Key Concepts. *Obshchaya Reanimatologiya = General Reanimatology.* 2025; 21 (3). https://doi.org/10.15360/1813-9779-2025-3-2566 [In Russ. and Engl.]

***Correspondence to:** Pavel G. Malkov, malkovp@yandex.ru

Summary

The issue of sepsis has been discussed extensively in the medical and scientific community for decades. However, a unified understanding of the biological nature of this condition has yet to be established.

Aim. To provide a structured review of the key concepts commonly used in clinical practice and in the scientific literature related to sepsis.

Materials and Methods. A review of the scientific literature combined with the authors' professional experience.

Results. From a methodological perspective, it is suggested to conceptualize sepsis as a pathological condition due to generalized suppurative process. In this case, typical sepsis and septic shock are proposed to be considered two pathogenically separate, independently developing anatomo-clinical forms of sepsis.

Conclusion. It is proposed to consider as sepsis only conditions associated with pathogens that are capable of causing purulent inflammation. Non–purulent conditions not associated with pathogens of purulent infections are considered as generalization of bacterial, viral, protozoal, fungal diseases that may acquire toxic and especially toxic clinical forms designated as bacterial-toxic, or infectious-toxic (but not septic) shock. Typical sepsis and septic shock are proposed to be considered as independently developing clinical and anatomical forms of sepsis rather than the sequentially developing stages of the pathological condition.

Keywords: sepsis; septic shock

Conflict of interest. The authors declare no conflict of interest.

Information about the authors:
Pavel G. Malkov: https://orcid.org/0000-0001-5074-3513
Georgy A. Frank: https://www.scopus.com/authid/detail.uri?authorId=57212995964

Introduction

Sepsis has long been one of the most debated topics in modern medicine [11]. The key terms used in the discussion of sepsis still lack clear and universally accepted definitions. The terminology and interpretations provided by official WHO bodies are highly ambiguous, hindering a deeper understanding of the biological nature of sepsis and the core principles for formulating a diagnosis.

According to the Third International Consensus Definitions for Sepsis and Septic Shock (Sepsis-3), sepsis is defined as «a life-threatening organ dysfunction caused by a dysregulated host response to infection» [1].

It is further noted that «Most types of microorganisms can cause sepsis, including bacteria, fungi, viruses and parasites, such as those that cause malaria. Bacteria such as *Streptococcus pneumoniae, Haemophilus influenzae, Staphylococcus aureus, Escherichia coli, Salmonella* spp. and *Neisseria meningitidis* are the most common etiological pathogens. Manifestations of sepsis and septic shock can be the fatal complication of infections with seasonal influenza viruses, dengue viruses and highly transmissible pathogens of public health concern such as avian and swine influenza viruses, severe acute respiratory syndrome coronavirus, Middle East respiratory syndrome coronavirus and most recently, Ebola and yellow fever viruses». [2].

This broad interpretation effectively blurs the distinction between generalized suppurative infections and generalized forms of other (non-purulent) infections, as well as syndromes classified in ICD-10 [3], such as

— septicemia, including septic shock (A41.9),
— toxic shock syndrome (A48.3),
— septic shock (R57.2),
— other (endotoxin-mediated) shock (R57.8),
— systemic inflammatory response syndrome (SIRS), including severe sepsis (R65.1).

At the same time, the Sepsis-3 consensus introduced several notable advancements. First, systemic inflammatory response syndrome (R65) was removed from the diagnostic criteria for sepsis, removing a significant degree of clinical ambiguity. However, the current definition — «a life-threatening organ dysfunction caused by a dysregulated host response to infection» [1] — itself remains somewhat vague.

Table 1. Fundamental Differences Between Sepsis and Typical (Classical) Infections

Characteristic	Sepsis	Typical (Classical) Infections
Causative agent	Not monocausal	Monocausal*
Isolation of pure culture	Not always possible	Possible*
Experimental reproducibility	Impossible	Possible*
Contagiousness	Not contagious	Contagious**
Course pattern	Non-cyclic	Cyclic**
Immunity development	Does not occur	Occurs**
Typical organ-specific lesions	Absent	Present**
Primary infectious complex	Absent	Present
Primary septic focus	Present	Absent

Note. * — criteria from Koch's postulates. ** — consequences derived from Koch's postulates.

Second, a new definition of septic shock was introduced, described as «a subset of sepsis in which underlying circulatory and cellular/metabolic abnormalities are profound enough to substantially increase mortality» [1, 4].

By introducing the term septic shock, the Sepsis-3 international consensus effectively recognizes the conceptual model of sepsis developed more than 70 years ago by Academician I. Davydovsky [5]. In fact, septic shock closely corresponds to the variant of sepsis without the formation of purulent metastatic foci — previously referred to as septicemia in the Soviet and Russian literature.

To the best of our knowledge, this condition does not correspond to the «purulent-resorptive fever» described by Davydovsky, which he defined as «a fairly routine intoxication originating from a wound and associated with the periodic entry of non-sterile degradation products from the wound into the circulation» [6].

Main Provisions of the Paper

The purpose of this publication is to present in a structured manner the key concepts traditionally used in clinical practice and the scientific literature when discussing sepsis. The issues of postmortem verification of organ dysfunction — as critical diagnostic features of typical sepsis and septic shock — have been comprehensively addressed in the article by Rybakova M. (2021) [7].

Although sepsis is caused by microorganisms (infectious agents), it is clear that it does not fulfill all the classical criteria of a typical infectious disease (Table 1):

- it lacks a single, typical causative agent (i.e., it is not monocausal);
- in most cases, the pathogen cannot be isolated in pure culture;
- it cannot be reliably reproduced in experimental models;
- it is not contagious;
- it does not follow a cyclical course;
- it does not induce specific immunity;
- it does not produce characteristic organ lesions;
- it does not present with a classic infectious complex (e. g., primary affect, lymphangitis, lymphadenitis), but typically involves a primary septic focus.

It is important to emphasize that the first three criteria represent the essential characteristics of infection according to the classical Koch's postulates, while the remaining ones are direct logical consequences. As a result, sepsis has characteristics that are in many ways the exact opposite of those of classical infections. Therefore, the direct attribution of sepsis to infection as its cause seems to be fundamentally incorrect.

According to I. V. Davydovsky, neither sepsis nor purulent-resorptive fever — although caused by infectious agents — should be considered «infectious diseases in the strict sense» [5, 6].

It is also noteworthy that sepsis is extremely difficult to reproduce in experimental settings [8, 9], despite numerous modeling attempts. The pathological processes induced in these experiments differ significantly from clinical human sepsis.

Sepsis is currently defined as «life-threatening organ dysfunction caused by a dysregulated host response to infection» [8]. However, such a definition allows for the conflation of two distinct concepts — «infection» and «infectious agent» — a logical fallacy known as ignoratio elenchi, which violates the fundamental law of identity in classical logic. The use of the term «infection» without appropriate clarification serves as a rhetorical device that allows sepsis to be indiscriminately associated with any infectious disease or infectious agent. This is logically flawed: first, because sepsis does not meet the classical criteria of Koch's postulates (see Table 1); and second, because not every infectious agent is capable of inducing sepsis.

Traditionally, in the Russian medical literature, sepsis was described as a generalized purulent process characterized by the presence of a localized septic focus and systemic dissemination either in the form of purulent metastases (septicopyemia) or as infectious-toxic shock (septicemia) [5].

Given that the spread of the infectious process occurs in a wide range of bacterial (e. g. typhoid fever, epidemic typhus, tuberculosis, syphilis), viral (e. g. viral hepatitis, smallpox, viral hemorrhagic fevers), protozoal (e. g., schistosomiasis, trypanosomiasis), fungal (e. g., systemic candidiasis), chlamy-

dial (e. g., ornithosis), mycoplasmal, and other diseases, it is obvious that a clear distinction must be made between these conditions and sepsis. This requires careful consideration of the following points:

1. The concept of sepsis is not the same as that of infection, even when qualified by phrases such as «life-threatening organ dysfunction».

2. The concept of sepsis is not synonymous with that of generalized infection, regardless of similarities in their clinical presentations.

3. The ability — or inability — of a given infectious agent to induce purulent inflammation is a defining criterion.

It is important to emphasize that sepsis is not an infection in the classical sense, but rather a generalized suppurative process, underscoring the need to distinguish sepsis from generalized forms of common infections.

This definition logically leads to the following conclusions

1. Generalized forms of typical infections caused by pathogens incapable of inducing purulent inflammation (such as certain bacteria, mycoplasmas, viruses, protozoa, fungi, etc.) should not be classified as sepsis.

2. Generalized forms of typical infections that retain the basic characteristics of classical infectious diseases (e. g., transmissibility) should not be classified as sepsis.

3. Shock or toxic states associated with highly virulent forms of classical infections should be considered complications of the primary disease, not septic shock.

The spread of the septic process occurs by hematogenous or lymphatic routes. However, as noted, «the blood and lymph of healthy individuals regularly transport various microorganisms. In conditions such as malnutrition, surgery, or other traumatic insults, bacteremia is a common occurrence» and therefore «bacteremia alone is not evidence of sepsis» [5].

Examples of proper documentation of the cause of death in the medical death certificate.

Ia) Infectious-toxic shock (A48.3)
b) Typhoid fever (A01.0)
c) —
d) —

or

Ia) Endotoxic shock (R57.8)
b) Coronavirus infection (U07.1)
c) —
d) —

According to the Sepsis-3 consensus, there are two distinct clinicopathologic subsets of sepsis: typical sepsis (sepsis, septicemia) and septic shock. These are not sequential stages of a single disease, but rather mutually exclusive, independent clinicopathologic entities. It follows that typical sepsis should not be viewed as a condition that inevitably progresses to septic shock, nor should septic shock be viewed as a direct consequence of typical sepsis.

The immediate cause of death (line Ia of the medical death certificate) should include either sepsis (A40-A41) or septic shock (R57.2), but not both.

Example of an incorrect entry for the cause of death on the medical death certificate:

Ia) Septic shock (R57.2)
b) Sepsis due to *Staphylococcus aureus* (A41.0)
c) Skin abscess, furuncle and carbuncle of buttocks (L02.3)
d) —

Example of correct entry:

Ia) Sepsis due to *Staphylococcus aureus* (A41.0)
b) Skin abscess, furuncle and carbuncle of buttocks (L02.3)
c) —
d) —

Although it is well established that sepsis lacks a single specific causative pathogen — reflecting its polyetiologic or non-monocausal nature — some empirical observations have been reported regarding the etiologic features of different clinicopathologic forms of sepsis [10] (Table 2). However, these findings remain anecdotal and lack robust statistical validation.

The identification of Gram-negative bacteria as the more common etiologic agents in septic shock and Gram-positive bacteria as the more common culprits in typical sepsis underscores the fundamental distinction between the two major clinicopathologic forms of sepsis defined by the Sepsis-3 consensus, namely typical sepsis and septic shock. This supports the conclusion that they are not sequential stages of the same disease process, but rather distinct and mutually exclusive clinicopathologic entities.

Table 2. Selected Etiological Features of Sepsis [10].

Staphylococcus aureus
• Widespread small-focus purulent metastases
• Tricuspid valve septic endocarditis
Streptococcus pyogenes
• Large-focus purulent metastases
• Mitral valve septic endocarditis
Streptococcus pneumoniae
• Tendency toward granulomatous reactions
Gram-negative bacteria
• Bacterial shock (currently defined as septic shock)

Professor I. V. Davydovsky noted that «in practice, the question of the causative agent of sepsis is reduced [almost exclusively] to three of the oldest symbionts of the human body: staphylococci, streptococci, and Escherichia coli. These microbes are completely uncharacteristic for entering into complex nosological relationships with the host» [5].

The view that extensive purulent foci — such as diffuse purulent peritonitis, pleural empyema, deep fascial phlegmons, and multiple large pulmonary abscesses – may actually inhibit the formation of metastatic purulent lesions seems justified [10]. Therefore, they cannot be considered as sources of generalized purulent dissemination and, consequently, should not be considered as causes of sepsis. Shock or toxic syndromes associated with such extensive purulent foci should be interpreted as complications of the underlying disease rather than as manifestations of sepsis or septic shock.

Example of an incorrect entry of the cause of death on the medical death certificate:

I a) Sepsis due to *Staphylococcus aureus* (A41.0)

b) Generalized purulent peritonitis (K65.0)

c) Diverticular disease of the colon with perforation and abscess (K57.2)

d) —

Example of a correct entry of the cause of death on the medical death certificate:

I a) Toxic shock syndrome (A48.3)

b) Generalized purulent peritonitis (K65.0)

c) Diverticular disease of the colon with perforation and abscess (K57.2)

d) —

The core terms and concepts traditionally used in discussions of sepsis require further clarification.

The term sepsis is equivalent to septicemia, and in the English-language literature the two are conventionally used interchangeably — they are considered complete synonyms.

Historically, in the Russian medical literature, septicemia referred specifically to sepsis without the formation of purulent metastases. However, this interpretation was not accepted by the international professional community. It was only with the Sepsis-3 consensus (2016) that the new term septic shock was introduced, which effectively describes the same condition — sepsis without suppurative metastasis.

Given the introduction of the term septic shock, the term septicemia should now be reserved for its original meaning: in English, septicemia is synonymous with sepsis.

The term septic shock, newly defined by the Sepsis-3 Consensus (2016), refers to a form of sepsis characterized by the absence of purulent metastases and accompanied by severe systemic intoxication and clinical signs of shock.

The term severe sepsis is used to describe typical sepsis with the formation of purulent metastases and prominent infectious and toxic manifestations, but without being classified as septic shock.

The term septicopyemia still used in the Russian literature has no equivalent in English; it was introduced as the opposite of septicemia, referring to typical sepsis with purulent metastasis development.

The term bacteremia refers to a transient condition characterized by the transport of bacteria (or bacterial colonies) through the bloodstream, often accompanied by bacterial embolism. Blood cultures are not consistently positive, which can only be explained by the fact that blood is not a habitat, but a transport medium in the hematogenous dissemination of the suppurative process. It is no coincidence that bacteremia (A49.9) is excluded from the diagnostic criteria for sepsis.

The terms toxic shock and infectious toxic shock are combined in ICD-10 into a single category, toxic shock syndrome, including bacterial toxic shock (A48.3).

The term endotoxin-associated shock is included into a separate ICD-10 category «Other shock» (R57.8), although all of these conditions are clinically identical and differ only in the primary damaging effect, which is of an «overwhelming force» nature.

The term systemic inflammatory response syndrome (SIRS) is classified under the three-character code R65 in ICD-10. The Sepsis-3 Consensus (2016) does not remove the term completely, but only excludes it from the diagnostic criteria for sepsis. In addition, one of the four-digit subcategories is recommended for use in coding severe sepsis (R65.1).

Conclusion

1. Sepsis is a generalized suppurative process that is fundamentally different from typical infections. It is polyetiologic (not caused by a single agent), the pathogen usually cannot be isolated in pure culture, it cannot be reliably reproduced experimentally, it is not contagious, it does not follow a cyclical course, it does not induce specific immunity, and it lacks characteristic organ involvement. It typically originates from a primary septic focus rather than a primary infectious complex.

1.1 Generalized forms of infection caused by pathogens that do not induce purulent inflammation and that have characteristic features of classical infections should not be classified as sepsis.

1.2 Generalization of the suppurative process occurs by hematogenous or lymphogenous routes. However, bacteremia (A49.9) is not a defining diagnostic feature of sepsis because the blood does not serve as a habitat but merely as a transport medium during the hematogenous spread of the suppurative process.

2. Typical sepsis (A40-A41), including severe sepsis (R65.1), is primarily caused by Gram-positive flora and is characterized by the presence of multiple purulent metastases. Septic shock (R57.2), typically caused by gram-negative flora, presents predominantly with features of bacterial toxin-mediated shock, while purulent metastases generally do not have time to form by the time of death. Special types of sepsis — such as bacterial (infective) endocarditis (I33) and chronic sepsis (sepsis lenta) — do not have distinct ICD-10 codes.

2.1 Typical sepsis (including severe sepsis) and septic shock should be considered distinct clinicopathologic entities. Sepsis should not be considered a condition that necessarily progresses to septic shock, nor should septic shock be considered a direct consequence of sepsis.

2.2 Extensive purulent foci such as diffuse purulent peritonitis, pleural empyema, compartmental pleural effusions, and multiple large pulmonary abscesses tend to inhibit the development of purulent metastases. Therefore, they should not be considered sources of generalized purulent spread and, consequently, should not be considered causes of sepsis. Shock states or intoxication syndromes associated with extensive purulent foci should be considered a complication of the underlying disease rather than manifestations of sepsis or septic shock.

2.3 Despite similarities in clinical presentation between septic shock and shock syndromes associated with typical infections, the latter should be distinguished from sepsis by the presence of features characteristic of classical infections. Shock associated with highly toxic forms of typical infections should be considered a complication of the primary disease rather than septic shock.

3. It is suggested not to use the terms septicopyemia and septicemia anymore. The contemporary equivalent of septicopyemia could be «typical sepsis», while septicemia corresponds to the term defined as «septic shock».

References

1. *Singer M., Deuschman C. S., Seymour C. W., Shankar-Hari M., Annane D., Bauer M., Bellomo R., et al.* The Third International Consensus definitions for sepsis and septic shock (Sepsis-3). *JAMA.* 2016; 315 (8): 801–810.
   DOI: 10.1001/jama.2016.0287. PMID: 26903338.
2. Совершенствование профилактики, диагностики и клинического ведения сепсиса. Доклад Исполнительного комитета Всемирной организации здравоохранения по пункту 7.2 предварительной повестки дня к 140-й сессии Исполнительного комитета (EB 140/12). 2. Improving the prevention, diagnosis, and clinical management of sepsis. Report of the Executive Committee of the World Health Organization on item 7.2 of the provisional agenda for the 140th session of the Executive Committee (EB 140/12). 2017. (in Russ.). https://apps.who.int/gb/ebwha/pdf_files/EB140/B140_12-ru.pdf.
3. Международная статистическая классификация болезней и проблем, связанных со здоровьем: Десятый пересмотр. Всемирная организация здравоохранения. 1992, 2003, 2021. Официальное издание на русском языке в 3-х т. Министерство здравоохранения Российской Федерации. 2003. International Statistical Classification of Diseases and Related Health Problems: The tenth revision. The World Health Organization. 1992, 2003, 2021. The official publication in Russian in 3 volumes. Ministry of Health of the Russian Federation. 07.04. 2021. (in Russ.).
4. *Shankar-Hari M., Phillips G. S., Levy M. L., Seymour C. W., Liu V. X., Deutschman C. S., Angus D. C., et al.* Developing a new definition and assessing new clinical criteria for septic shock for the Third International Consensus Definitions for Sepsis and Septic Shock (Sepsis-3). *JAMA.* 2016; 315 (8): 775–787.
   DOI: 10.1001/jama.2016.0289. PMID: 26903336.
5. *Давыдовский И. В.* Сепсис. В кн.: Патологическая анатомия и патогенез болезней человека. Том 1. Инфекционные болезни. М.: Медгиз; 1956: 541–574. *Davydovsky I. V.* Sepsis. In: Pathological anatomy and pathogenesis of human diseases. Volume 1. Infectious diseases. Moscow: Medgiz; 1956: 541–574. (in Russ.).
6. *Давыдовский И. В.* Гнойно-резорбтивная лихорадка. В кн.: Патологическая анатомия и патогенез болезней человека. Том 1. Инфекционные болезни. М.: Медгиз; 1956: 574–595. *Davydovsky I. V.* Purulent-resorptive fever. In: Pathological anatomy and pathogenesis of human diseases. Volume 1. Infectious diseases. Moscow: Medgiz; 1956: 574–595. (in Russ.).
7. *Рыбакова М. Г.* Сепсис: от синдрома системной воспалительной реакции до органной дисфункции. *Архив патологии.* 2021; 83 (1): 67–72. *Rybakova M. G.* Sepsis: from systemic inflammatory response syndrome to organ dysfunction. *Russian Journal of Archive of Pathology = Arkhiv Patologii.* 2021; 83 (1): 67–72. (in Russ.).
   DOI: 10.17116/patol20218301167.
8. *Черкасова М. Н.* К проблеме экспериментального моделирования сепсиса. *Успехи современной биологии.* 2021; 141 (4): 368–381. *Cherkasova M. N.* On the problem of experimental modeling of sepsis. *The Successes of Modern Biology = Uspekhi Sovremennoy Biologii.* 2021; 141 (4): 368–381. (in Russ.).
   DOI: 10.31857/S0042132421030054.
9. *Rittirsch D., Hoesel L. M., Ward P. A.* The disconnect between animal models of sepsis and human sepsis. *J Leukoc Biol.* 2007; 81 (1): 137–143.
   DOI: 10.1189/jlb.0806542. PMID: 17020929.
10. *Пархоменко Ю. Г.* Сепсис: Современное состояние, диагностика и спорные проблемы классификации. *Архив патологии.* 2005; 67 (6): 53–57. *Parkhomenko Yu. G.* Sepsis: state of the art, diagnosis and disputable problems of classification. *Russian Journal of Archive of Pathology = Arkhiv Patologii.* 2005; 67 (6): 53–57. (in Russ.).
11. *Мишнев О. Д., Гринберг Л. М., Зайратьянц О. В.* Актуальные проблемы патологии сепсиса: 25 лет в поисках консенсуса. *Архив патологии.* 2016; 78 (6): 3–8. *Mishnev O. D., Grinberg L. M., Zairatyants O. V.* Actual problems of the pathology of sepsis: 25 years in search of a consensus. *Russian Journal of Archive of Pathology = Arkhiv Patologii.* 2016; 78 (6): 3–8. (in Russ.).
    DOI: 10.17116/patol20167863-8.

Received 28.03.2025
Accepted 23.04.2025
Online first 29.04.2025

Basic information for the manuscript submission (v. April 21, 2025)

1. Initial submission

Authors should submit a single Word file containing the complete manuscript. Language of submission: Russian — for Russian-speaking authors. English — for non-Russian-speaking authors.

The file must include the following components:

- Title of the paper
- Full names of all authors
- Institutional affiliations of all authors
- Full manuscript text, including all sections
- Tables, figures, and photographs with captions and explanatory note
- Reference list

2. File Naming Format

Name the file using the first author's last name and the submission date in the format: LastName_YYYYMMDD.docx . For revised versions, only the date should be updated.

3. Manuscript Length

Original article: approximately 40,000 characters with spaces

Short communication: no more than 2,500 words

Review or meta-analysis: between 25,000 and 40,000 characters with spaces

4. Title Page Information

Title: must not exceed 12 words

Authors: full names (e.g., Peter A. Johnson)

Affiliations: full institutional names and postal addresses with zip code

Corresponding author: full name, email address, and phone number

5. Structure of summary, body text, References

Summary (Abstract): must be between 250 and 300 words and structured into the following sections:

- Introduction (background/scope of the problem)
- Aim
- Materials and Methods
- Results
- Conclusion

Highlights (optional): one to three main messages may be presented either in textual or infographic form. Text highlights should not exceed 40 words each.

Keywords: 6–8 keywords, separated by semicolons (;). Do not place a period at the end.

Post-keyword Informational Sections:

- Conflict of interest
- Study funding
- Acknowledgements (optional)
- Information about the Authors (ID, contributions)

Body text:

- Introduction (Background)
- Materials and Methods
- Results
- Discussion
- Conclusion

References: at least 70% of the references should be published within the last 5 years, and at least 30% within the last 3 years. Number of references: original articles — 25 to 45; short communications — 10 to 25; reviews — 80 to 120. Formatting: must comply with the Author Guidelines «3.14. References» section.

Illustrations (including tables): for original articles — up to 8; for short communications — up to 3; for reviews — up to 8.

6. Formatting

Font: Times New Roman, 12 pt. Section headings: bold. Line spacing: 5. Paragraph formatting: no extra space before or after paragraphs; one additional line between sections. First-line indent: 1.25 cm. Margins: 2.5 cm on all sides. Page numbers: bottom right corner of each page

СКОРО СПЕЦИАЛЬНЫЙ ВЫПУСК

Клинические рекомендации «Остановка сердца (взрослые пациенты)» — первые в Российской Федерации —

Кодирование по Международной статистической классификации болезней и проблем, связанных со здоровьем: I46, I46.0, I46.9

Клинические рекомендации (КР) «Остановка сердца (взрослые пациенты)» подготовлены коллективом ведущих специалистов и представителей Общероссийской общественной организации «Федерация анестезиологов и реаниматологов», Российского общества скорой медицинской помощи, Национального совета по реанимации, Российского общества первой помощи и регламентируют проведение реанимационных мероприятий при остановке кровообращения у взрослых пациентов.

В КР изложена терминология по проблеме остановки кровообращения, этиология и патогенез, эпидемиология внебольничной и внутрибольничной остановки кровообращения, принципы диагностики, алгоритмы базовой (с применением автоматического наружного дефибриллятора) и расширенной сердечно-легочной реанимации, особенности экстракорпорального жизнеобеспечения, а также проведения реанимационных мероприятий в рентген-операционной, у кардиохирургических пациентов и у беременных. Отражены юридические аспекты прекращения и обоснованного отказа от проведения реанимационных мероприятий, критерии качества оказания медицинской помощи. Приведены иллюстрированные алгоритмы проведения реанимационных мероприятий.

КР «Остановка сердца (взрослые пациенты)» содержат 14 приложений и 231 источник литературы.